

Review

The Progress of Additive Engineering for $\text{CH}_3\text{NH}_3\text{PbI}_3$ Photo-Active Layer in the Context of Perovskite Solar Cells

Mayuribala Mangrulkar *  and Keith J. Stevenson

Center for Energy Science and Technology, Skolkovo Institute of Science and Technology, 121205 Moscow, Russia; k.stevenson@skoltech.ru

* Correspondence: mayuribala.mangrulkar@skoltech.ru

Abstract: Methylammonium lead triiodide ($\text{CH}_3\text{NH}_3\text{PbI}_3/\text{MAPbI}_3$) is the most intensively explored perovskite light-absorbing material for hybrid organic–inorganic perovskite photovoltaics due to its unique optoelectronic properties and advantages. This includes tunable bandgap, a higher absorption coefficient than conventional materials used in photovoltaics, ease of manufacturing due to solution processability, and low fabrication costs. In addition, the MAPbI_3 absorber layer provides one of the highest open-circuit voltages (V_{oc}), low V_{oc} loss/deficit, and low exciton binding energy, resulting in better charge transport with decent charge carrier mobilities and long diffusion lengths of charge carriers, making it a suitable candidate for photovoltaic applications. Unfortunately, MAPbI_3 suffers from poor photochemical stability, which is the main problem to commercialize MAPbI_3 -based perovskite solar cells (PSCs). However, researchers frequently adopt additive engineering to overcome the issue of poor stability. Therefore, in this review, we have classified additives as organic and inorganic additives. Organic additives are subclassified based on functional groups associated with N/O/S donor atoms; whereas, inorganic additives are subcategorized as metals and non-metal halide salts. Further, we discussed their role and mechanism in terms of improving the performance and stability of MAPbI_3 -based PSCs. In addition, we scrutinized the additive influence on the morphology and optoelectronic properties to gain a deeper understanding of the crosslinking mechanism into the MAPbI_3 framework. Our review aims to help the research community, by providing a glance of the advancement in additive engineering for the MAPbI_3 light-absorbing layer, so that new additives can be designed and experimented with to overcome stability challenges. This, in turn, might pave the way for wide scale commercial use.



Citation: Mangrulkar, M.; Stevenson, K.J. The Progress of Additive Engineering for $\text{CH}_3\text{NH}_3\text{PbI}_3$ Photo-Active Layer in the Context of Perovskite Solar Cells. *Crystals* **2021**, *11*, 814. <https://doi.org/10.3390/cryst11070814>

Academic Editor: Stefano Carli

Received: 14 June 2021

Accepted: 9 July 2021

Published: 13 July 2021

Publisher's Note: MDPI stays neutral with regard to jurisdictional claims in published maps and institutional affiliations.



Copyright: © 2021 by the authors. Licensee MDPI, Basel, Switzerland. This article is an open access article distributed under the terms and conditions of the Creative Commons Attribution (CC BY) license (<https://creativecommons.org/licenses/by/4.0/>).

Keywords: additive; MAPbI_3 ; stability; ambient; inert; perovskite solar cell; efficiency

1. Introduction

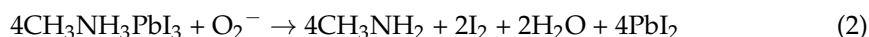
Alternative renewable energy sources are considered reliable options for long-term usage due to the limited availability of traditional energy resources (i.e., coal, oil, and gas). Since solar energy is abundant and free (i.e., it comes from a natural source), it is referred to as clean and green energy. Also, solar energy can help reduce air pollution and global warming caused by greenhouse gas emissions if low-cost manufacturing is achieved [1]. This notion of utilizing solar energy further led to the development of photovoltaic technology, resulting in three generations. The first generation of photovoltaic technology was silicon wafer-based solar cells. However, they were not commercially successful due to their high cost. In contrast, second generation solar cells offered a low cost, but compromised in efficiency. Hence, the third generation was developed to be cost-effective and efficient. In this context, perovskite solar cells are considered advanced level third generation photovoltaic technology that could offer low-cost processing with ease of manufacturing and equally high efficiency when compared to their traditional counterparts [2]. This is why the research community has paid attention to perovskite solar cells in the last decade.

“Perovskite” is the name of the mineral CaTiO_3 discovered in the Ural Mountains of Russia; it is named after the Russian nobleman and mineralogist, Lev Perovski. Nevertheless, this term is being used for all compounds, with the general formula ABX_3 , with the same crystal structure as CaTiO_3 or derived from this structure. These materials consist of two cations. Cation A is 12-fold coordinated by anion X, and cation B is 6-fold, where X can be either oxygen or a halide. In terms of perovskite solar cells, the most commonly used A-site cations are MA/ $[\text{CH}_3\text{NH}_3]^+$, FA/ $[\text{H}_2\text{NCHNH}_2]^+$, Rb^+ , Cs^+ , B site cations are Pb^{2+} , Sn^{2+} , Ge^{2+} . While the X site is halogen atoms, I^- , Cl^- , Br^- [3]. Among many different perovskite absorber layers, methyl ammonium lead iodide (MAPbI_3) is the most prominently studied hybrid organic–inorganic perovskite for perovskite solar cell application. MAPbI_3 offers several unique properties and advantages to be applicable in perovskite solar cells (PSC). It has a suitable bandgap ~ 1.6 eV, a high absorption coefficient (the absorption coefficient of MAPbI_3 lies in the range of 10^4 – 10^5 cm^{-1} , which is more than one order of magnitude larger than that of silicon for the visible light spectrum). The high absorption coefficient of MAPbI_3 allows it to absorb in the low light region. Moreover, a high absorption coefficient allows light to be absorbed by a thin film (generally in the range of 0.3–0.6 μm) of the perovskite layer, while crystalline silicon-based solar cells are usually made thicker ~ 300 μm . This, in turn, reduces the quantity of required material, thereby reducing the cost. Besides, MAPbI_3 can be easily solution-processed to produce efficient solar cells, which further lowers manufacturing costs. Moreover, MAPbI_3 can result in high open-circuit voltages (V_{oc}), low V_{oc} loss/deficit, and low exciton binding energy: 2–70 meV, resulting in better charge transport with decent charge carrier motilities of 2–66 $\text{cm}^2 \text{V}^{-1} \text{s}^{-1}$, long diffusion lengths of charge carriers ~ 1 μm . Because of these properties, scientists and researchers have recommended the fabrication of perovskite solar cells using MAPbI_3 as the active layer [4–6]. Nevertheless, long-term operational stability has been a significant factor that acts as a blockade for the commercialization of PSCs. In comparison, the traditionally made silicon-based solar cells remain operational for up to 20–25 years. On the contrary, perovskite solar cells are stable for a few hundred hours to a maximum of one year [4]. Thus, PSCs face serious stability issues compared to already available PV technology in the market. These stability issues involve both extrinsic and intrinsic challenges to overcome.

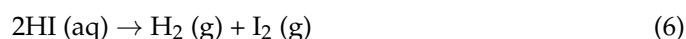
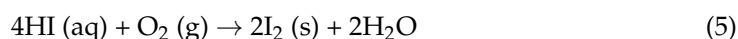
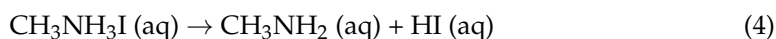
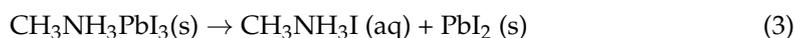
The perovskite-based active layer is susceptible to external factors, such as water, air, and moisture [7–9]. Reports have shown that, upon exposure to these external factors, PSC degrades and loses its operational stability [10]. It was found that, in the presence of water, MAPbI_3 crystal structure forms hydrates/complex with H_2O (Equation (1)), and deforms the perovskite structure, destroying optoelectronic properties, resulting in loss of photovoltaic performance [7,11,12].



Moreover, it was demonstrated that exposure of $\text{CH}_3\text{NH}_3\text{PbI}_3$ photoactive layers to light and oxygen results in the formation of superoxide (O_2^-) species. This reactive O_2^- species can deprotonate the methyl ammonium cation (CH_3NH_3^+), leading to the formation of PbI_2 , water, methylamine and iodine [13–15], as shown in Equation (2).

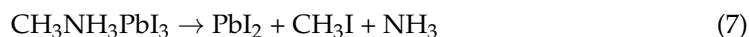


Furthermore, when MAPbI_3 is exposed to moisture, methyl-ammonium cation degrades and results in PbI_2 , I_2 and water formation (Equations (3)–(6)) [4], and the solar cell is destabilized.

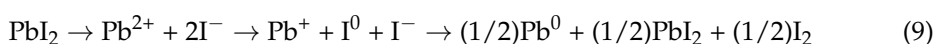


Nevertheless, the impact of these external factors can still be minimized by encapsulating the active layer. However, it may affect performance and the cost. Ironically, MAPbI₃ is intrinsically unstable as well. It means that, in the presence of light and heat, MAPbI₃ tends to decompose. Sadly, these conditions are unavoidable for the operation of a solar cell.

When the temperature exceeds 85 °C in the dark, MAPbI₃ forms ammonia or some other volatile species, and PbI₂ (Equation (7)) [12,16].



Whereas, in the presence of light and temperature, PbI₂ intermediate forms and further decomposes, resulting in the formation of metallic lead and molecular iodine. At the same time, volatile species/by-product may rise from CH₃NH₃I. In the presence of light and heat, the identified degradation pathways are presented in Equations (8) and (9) [2,17–23]:



Thus, these Pb and iodine sites create defect sites/trap states, resulting in instability of the CH₃NH₃PbI₃ active layer and CH₃NH₃PbI₃-based perovskite solar cell devices overall. These defect sites are often reported to be within the grains, at grain boundaries or at the surface of the CH₃NH₃PbI₃ perovskite layer. Moreover, these trap states can also alter the energy level alignment and destroy charge transfer properties in CH₃NH₃PbI₃ solar cell devices. Additionally, non-radiative recombination becomes more prominent in such a scenario, a clear indication of deterioration of device performance. Therefore, it is crucial/important to chemically passivate these defect sites to achieve longer stability of the CH₃NH₃PbI₃ layer [14]. To achieve the aforementioned, additive engineering has been widely applied. Although, the passivation can also be achieved by physically passivating the defects with the help of encapsulating layer [24–27].

In this review, however, we will focus only on the additive approach. To accomplish this, we have analyzed/scrutinized additives used in the CH₃NH₃PbI₃ photoactive layer. Further, the role of the additive and mechanism of the additive interaction with CH₃NH₃PbI₃ has also been discussed. Their impact on film morphology, charge transport properties, and impact on stability has been intensively described. It should be noted that, here, we discussed only those additives that are added in the CH₃NH₃PbI₃ layer. In addition, scrutiny of the physical passivation layers/encapsulation approach that may result in the same is beyond the scope of this review, as we mainly focused only on the aspect of additive engineering. Further, we aim to discuss those additives that do not alter/destroy the perovskite structure of CH₃NH₃PbI₃, i.e., do not result in mixed cation or mixed halide perovskite. The additives are mainly classified as organic additives and inorganic salt additives. Furthermore, organic additives are analyzed based on the functional group associated with the N/O/S donor atom. At the same time, the inorganic salt additives are further classified as per the group name in the periodic table, i.e., alkali metals, transition metals, other metals, and non-metals. This review aims to analyze the research progress/advancement in the context of additives employed to improve the performance and stability of the CH₃NH₃PbI₃ photoactive light-absorbing layer. This can further help design additives, ultimately resolving stability challenges to commercialize the CH₃NH₃PbI₃-based perovskite solar cell.

2. Organic Additives

Organic additives are the most common types of additives used in perovskite solar cells. These organic additives can be further categorized based on N donor, O donor, and S donor atoms. These electron donor atoms can bind/coordinate with the Pb²⁺ species, resulting in adduct formation, passivating the grain boundaries and, thus, improving efficiency and stability. Subsequently, based on the electron-donating atoms, additives can be further subcategorized as amines, nitriles belonging to the N donor atom, amides,

acids, acetates, alcohol, esters, and ethers, belonging to oxygen donor atoms and sulfides, thiocyanates belonging to the S donor atom [28].

2.1. N Donor Atom-Based Additives

2.1.1. Amine Additives

Following the notion of amine-based additives, the non-stoichiometric use of methylammonium iodide as an amine additive was advised in the early phases of developing perovskite solar cells. It was established that adding excess MAI reduces trap density, increases PL lifetime, and further increases PCE regardless of fabrication methods [29–31]. Likewise, some other organic amine derivatives, such as benzylammonium iodide (BAI) and phenethylammonium iodide (PEAI), have also been investigated as additives and were found to improve light harvesting properties and exciton lifetime with reduced charge recombination [32,33]. Moreover, it was discovered that, if hydrophobic cations containing amine additives are employed, such as hexylamine hydrochloride (1-HH), 1,6-diaminohexane dihydrochloride (1,6-DD) and phenylhydrazinium iodide (PHAI), it may even work as a protection for the MAPbI₃ film against moisture, improving the stability in ambient conditions [34,35]. Later, it was found that, if instead of an iodide, a chloride-based counterpart (i.e., MACl instead of MAI) was used as an additive, perovskite films became more crystalline, with increased grain size and homogenous, smooth morphology, which further resulted in grain boundary passivation, resulting in better performance. Unfortunately, the addition of MACl was reported to form mixed halide perovskite CH₃NH₃PbI_{3-x}Cl_x [36–38]. Although there were opposite reports about mixed halide formation. It was shown that when other halide ions, i.e., X = Br/Cl, are used with a minimum concentration in MAPbI₃ precursor, it does not affect MAPbI₃ characteristics, and the final perovskite remains crystalline MAPbI₃ phase-only instead of mixed halide perovskite. This is because a low concentration of halide ions can quickly evaporate as the films are annealed during the fabrication process. Some of the examples of such additives are amphiphilic hexadecyl trimethyl ammonium bromide (CTMAB), ethyl ammonium chloride (EACl), 1,3-diaminoguanidine monohydrochloride (DAGCl), benzamidine hydrochloride (BMCl), acetamidine hydrochloride (AcHc), methoxyammonium chloride (MeOCl), 2, 2, 2-trifluoroethylamine hydrochloride (TFEACl), benzenamine hydrochloride (BACl), 3-chloropropylamine Hydrochloride (3-CPACl), diethylamine hydrochloride (DEACl) [39–45].

Furthermore, nitrogen-containing heterocyclic amines play a great role in improving stability [46]. For instance, the introduction of 4,4'-bipyridine in MAPbI₃ demonstrated complex formation with PbI₂, thus improving intrinsic stability against illumination [47]. Additionally, it has been shown that the presence of N atoms prevents the loss of volatile species from the perovskite film and acts in a similar way as polymeric passivation coating. Further, such a passivation effect was visible, morphologically (in the SEM cross-section images and energy dispersive X-ray analysis), when PVC was added in MAPbI₃ [48]. Later, scientists designed pyridine derivatives with units containing different multifunctional groups. One such additive is (C₆₀-PyP), which contains C₆₀ units that are hydrophobic in nature and pyridine units, which chelates Pb²⁺ by donating the lone electron pair on the N atom. It is known that uncoordinated Pb²⁺ ions are considered trap states at grain boundaries and can block charge extraction [49]. Thus, grain boundaries are passivated by assisting coordination interactions with the Pb²⁺ ion of MAPbI₃ and PyP unit that further improved short circuit current density J_{sc} and eliminated ion migration. While the hydrophobic C₆₀ unit does not let moisture directly affect the film [49]. Similar results were noticeable when pyridine-2-carboxylic lead salt (PbPyA₂) and polyvinylpyrrolidone (PVP) additives were employed in MAPbI₃ precursor [36,50]. Additionally, solvent additives with heterocyclic nitrogen-containing units also demonstrated similar results. In an investigation, Zhang and co-workers demonstrated that NMP as a solvent additive (when added in DMF) resulted in a high quality of perovskite film due to the Lewis acid–base reaction with Pb atom. The study revealed that intermediates obtained with different PbI₂/NMP

ratios are of the same kind, because of which, the solar cell performance and stability do not depend on the NMP ratio in the precursor [51]. Following the idea of the Lewis acid–base interaction, KIM and co-workers explored pyrrolidone-based solvent additives and compared with commonly used DMF-based precursor [52]. For pyrrolidone-based solvent additives, different *N*-substituents: *N*-methyl-2-pyrrolidone (NMP), *N*-ethyl-2-pyrrolidone (NEP), *N*-cyclohexyl-2-pyrrolidone (CHP), and *N*-octyl-2-pyrrolidone (NOP) was employed. During the in situ crystal growth, it was observed that solvent additive containing pyrrolidone structure with higher boiling point results in lower vapor pressure over pristine DMF-based precursor. Thus, it resulted in a further improvement in the morphology of perovskite film since the *N* substituent becomes bulkier with a higher boiling point (the boiling points of NMP, NEP, CHP, and NOP are 154 °C, 202 °C, 204 °C, 286 °C, 303 °C). Furthermore, it was discovered that the strength of coordination of solvent component influenced intermediate formation with PbI_2 , which, in turn, was influenced by the boiling point of the solvent. This was based on the evidence when the intermediate phase vanished with the CHP solvent additive, whereas pure DMF solvent without pyrrolidone-based solvent additives showed DMF: PbI_2 solvate formation. Therefore, it was suggested that the bulkier additive solvent suppress DMF: PbI_2 solvate formation, which shows lack of stability when used without any cosolvent [52]. Some other derivatives, such as DMI, 1-(4-ethenylbenzyl)-3-(3,3,4,4,5,5,6,6,7,7,8,8,8-tridecafluorooctylimidazolium iodide (ETI), 1-methyl-3-propylimidazolium bromide (MPIB), 1-butyl-3-tetrafluoroborate (BMIMBF₄) are other examples that result in improved PCE and ambient stability due to hydrophobicity of *N* atoms with a ring-like structure [53–55]. Figure 1 below shows the chemical structures of additives based on amine derivatives.

2.1.2. Cyano/Nitrile Additives

Subsequently, it was observed that the cyano group-containing *N* atom could be equally effective to passivate grain boundaries [56]. Triazine-graphdiyne (Tra-GD) is a graphene-like material that consists of pyridine-like nitrogen in the highly conjugated framework. It was suggested that balanced charge distribution in the $\text{C}=\text{N}$ bond in the triazine ring promotes stronger interaction with Pb^{2+} , resulting in very tight contact between these two materials. This, in turn, did not allow the ion migration on the surface and successfully passivated grain boundaries [56]. Similarly, graphitic carbon nitride addition also resulted in good morphology due to highly compact bonding between Pb^{2+} and *N* of $\text{C}=\text{N}$ that further endorsed to achieve power conversion efficiencies (PCEs) up to 21.1% (aperture 0.16 cm²) and 19.5% (aperture 1.0 cm²), featuring an open-circuit voltage of 1.16 V (corresponding to a slight voltage loss of 0.39 V), and improved operational device stability (~90% initial efficiency retained after constant one sun illumination for 500 h) [57,58]. Further, Zhou and co-workers demonstrated that, by employing 1,8-Diazabicyclo[5.4.0]undec-7-ene (DBU), the formation of I^- can also be suppressed due to adduct formation with PbI_2 [59]. Moreover, another solvent additive, acetonitrile (ACN), also showed improvement in morphology due to adduct formation with PbI_2 when added in a DMF-based precursor. This further proved to increase PCE from 15.04% to 19.7%, which remained stable without encapsulation for 160 h, with the PCE remaining ~60% of the initial value when exposed to the white light [60]. The chemical structures of the mentioned nitrile-based additives are illustrated in Figure 2.

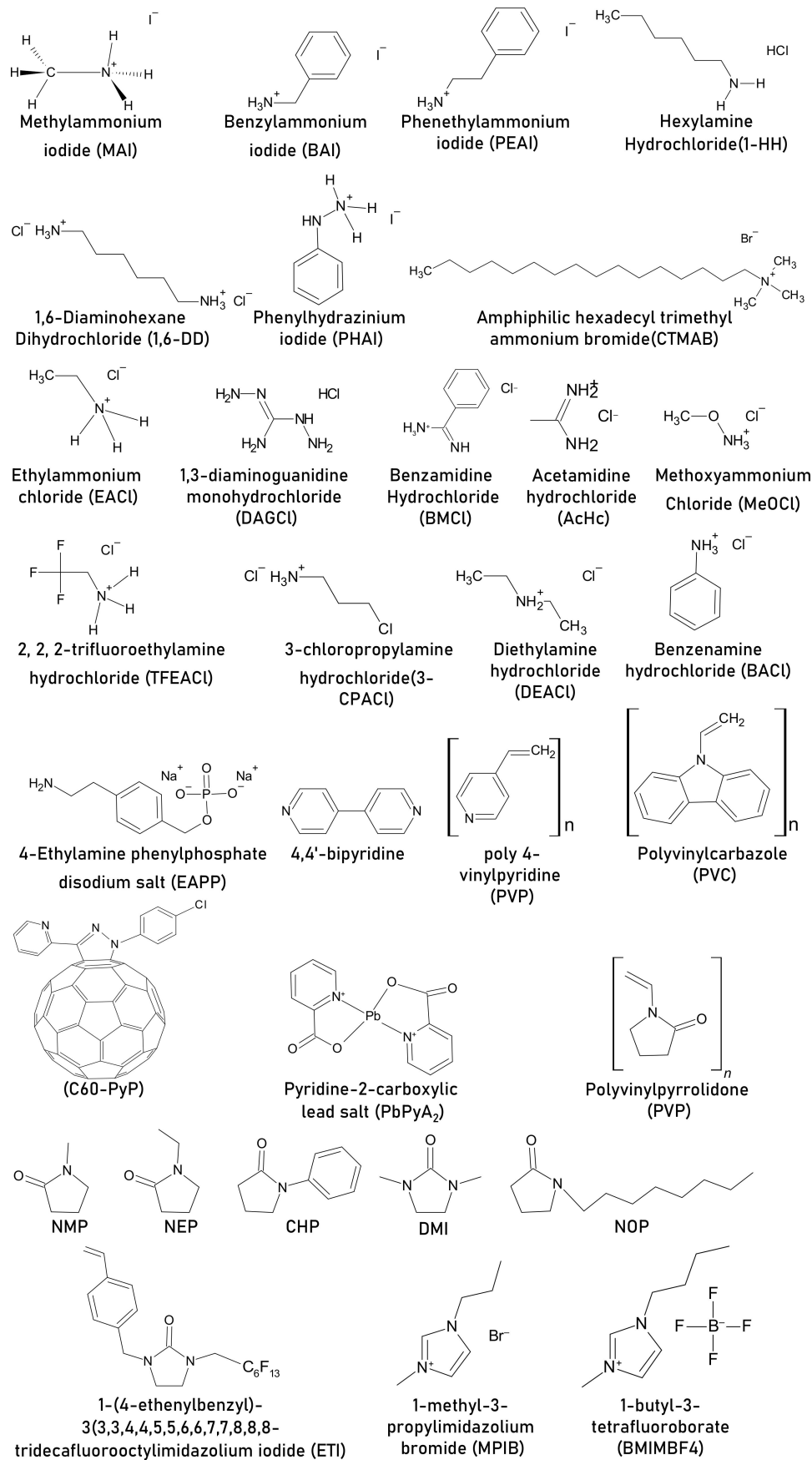


Figure 1. Chemical structures of amine-based additives for MAPbI₃ PSC.

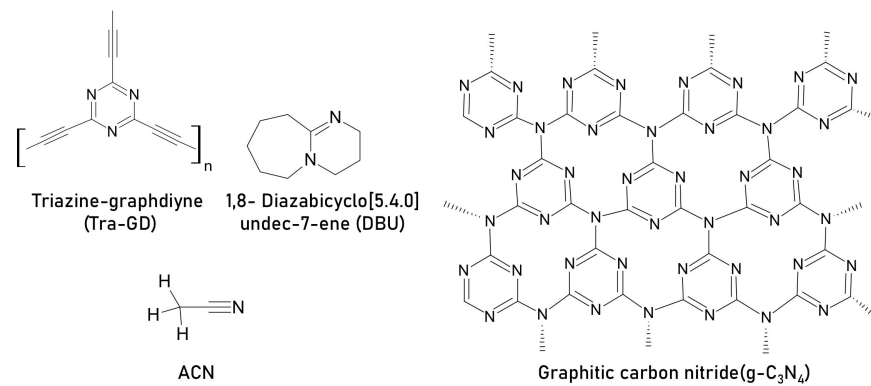


Figure 2. Chemical structures of nitrile additives in MAPbI₃ PSC.

Further, at a glance, the summary of additives that improve stability is presented in Figure 3. In Figure 3, “Extrinsic” represents results reported by conducting stability tests in air, moisture, or in ambient conditions, whereas “Intrinsic” represents results reported by conducting stability tests in inert, inside glovebox (nitrogen or argon filled), or vacuum. All subsequent figures depicting stability time versus additive will use these terms and represent the aforementioned. Here, the stability time refers to the time for which the active layer with additives was reported to be operational/functional in corresponding references. Additional details of additive influence on power conversion efficiency (PCE) and stability are described in Table 1, displaying the additives based on the N donor atom for the MAPbI₃ active layer.

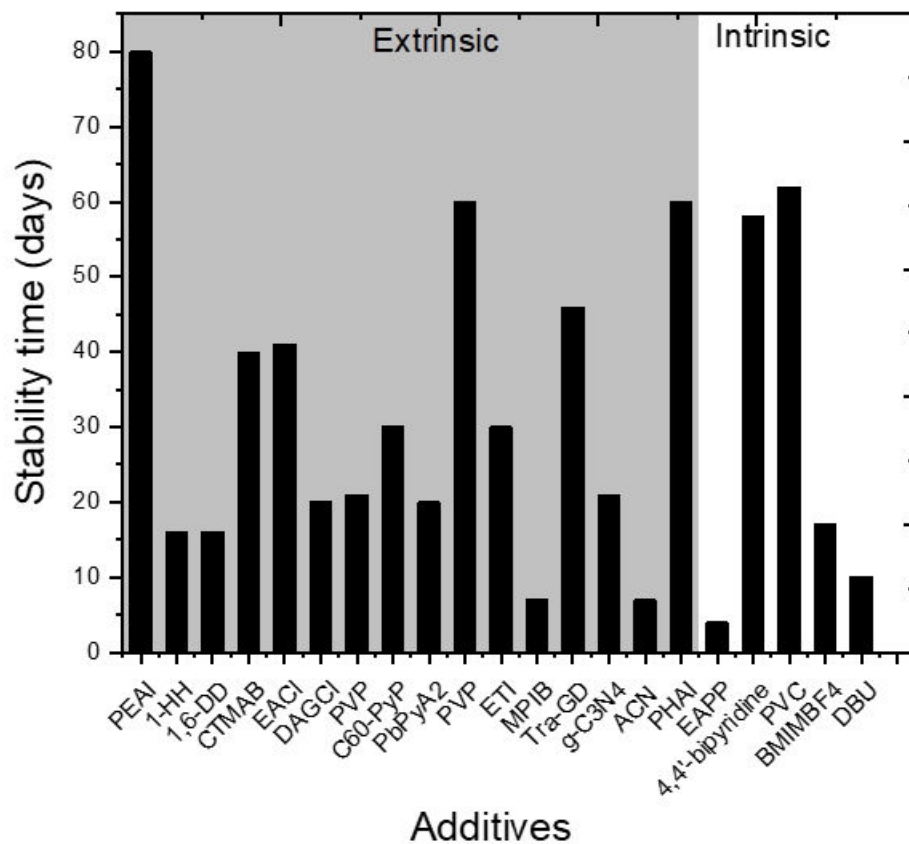


Figure 3. Stability of MAPbI₃ photoactive layer due to various additives containing N donor atom. The data are taken from references [33–35,39–41,47–50,53–57,59–62] respectively.

Table 1. Investigated additives based on nitrogen donor atom containing amines or nitrile.

Additive in Active Layer	Architecture	PCE, % (Pristine)	Stability (Pristine)	PCE, % (with Additive)	Amount of Additive	Stability with Additive	Stability Conditions	Role of Additive	Ref
excess MAI	FTO/SnO ₂ /CH ₃ NH ₃ PbI ₃ /PCBM/Ag	15.14	N/A	17.24	molar ratio PbI ₂ : MAI = 1:1.05	N/A	N/A	Hot casting, improved crystallinity, decrease in defect density, increased PL lifetime	[29]
excess MAI	ITO/PCBM/CH ₃ NH ₃ PbI ₃ /HTL/Au	N/A	N/A	N/A	molar ratio MAI: PbI ₂ = 3:1	N/A	N/A	Vacuum deposition, increased PL lifetime, reduced trap states	[30]
excess MAI	FTO/TiO ₂ /CH ₃ NH ₃ PbI ₃ /Spiro-OmATAD/Au	11.13	N/A	13.37	0.2 mM	N/A	N/A	Sequential deposition, good quality perovskite film	[31]
benzylammonium iodide (BAI)	FTO/TiO ₂ /CH ₃ NH ₃ PbI ₃ /HTL/metal	6.83	N/A	9.05	molar ratio BAI:MAI = 0.2	N/A	N/A	Better light harvesting property and low charge recombination	[32]
phenethylammonium iodide (PEAI)	FTO/ c-TiO ₂ /m-TiO ₂ /mp-ZrO ₂ /CH ₃ NH ₃ PbI ₃ /Carbon	6.3	Retained ~77% PCE after 80 days	8.60	molar ratio PEAI: MAI = 1:20	Retained 90% PCE after 80 days	air, light 100 mW cm ⁻²	Better contact with TiO ₂ , longer exciton lifetime, good quality of perovskite film	[33]
hexylamine hydrochloride (1-HH)	Glass/ITO/PEDOT:PSS/CH ₃ NH ₃ PbI ₃ /PCBM/BCP/Ag	14.37	Retained 43% PCE from initial after 16 days	15.70	0.05 wt%	Retained ~85% PCE from initial after 16 days	Unencapsulated, ambient, RT, air, RH = 10–20%	Increases grain size and passivate defects, NH ₃ ⁺ group could form N-H . . . I. hydrogen bond with the I- of the [PbI ₆] ⁴⁻ passivating "A" vacancy; hydrophobic hexane alkyl chain protects against moisture	[34]
1,6-diaminohexane dihydrochloride (1,6-DD)						Retained 90% PCE from initial after 16 days			
phenylhydrazinium iodide (PHAI)	FTO/PEDOT:PSS/CH ₃ NH ₃ PbI ₃ /PCBM/Rhodamine/Ag	14.63	(a) Retained ~53% PCE after 60 days (b) died in 20 days	17.2	10 mg mL ⁻¹	(a) Retained ~90% PCE after 60 days (b) Retained ~85% PCE after 20 days	(a) unencapsulated, N ₂ , dark, RH = 20%, T = 26 °C (b) unencapsulated, ambient room environment, dark, 30 ± 5% RH, 24 ± 2 °C	PbI ₂ and PHAI complex/intermediate formation results in passivation against vacancy defects, hydrophobic phenyl rings acts as a barrier against moisture	[35]
amphiphilic hexadecyl trimethyl ammonium bromide(CTMAB)	Glass/FTO/TiO ₂ /CH ₃ NH ₃ PbI ₃ /Spiro-OMeTAD/Au	17.05	Retained 70% PCE after 40 days	18.03	10 mg CTMAB in 1 mL DMSO. Used 20 uL of this to add in 1 mL precursor	Retained 95% PCE after 40 days	Non-encapsulated, RH~40%, T = 25 °C, dark	Improved crystallinity and morphology	[39]
ethylammonium chloride (EACl)	Glass/FTO/c-TiO ₂ /meso-TiO ₂ /CH ₃ NH ₃ PbI ₃ /HTL/Au	17.35	Retained ~30% of the original PCE after 1000 h	20.3	2.5%, molar %	Retained ~89% of the original PCE after 1000 h	encapsulated	Improves morphology, grain boundary passivation	[40]
1,3-diaminoguanidine monohydrochloride (DAGCl)	Glass/ITO/PolyTPD/CH ₃ NH ₃ PbI ₃ /PC ₆₁ BM/ZrAcac/Ag	19.1	Retained 70% PCE after 20 days	20.3	0.6%, wt% of MAI	Retained 80% PCE after 20 days	Non-encapsulated, ambient, RH ~ 50%	Increased grain size, reduced trap density, DAG cation can bond with I ⁻ via hydrogen	[41]
benzamidine hydrochloride (BMCl)	ITO/TiO ₂ /PC ₆₁ BM/CH ₃ NH ₃ PbI ₃ /PTAA/MoO ₃ /Ag	17.8	N/A	18.4	N/A	N/A	N/A	Enhance work function of perovskite film improves efficiency	[42]

Table 1. Cont.

Additive in Active Layer	Architecture	PCE, % (Pristine)	Stability (Pristine)	PCE, % (with Additive)	Amount of Additive	Stability with Additive	Stability Conditions	Role of Additive	Ref
acetamidine salt (AcHc)	ITO/TiO ₂ /CH ₃ NH ₃ PbI ₃ /Spiro-OMeTAD/Au	15.45	N/A	16.54	molar ratio MAI:AaHc = 1:0.08	N/A	N/A	Smooth film, full and uniform coverage, large grain size, improve carrier lifetime,	[43]
methoxyammonium chloride (MeOCl)	FTO/compact-TiO ₂ layer/mesoporous-TiO ₂ layer/CH ₃ NH ₃ PbI ₃ /Spiro-MeOTAD/Ag	17.15	N/A	19.71	molar ratio PbI ₂ :MeOCl =1:0.10	N/A	N/A	Improvement in grain size and crystallinity	[44]
2, 2, 2-trifluoroethylamine hydrochloride (TFEACl)				4.98					
benzenamine hydrochloride (BACl)	Glass/ITO/PEDOT:PSS/CH ₃ NH ₃ PbI ₃ /PCBM/Al	N/A	N/A	11.07	molar ratio of additive:MAI: PbI ₂ = 0.4:1:1	N/A	N/A	Compact smooth high quality film	[45]
3-chloropropylamine hydrochloride (3-CPACl)				8.21					
diethylamine hydrochloride (DEACl)				9.89					
4-ethylamine Phenylphosphate disodium salt (EAPP)	FTO/C-TiO ₂ /mp-TiO ₂ /CH ₃ NH ₃ PbI ₃ /Spiro-OMeTAD/Ag	18.83	(a) Dead in 6 h (b) Remained 60% from initial PCE after 100 h	17.61	1 mol%	(a) Remained 90% from initial PCE after 12 h (a) Remained ~99% from initial PCE after 100 h	(a) ATM condition, RH = 80%, unencapsulated, (b) inert, N ₂ , unencapsulated,	Phenylethylamine group protects against moisture and improves ambient stability, phosphate sodium prevents the formation of (CH ₃ NH ₃) ₄ PbI ₆ ·H ₂ O	[62]
4,4'-bipyridine	Glass/CH ₃ NH ₃ PbI ₃	N/A	Died in ~900 h	N/A	5 wt%	Remained active for 1400 h	inert, unencapsulated, light 70-80 mW cm ⁻² , 50-60 °C	Forms complex with PbI ₂ , thus slows down the formation of metallic lead	[47]
poly 4-vinylpyridine (PVP)	FTO/TiO ₂ /CH ₃ NH ₃ PbI ₃ /Spiro-OMeTAD/Au	6.09	Remained 1.55% PCE as of final PCE (absolute value) after 3 weeks	13.07	0.4 wt%	Remained 6.6% PCE as of final PCE (absolute value) after 3 weeks.	Air, 50% RH, non-encapsulated	Inhibits carrier recombination, reduced defects	[61]
Polyvinylcarbazole (PVC)	ITO/PTAA/CH ₃ NH ₃ PbI ₃ /PCBM/Al	17.4	Died in 1500 h	18.7	1 mass%	Retained ~70% of the initial efficiency after light soaking for 1500 h,	light 50 ± 3 mW cm ⁻² , 65 ± 2 °C, inert nitrogen,	Defect passivation due to interaction with lone pair of electrons from N atom with Pb ²⁺	[48]

Table 1. Cont.

Additive in Active Layer	Architecture	PCE, % (Pristine)	Stability (Pristine)	PCE, % (with Additive)	Amount of Additive	Stability with Additive	Stability Conditions	Role of Additive	Ref
pyridine-functionalized fullerene derivative (C60-PyP)	ITO/TiO ₂ /CH ₃ NH ₃ PbI ₃ /Spiro-OMeTAD/Au	17.61	Retained 70% PCE after 30 days	19.82	0.13 wt%	Retained 90% PCE after 30 days	25 °C, RH = 30%, dark, non-encapsulation,	Enlarged grain size, improved crystallization, interaction b/w N atom of the pyridine moiety within C60-PyP and Pb ²⁺ ion within MAPbI ₃ leads to the passivation of trap states of perovskite layer, hydrophobic nature of C60-PyP molecule increases ambient stability	[49]
pyridine-2-carboxylic lead salt (PbPyA ₂)	ITO/P3CT-N/CH ₃ NH ₃ PbI ₃ /(PCBM)/C ₆₀ /(BCP)/Ag	18.86	(a) Retained 20% of PCE after 480 h (b) retained 20% of PCE after 540 h (c) retained 30% of PCE from initial after 480h	19.96	4 mg mL ⁻¹	(a) Retained 80% PCE after 480 h (b) retained 93% of initial PCE after 540 h (c) retained 90% PCE from initial after 480h	(a) 90 °C, RH = 40–60%, dark, not encapsulated, (b)MPP- tracking, non-encapsulated, white light-100 mW cm ⁻² , inert, 25 °C, (c) Air, non-encapsulated, dark, RH = 40–60%	Controlled crystallization, passivation of grain boundaries, the interaction of pyridine and carboxylate to cations increases hydrophobicity	[50]
polyvinylpyrrolidone (PVP)	Ito/SnO ₂ /CH ₃ NH ₃ PbI ₃ /Spiro-OMeTAD/Au	15.33	Retained 76% from initial PCE after 400 h	15.19	1 mg mL ⁻¹	Retained 80% of the initial PCE after 60 days	encapsulated, ambient, RH = 10%, RT	Lewis base, the pyridine part (side chain) of the PVP polymer, can passivate the surface defects caused by misaligned lead ions and can fill the iodine vacancy traps on the surface of the perovskite film, C=O also stabilizes, allows not to degrade	[36]
NMP	FTO/ZnO-MgO-EA+ /mesoporous-TiO ₂ /CH ₃ NH ₃ PbI ₃ /Spiro-OMeTAD/Au	18.0	N/A	19.2	molar ratio PbI ₂ :NMP =1:2	N/A	N/A	The same kind of intermediate, regardless of NMP ratio, results in excellent morphology	[51]
NMP		1.50		7.03	60 µL in 1 mL precursor			Lewis acid base interaction	
NEP	Glass/ITO/PEDOT:PSS/CH ₃ NH ₃ PbI ₃ /PC ₆₁ BM/Al		N/A	10.04		N/A	N/A	-	[52]
CHP				12.87				Suppression of solvate formation	
NOP				2.79				Lewis acid–base interaction	
DMI	FTO/compact-TiO ₂ /CH ₃ NH ₃ PbI ₃ /Spiro-OMeTAD/Au	10.72	N/A	14.54	10 vol%	N/A	N/A	Pb-O bond formation due to Lewis adduct between DMI and Pb	[63]

Table 1. Cont.

Additive in Active Layer	Architecture	PCE, % (Pristine)	Stability (Pristine)	PCE, % (with Additive)	Amount of Additive	Stability with Additive	Stability Conditions	Role of Additive	Ref
1-(4-ethenylbenzyl)-3-(3,3,4,4,5,5,6,6,7,7,8,8,8-tridecafluorooctylimidazolium iodide (ETI))	FTO/C-TiO ₂ /mp-TiO ₂ /CH ₃ NH ₃ PbI ₃ /Spiro-OMeTAD/Au	19.2	(a) Retained 49% PCE from initial 700 h (b) Retained 60% PCE from initial 700 h	19.5	1 mol%	(a) Retained 85% PCE from initial 700 h (b) Retained 80% PCE from initial 700 h	(a) MPPT inert, 60 °C, light 100 mW cm ⁻² , unencapsulated, (b) RH = 40%, RT, dark, air	Enables the full transformation into precursor, suppresses thermal decomposition pathway and, provides outstanding hydrophobicity within the active material	[53]
1-methyl-3-propylimidazolium bromide (MPIB)	ITO/PEDOT:PSS/CH ₃ NH ₃ PbI ₃ /PC ₆₁ BM/BCP/Ag.	15.9	retain ~50% of its original PCE after 150 h	18.2	0.5 mg mL ⁻¹	retain 78% of its original PCE after 150 h	atmospheric environment, RT,	Passivation of the uncoordinated Pb ²⁺ to reduce the defects in the perovskite film due to the lone-pair electron in its cation group, and beneficial to promote crystal growth to improve film quality	[54]
1-butyl-3-tetrafluoroborate (BMIMBF ₄)	ITO/NiO _x /CH ₃ NH ₃ PbI ₃ /C ₆₀ /Ag	18.13	retaining 30% of their initial PCE after thermal ageing of 400 h at 85 °C	18.07	0.4 mol%	retaining 80% of their initial PCE after thermal ageing of 400 h at 85 °C	85 °C, unencapsulated	Thermal stability by effective suppression of perovskite decomposition	[55]
Spiro-OMeTAD	FTO/Den TiO ₂ /mp-TiO ₂ /CH ₃ NH ₃ PbI ₃ /Spiro-OMeTAD/Au	15.52	N/A	17.77	0.01 wt%	N/A	N/A	Facilitates charge transport	[64]
triazine-graphdiyne (Tra-GD),	ITO/P3CT-K/CH ₃ NH ₃ PbI ₃ /PC ₆₁ BM/ZnO/Al	17.90	Died in 1100 h	20.33	2 mg mL ⁻¹	Retain above 90% after 1100 h	Unencapsulated	Interacts with Pb ²⁺ at grain boundaries and passivates grain boundaries and inhibits ion migration	[56]
graphitic carbon nitride(g-C ₃ N ₄)	FTO/compact TiO ₂ /CH ₃ NH ₃ PbI ₃ /Spiro-MeOTAD/Au	18	Retained 46% PCE after 300 h	21.6	0.1 wt%	Retained 90% PCE from initial after 500 h	Encapsulated, light 100 mW cm ⁻²	Improves grain size and crystallinity, passivates grain boundaries, C=N to interact with Pb ²⁺ that forms compact tight bonding resulting in good morphology	[57]
graphitic carbon nitride (g-C ₃ N ₄)	FTO/compact TiO ₂ /CH ₃ NH ₃ PbI ₃ /Spiro-OMeTAD/MoO ₃ /Ag	16.22 ± 0.83	N/A	19.34 ± 0.63	0.4 mg mL ⁻¹	N/A	N/A	Passivation, enhanced crystallinity, C=N to interact with Pb ²⁺ , increases the conductivity and carrier mobility	[58]
1,8-Diazabicyclo [5.4.0]undec-7-ene (DBU)	Glass/ITO/NiO _x /CH ₃ NH ₃ PbI ₃ /PCBM/PEI/Ag	15.98	Retained 50% PCE from initial after 10 days	18.13	3% weight ratio	Retained 80% PCE from initial after 10 days	unencapsulated, inert (N ₂), mpp tracking	Iodine quencher, adduct with PbI ₂ (C=N interaction with Pb ²⁺), reduced defects, high-quality perovskite film	[59]
ACN	ITO/TiO ₂ /CH ₃ NH ₃ PbI ₃ /Spiro-OMeTAD/Au	15.04 ± 0.48	Remained ~20% of initial PCE after 150 h	19.7	molar ratio ACN: PbI ₂ = 0.5	Remained ~60% PCE after 150 h	light 100 mW cm ⁻² RH = 60%–90%, in air without encapsulation	Morphology enhancement	[60]

2.2. O Donor Atom-Based Additives

Similar to N donor, O donor and S donor can also act as Lewis bases due to lone pair of electrons available to co-ordinate with Pb defect site. Additives containing O atom as the Lewis base may consist of various functional groups, such as carbonyls, carboxyl, carboxylates, ester, ethers, and alcohols [28].

2.2.1. Carbonyl and Amide Additives

One such systematically investigated additive is urea. Urea is an eco-friendly compound consisting of a carbonyl group known to interact with PbI_2 [65]. It has been illustrated that PbI_2 and urea forms an intermediate $\text{PbI}_2 \cdot \text{O}=\text{C}(\text{NH}_2)_2$ when added to the PbI_2 precursor solution in the double-step spin coating process. The oxygen atoms act as a Lewis base. Whereas Pb^{2+} acts as Lewis acid, resulting in the formation of Lewis acid–base adduct. This adduct formation further results in large, flat grains [66,67]. Similar results were observed for the single-step spin coating process, resulting in grain boundary passivation, improved crystalline film, and suppressed non-radiative recombination losses, further improving the efficiency of solar cells [67–69]. Moreover, it was shown that incorporating amides in MAPbI_3 reduces the Fermi level by interacting I^- defect vacancy, reducing the trap sites, and increasing the work function of MAPbI_3 perovskite. At the same time, the carbonyl group transfers electrons to perovskite, reducing the Fermi level, which in turn helps to achieve better charge transport properties [70]. Recently, a variant of urea, biuret incorporation in MAPbI_3 precursor attributed the intermediate formation with PbI_2 to the electron delocalization in the $\text{N}-\text{C}=\text{O}-\text{N}$ system in the presence of carbonyl group and explained this is why the peak shift for $\text{C}=\text{O}$ vibration is noticed in FTIR spectra (from 1722 to 1713 cm^{-1} in case of biuret-modified MAPbI_3 film) [71], resulting in higher PCE over urea incorporated devices [72]. Some other additives, such as benzoquinone (BQ), triazine perylene diimide (TPDI), 3,4-dihydroxybenzhydrazide (DOBD), containing the carbonyl group have shown similar properties [73–76]. Similarly, it was also shown that, if a hydrophobic ring is attached within the additive framework in combination with the carbonyl group (Isatin-Cl additive), it also acts as a shield against humidity in ambient conditions, helping to maintain the PCE nearly to 95% of the initial state [77]. Moreover, the usage of the carbonyl group can also be expanded to improve the flexibility of flexible, printable solar cells (FPSC). Polycaprolactone (PCL) additive in MAPbI_3 has shown desirable improvement in PCE as well as mechanical strength. This improvement in mechanical stability was ascribed to a two-fold increase in grain size (from 200 to 400 nm) and homogenous grain distribution, leading to improved mechanical stability that maintained PCE more than 90% of the initial state after 300 bending cycles for the radius from 20 to 4 mm and stability under illumination for 350 h [78].

2.2.2. Sulfonyl Additives

Furthermore, carbonyl-based additives are often compared with the sulfonyl-based group, where the O atom is connected to different species, (i.e., S atom instead of C atom). Fang and co-workers have done one such study in which the strength of Pb coordination of the sulfonyl group containing additive was compared with the carbonyl-based additive. For this purpose, two novel fused ring non-fullerene acceptor materials IDIS-Th and IDIC-Th were introduced into MAPbI_3 . IDIC-Th had the Lewis base functional group carbonyl ($\text{C}=\text{O}$), and IDIS-Th had a sulfonyl group ($\text{O}=\text{S}=\text{O}$). Since the sulfonyl group ($\text{O}=\text{S}=\text{O}$) is a stronger electron-withdrawing group compared with carbonyl ($\text{C}=\text{O}$); the sulfonyl group was predicted to have a stronger interaction with Pb ions than carbonyl ($\text{C}=\text{O}$) because the two sulfur-oxygen double bonds can chelate Pb^{2+} with stronger interaction. Moreover, it was noticed that replacing carbonyl with the sulfonyl group could effectively downshift the lowest unoccupied molecular orbital (LUMO) level of IDIS-Th, which indicated the sulfonyl group is a stronger electron-withdrawing group. Thus, the interaction with Pb would reduce the defect traps density. Further, to confirm the defect passivation effect of IDIC-Th and IDIS-Th, the trap densities (n_{trap}) in bulk MAPbI_3 films were calculated

and found to be $8.85 \times 10^{15} \text{ cm}^{-3}$ and $4.20 \times 10^{15} \text{ cm}^{-3}$, respectively. Undoubtedly, the sulfonyl group reduced the defect states. This further reflected improvements in the contact angles of the film (the hydrophobicity of the films). The improvement in hydrophobicity indicated that the additive molecules at the GBs and surface could inhibit the raid of moisture to MAPbI₃ films. However, both IDIC-Th and IDIS-Th are known for their hydrophobic nature. Nevertheless, these changes reflect improvement in hydrophobic nature. Moreover, the influence of the two molecules on photovoltaic performance was also examined. The PSC with IDIS-Th molecule showed significant improvement in PCE and reached up to 20.01%. Additionally, due to the strong passivation effect of IDIS-Th, PSC with IDIS-Th demonstrated superior stability over PSC with IDIC-Th in ambient conditions, under solar radiation and in the dark at high temperature [79]. Likewise, a comparison of solvent additives hexamethylphosphoric triamide (HMPA) and dimethyl sulfoxide (DMSO) was made, which was further compared to solvent additive NMethyl-2-pyrrolidone (NMP). Here, Lewis basicity, donor number (D_N), and the boiling point of solvents were utilized as comparison parameters to correlate the role of solvents in regulating morphology. This investigation, conducted by Cao and Wei, and co-workers, highlighted that the larger the donor number, the stronger is the Lewis basicity of the solvent additive. The donor number of DMF, NMethyl-2-pyrrolidone (NMP), dimethyl sulfoxide (DMSO), and hexamethylphosphoric triamide (HMPA) are 26.6, 27.3, 29.8, and 38.8, respectively. Therefore, it was suggested that Pb–O bond strength would increase with an increase in the donor number of the additive [80,81]. Hence, NMP, DMSO, and HMPA were expected to form stronger intermediates over pure DMF. In addition, it is also observed that the strong Lewis base additives exhibit higher boiling points. (The boiling points of the DMF, NMP, DMSO, and HMPA are 152, 202, 189, 235 °C, respectively) [82,83]. This, in turn, reduces the evaporation rate of the solvent during the spin-coating process, resulting in a good film morphology. As a result, DMSO followed by NMP cosolvents displayed excellent PCE of 14.66% and 16.17% over pristine (DMF) (12.25%). No residue of PbI₂ remained and complete conversion into perovskite resulted in less resistance [84]. Further, other solvent additives based on O donor atoms, such as tetramethylene sulfone (TMS) [85] and tetrahydrothiophene oxide (THTO), also utilized a similar mechanism of forming the Pb–O bond and improved performance and stability [86]. The chemical structures and influence of amides/carbonyl/sulfonyl group-based additives onto the stability of the MAPbI₃ layer are presented in Figures 4 and 5, respectively, with a glance summary shown in Table 2.

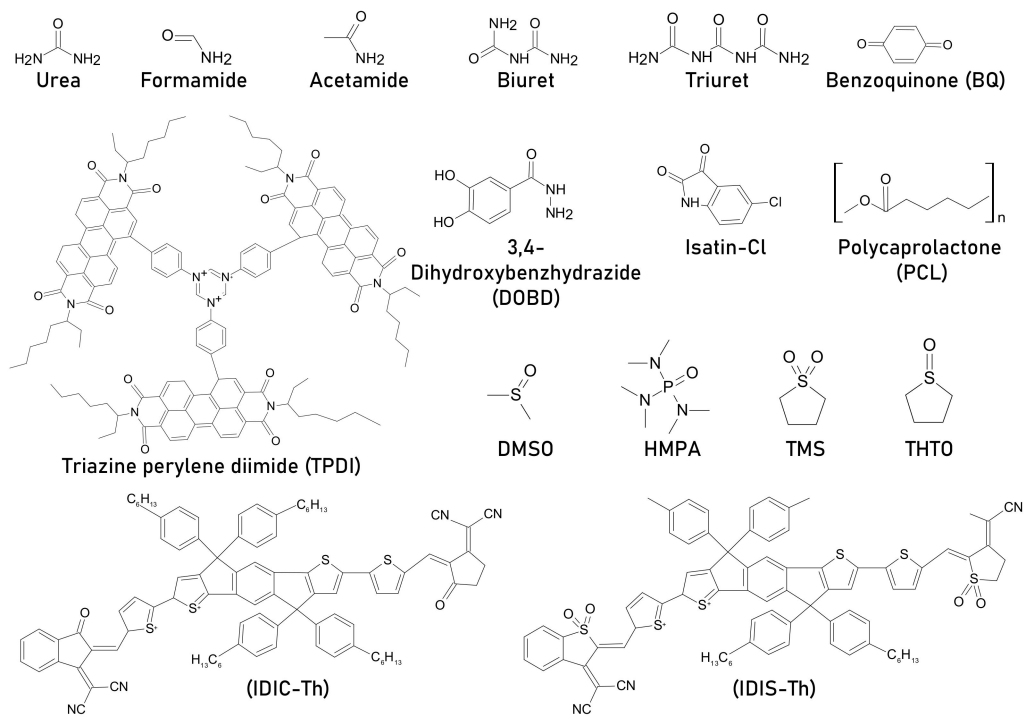


Figure 4. Chemical structures of amide/carbonyl/sulfonyl based additives for MAPbI₃ PSC.

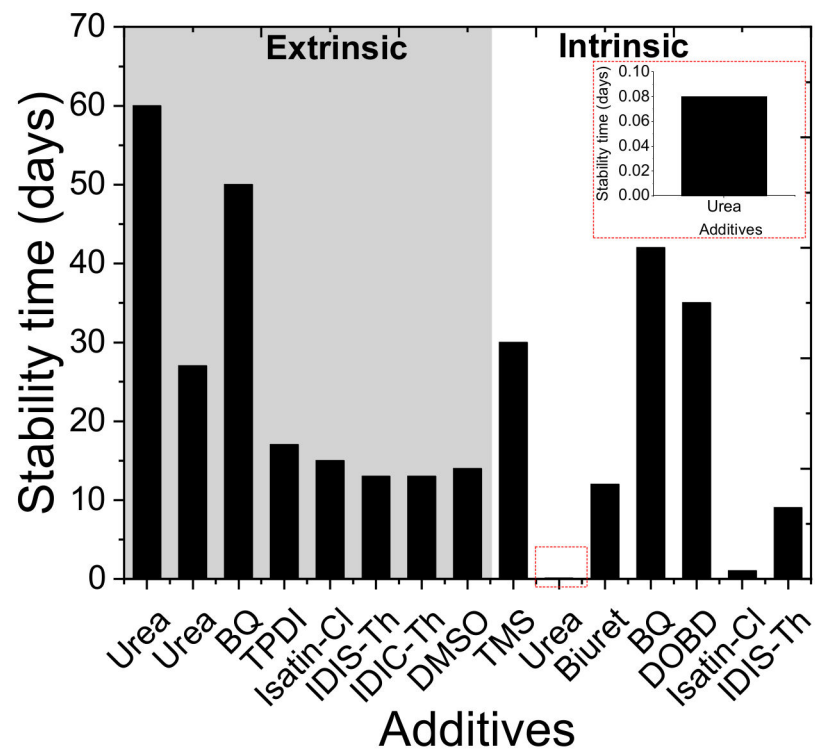


Figure 5. Influence of carbonyl/sulfonyl group onto stability of MAPbI₃-based PSCs. The data are collected from references [65,67,68,71,73–77,79,84,85] respectively.

Table 2. A summary of additives containing amides/carbonyls/sulfonyl functional group in MAPbI₃ active layer.

Additive in Active Layer	Architecture	PCE, % (Pristine)	Stability (Pristine)	PCE, % (with Additive)	Amount of Additive	Stability with Additive	Stability Conditions	Role of Additive	Ref
urea	Glass/ITO/PEDOT:PSS/CH ₃ NH ₃ PbI ₃ /PCMB/BCP/AI	15.1	Retained ~35% from original PCE after 2 h	17	molar ratio urea: lead acetate = 0.5	Retained ~60% from original PCE after 2 h	light, 100 mW cm ⁻² , 50–60 °C, inert, unencapsulated	Interaction of carbonyl group of urea with PbI ₂ results in crystalline film, resulting passivation and improvement in stability	[65]
urea	ITO/PEDOT:PSS/PbI ₂ /MAI/PCBM/BPhen/Ag	12.75	N/A	18.01	5 wt%, wt% of PbI ₂	N/A	N/A	Double step spin coating, urea and PbI ₂ together form PbI ₂ ·O=C(NH ₂) ₂ complex/intermediate, resulting big flat grains	[66]
urea	FTO/SnO ₂ /CH ₃ NH ₃ PbI ₃ /Spiro-OMeTAD/Au	15.48	Remained 50% from original PCE after 60 days	18.52	20 mol%	Remained 80% from original PCE after 60 days	air, 50% humidity, without any encapsulation	PbI ₂ -urea adduct results increment in grain size and passivate grain boundaries	[67]
urea	ITO/SnO ₂ /CH ₃ NH ₃ PbI ₃ /Spiro-OMeTAD/Ag	16.80	a) Retained 10% PCE as of final PCE after ~27 days b) retained nearly 90% PCE from initial after 60 min	18.5	4 mol%	(a) Remained 12% PCE as of final PCE after ~27 days (b) retained nearly 100% PCE from initial after 60 min	mppt tracking (a) dark, ambient, (b) 1 sun, in-situ	Adduct formation, high crystallinity, good film, suppress non-radiative recombination and passivates grain boundaries	[68]
formamide	FTO/c-TiO ₂ / mp-TiO ₂ //CH ₃ NH ₃ PbI ₃ /ZrO ₂ layer mp-ZrO ₂ /carbon electrode	14.26	N/A	15.21	N/A	N/A	N/A	the amide additives shifted the Fermi level of the MAPbI ₃ perovskite from −4.36 eV to −4.63, −4.65, and −4.61 eV, respectively for formamide, acetamide and urea and suppressed non-radiative recombination. Reduced iodide defects vacancy	[70]
acetamide				15.57					
urea				15.07					
biuret	FTO/TiO ₂ /CH ₃ NH ₃ PbI ₃ /PCBM/Ag	18.26	Maintains ~50%PCE after 12 days	21.16	2 mol%	Preserves 94% of its initial efficiency after 12 day	85 °C, N ₂ , inert, non-encapsulated,	Increased grain size, reduced trap state, additive acts as Lewis base and interacted with uncoordinated Pb ²⁺ , improves the thermal stability	[71]
urea	Glass/ITO/NiO _x /CH ₃ NH ₃ PbI ₃ //PC ₆₁ BM/Ag	15	N/A	18.6	0.05 mmol	N/A	N/A	Passivate the defects and eliminate non-radiative charge recombination due to adduct with PbI ₂	[72]
biuret				20.1					
triuret				19.2					
benzoquinone (BQ)	ITO/PEDOT:PSS/CH ₃ NH ₃ PbI ₃ /C ₆₀ /BCP/Au	10.7	Remained ~50% PCE from initial after 900 h	15.6	0.5 mol%	Remained ~80% PCE from initial after 1000 h	unencapsulated, light 1 sun, open circuit, without UV-filter	Reduces trap density	[73]

Table 2. Cont.

Additive in Active Layer	Architecture	PCE, % (Pristine)	Stability (Pristine)	PCE, % (with Additive)	Amount of Additive	Stability with Additive	Stability Conditions	Role of Additive	Ref
benzoquinone (BQ)	FTO/TiO ₂ /CH ₃ NH ₃ PbI ₃ /SpiroOMeTAD/Au	17.37	(a) Dead in 1200 h (b) Dead in ~800 h	18.01	0.25%	(a) Retained 75% PCE from initial after 2400 h (b) Retained ~30% PCE from initial after 1200 h	unencapsulated, without UV-filter (a) RH ~ 20%, RT, (b) ambient air, RH = 40–70%, RT	Improves crystal quality, passivate grain boundary, reduce trap states, suppress PbI ₂ formation at GB	[74]
triazine perylene diimide (TPDI)	ITO/PEDOT:PSS/CH ₃ NH ₃ PbI ₃ /PC ₆₁ BM/Ag	8.32	Retained 30% from initial PCE after 400 h	10.84	1.2 mg mL ⁻¹	Retained 60% from initial PCE after 400h	Non-encapsulated, ambient	Minimize grain boundary defects and enhance the coverage and crystal grain sizes	[75]
3,4-Dihydroxybenzhydrazide (DOBD)	ITO/PEDOT:PSS/CH ₃ NH ₃ PbI ₃ /C ₆₀ /BCP/Al	14.47	Retained 70%PCE from initial after 35 days	17.58	3 mg mL ⁻¹	Retained 85%PCE from initial after 35 days	Non-encapsulated, inert, dark	Increases grain size and decrease of grain boundaries, both of which facilitate charge transportation and suppress charge recombination, due to Lewis acid–base interaction between Pb ²⁺ and C=O	[76]
Isatin-Cl	ITO/PTAA:F4TCNQ/CH ₃ NH ₃ PbI ₃ /PCBM/Al	18.13	(a) Retained 60% PCE from initial after 350 h. (b) Retained 30% PCE from initial after 24 h	20.18	0.0001 wt%	(a) Retained 95% PCE from initial after 350 h. (b) Retained 75% PCE from initial after 24 h	unencapsulated, (a) in ambient air, RH = 45%, room temperature, (b) in nitrogen atmosphere at 85 °C	The carbonyl groups and hydrogen-bond structures on Isatin-Cl passivate the defect states in the perovskite grain boundaries and improved charge transport, suppress charge recombination, hydrophobic ring attached to Isatin-Cl improves stability against humidity	[77]
polycaprolactone (PCL)	glass or PET/ITO/PEDOT:PSS/CH ₃ NH ₃ PbI ₃ /PC ₆₁ BM/BCP/Ag	10.52	Retained 32% of initial PCE (10.12%) after 300 bending cycles	14.49	0.025 wt%	Retained 90% of initial PCE (10.12%) after 300 bending cycle	mechanical bending stability	Carbonyl (C=O) and Pb ²⁺ bond helps the uniform coverage of perovskite, which avoids the defects and achieve the grain boundary regulation on flexible PSC	[78]
IDIS-Th	ITO/P3CT-N/CH ₃ NH ₃ PbI ₃ /PC ₆₁ BM/Bphen/Ag	17.78	(a) Retained 50% from initial PCE after 300h (b) Retained 78% from initial PCE after 200 h	20.1	0.05 mg mL ⁻¹	(a) Retained 80% from initial PCE after 300 h (b) Retained 85% from initial PCE after 200 h	(a) light 100 mW cm ⁻² , ambient, RH = 30%, non-encapsulated, (b) 85 °C, inert, dark,	Passivate grain boundary, reduce charge recombination, adduct between additive and under coordinated Pb ions can effectively inhibit ion migration and moisture diffusion to enhance the stability of PSC devices	[79]
IDIC-Th			18.78	(a) Retained 80% from initial PCE after 300 h (b) Retained 78% from initial PCE after 200 h					

Table 2. Cont.

Additive in Active Layer	Architecture	PCE, % (Pristine)	Stability (Pristine)	PCE, % (with Additive)	Amount of Additive	Stability with Additive	Stability Conditions	Role of Additive	Ref
NMP	FTO/TiO ₂ /PbI ₂ /MAI/Spiro-OMeTAD/Au	12.25	Died after 14 days	14.66	30% NMP in 1 mL precursor	N/A	in air	Morphology control based on Lewis basicity-based, donor number and boiling point	[84]
DMSO				16.17	20% DMSO in 1 mL precursor	Retained 66% PCE from initial after 14 days			
HMPA				12.06	5% HMPA	N/A			
tetramethylene sulfone (TMS)	FTO/bl-TiO ₂ /mp-TiO ₂ /CH ₃ NH ₃ PbI ₃ /Spiro-OMeTAD/Au	8.7	Retained ~70% from initial PCE after 30 days	16.2	molar ratio =PbI ₂ :MAI:TMS = 2:2:1	Retained 80% from initial PCE after 30 days	RT, RH = 10 - 40%, un encapsulated, dark	Intermediate phase via cross-linking. PbI ₂ act as Lewis acid TMS with S=O group acts as Lewis base	[85]
tetrahydrothiophene oxide (THTO),	ITO/PEDOT:PSS/CH ₃ NH ₃ PbI ₃ /PCBM/Al	N/A	N/A	12.1	molar ratio THTO:Pb = 3:1	N/A	N/A	Additive alters the nucleation and growth processes, lowered the free energy of the precursor by incorporating a sulfoxide (S=O), which strongly interacts with MAPbI ₃ precursors, allowing an unprecedented degree of control over the nucleation density and growth rate.	[86]

2.2.3. Carboxylic/Acid Additives

Acid additives have also been incorporated in the MAPbI₃ precursor. The most commonly reported acid additive is 5-amino valeric acid (5-AVA). Dauskardt and co-workers showed that the introduction of 5-AVA into MAPbI₃ precursor could be helpful to increase the mechanical robustness of the perovskite film. To test the mechanical reliability, the double cantilever beam method was used, and the cohesion energy (G_c) was calculated from the critical load at which the film created cracks. It was observed that the incorporation of 5% concentration of 5-AVA into MAPbI₃ precursor increased cohesion energy (G_c) from $0.61 \pm 0.27 \text{ J/m}^2$ (pristine) to $6.04 \pm 2.04 \text{ J/m}^2$ (with AVA additive) almost 12-fold. This improvement in G_c with 5-AVA was attributed to enhanced interaction forces due to the longer alkyl chains present in the 5-AVA [87]. Additionally, a further increase in plasticity and crack deflection around the additive-containing perovskite grain boundaries was observed. Later, the elastic moduli of MAPbI₃ perovskite films with 5-AVA showed a slight decrease in the elastic modulus from 20.5 GPa (pristine) to 18.9 GPa (5-AVA) (using the nanoindentation method). This decrease in stiffness of the planar perovskite structure made it more mechanically robust and less brittle. Moreover, it was confirmed that adding 5 AVA in MAPbI₃ precursor does not change MAPbI₃ lattice parameters [87]. Simultaneously, another study done by Durrant and the group reported enhanced photostability of MAPbI₃ solar cells due to surface defect passivation in screen printed, HTM free, carbon electrode-based PSC consisting of 5 AVA in MAPbI₃. They found a 40-fold increase in device lifetime measured under full sun illumination in ambient air (RH \pm 15%). Further, it was proposed that AVA is located at grain boundaries and, thus, able to passivate surface defect sites, resulting in enhanced resistivity to oxygen-induced degradation [88]. The impressive improvement in the stability due to the AVA additive is attributed to the interaction of halides with $-\text{COOH}$ and NH_3^+ group, through hydrogen bonding ($(\text{O}-\text{H}\cdots\text{I})$ and $(\text{N}-\text{H}\cdots\text{I})$), and further verified in the large area cell with an area of 0.25 cm^2 , which demonstrated the efficiency of 6.6% with a decent shelf life of 75 days, maintaining more than 90% of initial efficiency [89]. Later, using polyacrylic acid (PAA), Cao and workers demonstrated that acid additives could be useful for large area (1 cm^2) films using the doctor blade method. Using the carboxyl functional groups of PAA, iodide ion vacancies at the perovskite crystal surface could be cross-linked. Thus, the interaction of the PAA molecule with MAPbI₃ passivates defects and improves PCE and stability [90]. In addition, it was demonstrated that bifacial passivation could also be obtained by the interaction of a functional group of $-\text{COOH}$, combined with $-\text{C}$, $-\text{S}$ (of thioctic acid (TA)). Lewis acid–base reaction between under-coordinated Pb^{2+} and S atom in MAPbI₃ can passivate one side, and at the same time, TiO_2 can interact with COOH through hydrogen bonding, resulting in double-sided passivation [91]. Likewise, various studies reported that if multiple $-\text{COOH}$ groups are attached with hydrophobic phenyl ring—it can chelate with Pb^{2+} atom and act as a shield against moisture and humidity under ambient conditions, maintaining the overall crystallinity of film. Terephthalic acid (TPA) and trimesic acid (TMA) are examples. The proposed mechanism of stability in such a case is given as follows: negatively charged groups ($-\text{COO}^-$) strongly attract Pb^{2+} ions in the precursor solution via electrostatic interactions. At the same time, the hydrogen atom from carboxylic acid can bond covalently with halide anion in solution due to the strong electronegativity of halide ions. Thus, it overall suppresses the loss of iodine molecules and, in turn, slows down the decomposition of MAPbI₃ light absorbing layer. Simultaneously, benzene ring with rigidity and π – π bond effect does not allow interacting with water and protects against thermal stress and UV-illumination in ambient conditions [92,93]. Similar effects were observed when 3,3',5,5'-azobenzene-tetracarboxylic acid (H_4abtc) containing two benzene rings connected via azo bonding is introduced in PbI_2 precursor in optimum amounts (2 mass %). The purpose of using the azo group was to reduce the stiffness of the perovskite film [94]. However, due to the hydrophobic nature of the attached cation in the acid-containing additive, most of them increase ambient stability (see Figure 6 for chemical structures of acid-containing additives and Figure 7 for associated stability). Further details

of acid-based additives in MAPbI₃ are provided in Table 3 below.

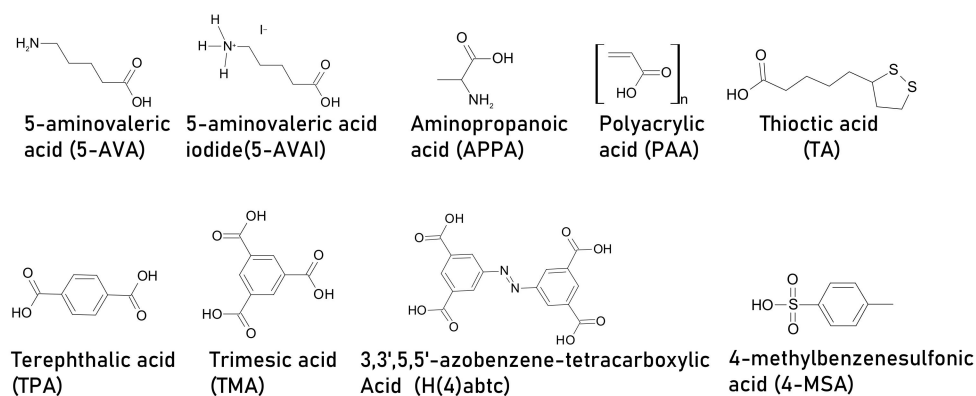


Figure 6. Chemical structures of acid containing additives for MAPbI₃ PSC.

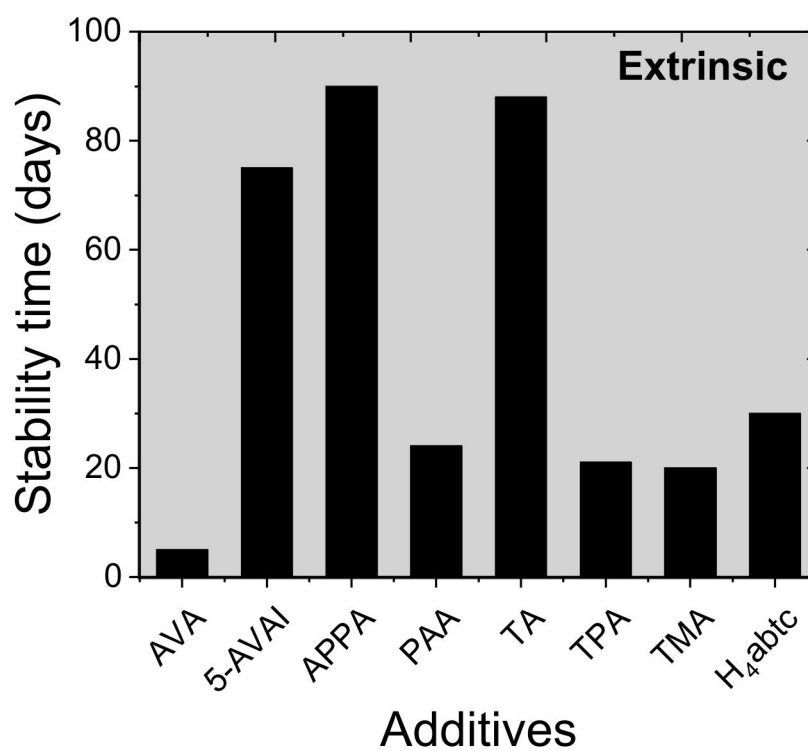


Figure 7. Impact of acidic additives on the stability of MAPbI₃-based solar cells. The graph is plotted using the data from references [88–95] respectively.

Table 3. A summary of acid additives for the MAPbI₃ active layer.

Additive in Active Layer	Architecture	PCE, % (Pristine)	Stability (Pristine)	PCE, % (with Additive)	Amount of Additive	Stability with Additive	Stability Conditions	Role of Additive	Ref
5-aminovaleric acid (5-AVA)	ITO/C ₆₀ /CH ₃ NH ₃ PbI ₃ /PTAA/Au	15.4	N/A	13.7	5% wt	N/A	N/A	Larger grain size, improved crystallinity, improved mechanical robustness	[87]
amino valeric acid AVA	FTO/compact TiO ₂ /mesoporous TiO ₂ /mesoporous ZrO ₂ /mesoporous carbon	11.1	Died in 110 h	9.1	molar ratio AVA: MAI=3%	Retained 50% PCE from initial after 110 h	RH = 15%, 1 Sun, non-encapsulated,	AVA located at grain boundaries is able to passivate surface defect sites, resulting in enhanced resistivity to oxygen-induced degradation.	[88]
5-ammonium valeric acid iodide (5-AVAI)	FTO/TiO ₂ /CH ₃ NH ₃ PbI ₃ /ZrO ₂ /Carbon	N/A	N/A	6.68	0.072M of AVAI	5.62% PCE as of final PCE after 75 days	ambient,	Big area 0.25 cm ² , lower charge transport resistance	[89]
aminovaleric acid iodide (AVAI)	TiO ₂ /ZrO ₂ /CH ₃ NH ₃ PbI ₃ /Spiro-OMeTAD/Au	~7	N/A	~9	AVA:PbI ₂ = 3 mol%	N/A	N/A	Controls ion migration-	[96]
aminopropanoic acid (APPA)	ITO/PTAA/CH ₃ NH ₃ PbI ₃ /PC ₆₁ BM/BCP/Ag _s	17.51	Remained 6% as of absolute value of PCE after 90 days	19.23	weight ratio MAI:APPA= 0.56	Remained 13% as of absolute value of PCE after 90 days	unencapsulated, RH = 10%	Smaller grain size, smooth surface, suppress non-radiative charge recombination, resulting in enhanced J _{sc} and V _{oc}	[95]
Polyacrylic acid (PAA)	FTO/ NiO _x :Zn/CH ₃ NH ₃ PbI ₃ /PC ₆₁ BM/bathocuproine (BCP)/Ag	10.3	Retained 60% from initial PCE after 24 days	14.9	5 mg mL ⁻¹	Retained 80% from initial PCE after 24 days	RT, air, ambient, RH ~ 30 ± 5%, non-encapsulated	Using the doctor blade method, a smooth, uniform, and pin-hole free film of high electronic quality, passivate defects in large area devices (1 cm ²)	[90]
thioctic acid (TA)	FTO/ c-TiO ₂ /TiO ₂ -Poly(TA)/CH ₃ NH ₃ PbI ₃ /Spiro-OMeTAD/Au	17.4	(a) Died after 180 min (b) Died after 400 h (c) N/A	20.4	20 mg mL ⁻¹	(a) Retained 98% of its original PCE after 450 min (b) 97% PCE after 2100 h (c) retained 92% PCE from initial after 600 h	(a) under UV irradiation (35.8 mW cm ⁻²). (b) air, RH = 50 ± 10%, (c) mppt, inert, 1.5 AMG	Carboxylic acid moieties binds at TiO ₂ surface. Then five-membered ring-containing the dynamic covalent disulfide is bonded to the other end of the molecule through the thermal-initiated ring-opening, and interacts with Pb, forming high-quality perovskite film due to the Lewis acid–base reaction between S and Pb ²⁺ . Extra passivation on TiO ₂ helps for efficient charge extraction and stability under UV illumination and ambient conditions	[91]
terephthalic acid (TPA)	FTO/compact-TiO ₂ /CH ₃ NH ₃ PbI ₃ /Carbon layer	11.5 ± 0.67	(a) Retained 81% PCE from initial after 21 days (b) ~6% PCE as of final PCE after 700 h (c) retained 79% PCE from initial after 40 min	14. 29 ± 0	8 mg mL ⁻¹	(a) Retained 94% PCE from initial after 21 days (b) 10.7% PCE as of final PCE after 700 h (c) retained 90% PCE from initial after 40 min	(a) unencapsulated, air, RH = 35%, 25 °C, ambient, dark, (b) 60 °C (c) 365 nm UV illumination 250 mW cm ⁻²	(–COO [–]) from TPA can strongly attract Pb ²⁺ ions crosslinking additive within perovskite, resulting in compact, dense improved morphology, the rigidity of the phenyl skeleton allows moisture and thermal resistance	[92]

Table 3. Cont.

Additive in Active Layer	Architecture	PCE, % (Pristine)	Stability (Pristine)	PCE, % (with Additive)	Amount of Additive	Stability with Additive	Stability Conditions	Role of Additive	Ref
trimesic acid (TMA)	FTO/TiO ₂ /CH ₃ NH ₃ PbI ₃ /Spiro-OMeTAD/Ag	14.27	(a) Retained 49% from initial PCE after 10h (b) retained 46% from initial PCE after 20 days	17.21	1.0 mol L ⁻¹ PbI ₂ precursor solution	(a) Retained 49% from initial PCE after 10 h (b) retained 71% from initial PCE after 20 days	(a) 100 °C, air, ambient, dark, non-encapsulated, (b) RT, air, RH ~ 30%, dark, non-encapsulated,	TMA with a benzene ring and three carboxyl groups maintained stability. The strong hydrogen bond between the hydroxyl group and iodide to suppress the loss of iodide ion, preventing the perovskite from decomposing. Moreover, the benzene ring with rigidity and the π-π bond effect, and the hydrophobic alkyl chains further protects the perovskite from reacting with water	[93]
3,3',5,5'-azobenzene-tetracarboxylic acid (H ₄ abtc)	FTO/TiO ₂ /CH ₃ NH ₃ PbI ₃ /Spiro-OMeTAD/Au	14.25	(a) Remained 25% after 20 h (b) retained 66% of its initial PCE after 30 d	17.67	2.0% (mass ratio with respect to PbI ₂)	(a) Remained 61% after 20 h (b) retained 84% of its initial PCE after 30 d	(a) 100 °C without encapsulation, air, light 100 mW cm ⁻² (AM 1.5), (b) RT, RH = 30% without encapsulation.	High-quality perovskite film, H ₄ abtc can passivate grain boundaries by reacting with the lead cation, therefore leading to good thermal stability and anti-moisture of perovskite films due to rigidity of the benzene ring and azo bond	[94]
4-methylbenzenesulfonic acid (4-MSA)	FTO/b1-TiO ₂ /mp-TiO ₂ /CH ₃ NH ₃ PbI ₃ /Spiro-OMeTAD/Au.	14.05	N/A	17.58	6 mg mL ⁻¹	N/A	N/A	Improved performance, reduced hysteresis, improve J-V characteristics, the sulfonic group is chemically bonded to mp-TiO ₂ and phenyl backbone has p-conjugated structure. J _{sc} and V _{oc} of 4-MSA doped PSC are enhanced.	[97]

2.2.4. Carboxylate/Acetate Additives

In a similar fashion, the acetates in the form of additives also show improvement in crystallinity and grain size, passivating the grain boundaries. One of the examples is formamidinium acetate salt (FAAc). It was reported that FAAc controlled the film morphology and improved fill-factor over 80%, which in turn improved PCE to 16.59%. The improved photovoltaic parameter was further associated with the incorporation of FAAc that eliminated the defect and trap density in the MAPbI₃ film and, thus, improved the charge transport efficiency and reduced the hysteresis [98]. On the contrary, methyl ammonium acetate (MAAc) resulted in lower crystallinity and a smaller grain size ~200 nm [99]. However, it was suggested to use MAAC together with thiosemicarbazide (TSC) salt in the precursor to overcome lower crystallinity. This combination of additives (10–15% MAAC (molar ratio) and a tiny amount of TSC (3–5% molar ratio)) gave a certified PCE of 19.19% for an aperture area of 1.025 cm², and the high-performing devices were able to sustain over 80% of the initial PCE after 500 h of thermal ageing at 85 °C [100]. Moreover, acetate additives were reported to be used as complementary to halogens. For instance, ammonium acetate (NH₄Ac) was found to produce full film coverage with higher crystallinity. It was speculated that NH₄Ac resulted in the formation of methylamine acetate salt by forming NH₄PbI₃ as an intermediate phase with a volatile by-product NH₃ resulting in a higher nucleation density of grains and full coverage of the surface. This, in turn, resulted in a higher efficiency of 13.9% in carbon-based solar cells (FTO/TiO₂/perovskite/Carbon), and 17.02% in the two-step spin coating in FTO/TiO₂/CH₃NH₃PbI₃/spiro-OMeTAD/Au configuration [101,102]. Further, the influence of NH₄Ac addition was compared with NaAc and ZnAc₂. Sadly, the incorporation of sodium acetate (NaAc) into MAPbI₃ precursor reported no improvement in photovoltaic performance. However, the PCEs were comparable. While compared to Zinc-acetate (ZnAc₂) additive, devices with ZnAc₂ demonstrated improved fill factor and short circuit current density over reference cells, resulting in improved PCE from 11.1% to 12.30%. Furthermore, against the speculation that Zn²⁺ might partially replace Pb²⁺, due to the smaller ionic radius, the small quantity of ZnAc₂ (MAI/PbI₂/ZnAc₂ (1:1–x:x, x = 7% as of molar ratio)) was reported to assimilate well within the MAPbI₃ framework, and maintained ~89% of initial PCE after 1900 h when stored in Rh=40%, dark. However, NH₄Ac incorporated devices exhibited ~96% PCE of the initial stage after 1900 h with the same conditions [101,102]. Later, lead acetate (PbAc₂) was employed as an additive, demonstrating excellent PCE improvement from 17.25% to 19.07%. It was further demonstrated that incorporation of PbAc₂ in precursor creates an intermediate phase by forming hydrogen bonding due to interaction with MA⁺ and O from acetate. Thus, this hydrogen bonding acts as a cross-linking agent for the intermediate phase, which later improves the intrinsic stability of devices that maintain almost 95% of the initial PCE for 20 days [103]. A similar mechanism was utilized in another study where the addition of barium acetate (BaAc₂) was explored in MAPbI₃ perovskite with a lower concentration (0–2 mg/mL), which suppressed ion migration and improved thermal stability. The devices could sustain ~90% PCE of the initial stage after exposure to thermal stress at 90 °C in the dark in inert conditions without any encapsulation up to 400 h [104]. Thus, by employing acetate-based additives (Figure 8), improved stability can be obtained both in ambient and inert conditions (Figure 9). Further, the acetate-based additives are summarized in Table 4.

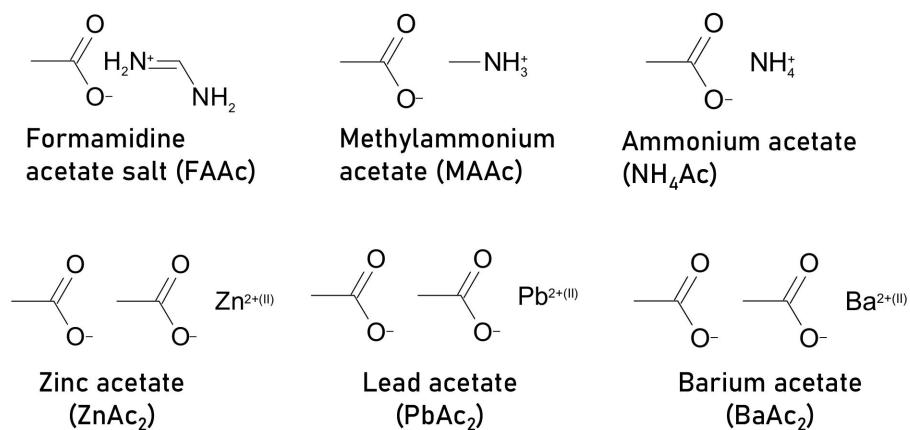


Figure 8. Chemical structures of acetate additives for MAPbI₃ PSC.

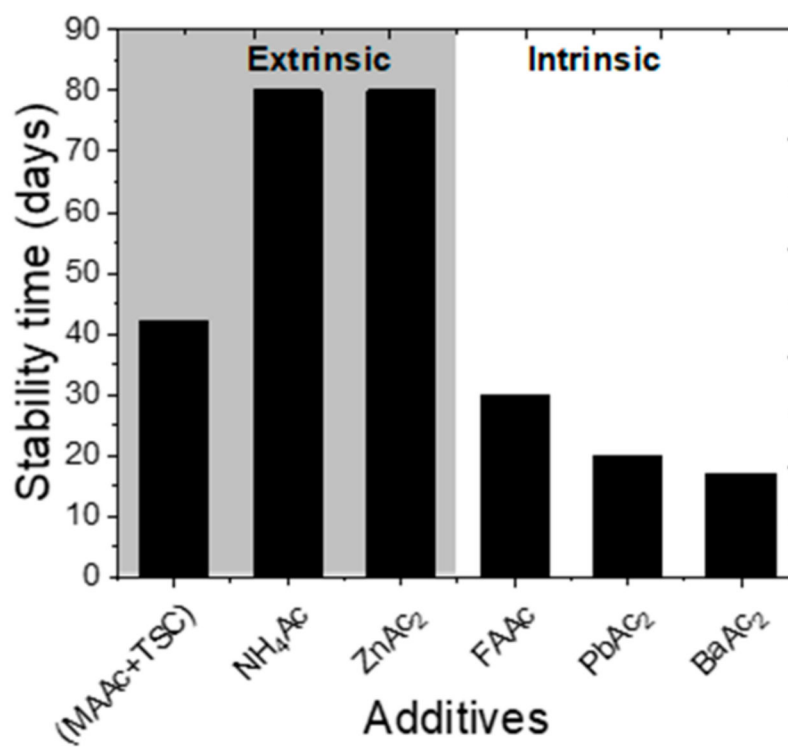


Figure 9. Influence of acetate-based organic additives onto stability of MAPbI₃ perovskite. The graph is plotted with the data taken from references [98,100,102–104] respectively.

Table 4. Acetate-based additives in MAPbI₃ active layer.

Additive in Active Layer	architecture	PCE, % (Pristine)	Stability (Pristine)	PCE, % (with Additive)	Amount of Additive	Stability with Additive	Stability Conditions	Role of Additive	Ref
formamidinium acetate salt (FAAc)	ITO/PEDOT:PSS/CH ₃ NH ₃ PbI ₃ /PCBM/Al	12.13	(a) N/A (b) N/A	16.59	5 mol%	(a) Retained 90% PCE from initial after 30 days (b) 16.10 as of final PCE after 320 s @ (0.87 V)	inert, unencapsulated,	control film morphology and crystallinity, improves optical and electrical properties reduces hysteresis	[98]
methylammonium acetate (MAAc) and thiosemicarbazide (TSC), combined	FTO/NiO/CH ₃ NH ₃ PbI ₃ /PCBM/Ag	N/A	N/A	19.19	10–15% MAAc (molar ratio) 3–5% TSC (molar ratio)	(a) Retained 90% PCE from initial after 1000 h (b) Retained 80% PCE from initial after 500 h	(a) light AM 1.5, 25 °C and RH < 25%, mppt (b) dark, 85 °C, RH < 25%	large-area (aperture area of 1.025 cm ²) using one step solution process, high crystalline quality of film	[100]
ammonium acetate (NH ₄ Ac)	FTO/TiO ₂ /CH ₃ NH ₃ PbI ₃ /Spiro-OMeTAD/Au	13.82	N/A	17.02	10 wt%	N/A	N/A	Improved film morphology and increased surface coverage	[101]
ammonium acetate CH ₃ COONH ₄ (NH ₄ Ac)	FTO/TiO ₂ /CH ₃ NH ₃ PbI ₃ /carbon devices	11.11	Remained 60% from initial PCE after 1900 h	13.9	molar ratio MAI/PbI ₂ /NH ₄ Ac 1:1:x = 0.08%	Remained 96% from initial PCE after 1900 h	Dark, RH = 40%	Carbon electrode-based device, improved crystallinity	[102]
zinc acetate Zn(CH ₃ COO) ₂ (ZnAc ₂)				12.30	molar ratio MAI/PbI ₂ /ZnAc ₂ 1:1–x:x = 7%	Remained 89% from initial PCE after 1900 h			
lead acetate (PbAc ₂)	Glass/ITO/PTAA/CH ₃ NH ₃ PbI ₃ /PCBM/BCP/Ag	17.25	Retained 80% PCE from initial after 20 days	19.07	molar ratio PbAc ₂ /PbI ₂ =3%	Retained 95% PCE from initial after 20 days	unencapsulated, inert	PbAc ₂ additive aids cross-linking to form a strong hydrogen bond with MAI, leading to a more stable perovskite intermediate phase, retards crystallization process, resulting, perovskite thin films with better morphology and larger grains	[103]
barium acetate (BaAc ₂)	ITO/P3CTN/CH ₃ NH ₃ PbI ₃ /PC ₆₁ BM/C ₆₀ /BCP/Ag	18.99	Retained only 20% from initial PCE after 400 h	19.82	2 mg mL ⁻¹	Retained 90% from initial PCE after 400 h	Non encapsulated, inert, 90 °C, dark,	suppression of ions migration, high quality perovskite film, grain boundary passivation	[104]

2.2.5. Ester- and Ether-Based Additives

Interestingly, phenyl-C61-butyric acid methyl ester (PCBM), which is commonly employed as a charge transport layer in organic–inorganic hybrid solar cells, was also examined as an additive in the perovskite layer to achieve hole transport material (HTM) free fully printable MPSC (mesoporous perovskite solar cell). It was shown that, when the concentration of PCBM increased from 0 to 0.25 mg/mL, the PCE significantly improved from 8.58% to 12.36%, achieving a PCE enhancement of more than 44%. This enhancement of PCE was further ascribed to increased J_{sc} from 14.56 mA cm⁻² to 20.26 mA cm⁻² due to higher photogenerated charge separation, and suppressed the charge recombination process. Later, it was illustrated that the PCBM-perovskite intermediate phase was facilitated due to the formation of an intermediate adduct with PbI₂ and carbonyl groups in PCBM [105]. Afterwards, Hu et al. compared PCBM incorporation with only the C₆₀ unit and C₆₀-taurine unit in a single-step spinning coating method in p-i-n configuration. It was reported that C₆₀ (16.59%), PCBM (15.94%), C₆₀-Ta (16.59%) all improved PCE over pristine (14.87%), which was consistent with the previously published report. Further, it was found that the addition of C₆₀ and its derivatives decreased the trap densities and exhibited higher stability when exposed to ambient conditions RH = 25–50% without encapsulation [106].

Moreover, investigations have shown that ethers can help passivate grain boundaries on the perovskite surface. Poly (propylene glycol) bis (2-aminopropyl ether) (PEA) and Jeffamine are some of the examples that showed interaction with Pb ions due to the lone pair of the electron on the oxygen-containing ether part of the additives. Simultaneously, the MA⁺ cation from perovskite forms hydrogen bonding with the counter ion of the additive. Thus, the polymer works as a cross-linking agent that decreases trap densities and hysteresis, improving the device performance and stability. Moreover, the cross-linking properties can also improve the ductility of the perovskite film while stretching when fabricated on a flexible substrate (such as D2000, a Jeffamine variation) [107,108]. Furthermore, using the mechanism above, ethyl cellulose (EC), a low cost, environmentally friendly, thermally stable, and water-insoluble compound, also demonstrated chemical passivation of defect traps. Thus, because of the passivation effect of EC additive, the MAPbI₃ crystal structure remained stable against moisture and air, maintaining 80% of PCE when exposed unencapsulated to ambient air at RH = 45% in the dark for 30 days [109]. Later on, tetra-orthosilicate (TEOS) additive in MAPbI₃ was also reported to lower the cost of processing by making the fabrication process feasible in the air instead of the glove box, which was found valid for both single and double step spin-coating methods. This achievement is due to the fact that, when TEOS is introduced to MAPbI₃ in air, SiO₂ precipitates, acting as a passivation for the perovskite surface and shielding it from moisture and air. This improved the overall stability in ambient conditions [110–112]. Further, cyclic ether compound THF (tetrahydrofuran) also reported improving stability in ambient air, which the pioneer of the PSCs, the Miyasaka group, investigated. The study demonstrated that THF and PbI₂ in DMF interact and form a complex, resulting in dense, homogenous, and pinhole-free film due to complex formation between the Pb and O donor from THF, because of the Lewis acid nature of Pb and Lewis basicity of THF. This, in turn, avoids a direct interaction of PbI₂ with water, improving T80 (T80 is the time at which PCE is degraded to 80% of initial PCE) for 20 days in the ambient environment, with 50% RH, when devices were exposed unencapsulated [113]. Similarly, the liquid additive diethyl ether was also found to influence the crystallization process, resulting in large grains, leading to improved photocurrent properties and performance [114]. The chemical structures (Figure 10) and an overview illustrating the influence of ester and ether-based additives on the stability of MAPbI₃-based solar cells is shown in Figure 11, respectively. Further, a table describing ester and ether containing additives and their role in the MAPbI₃ layer is presented in Table 5.

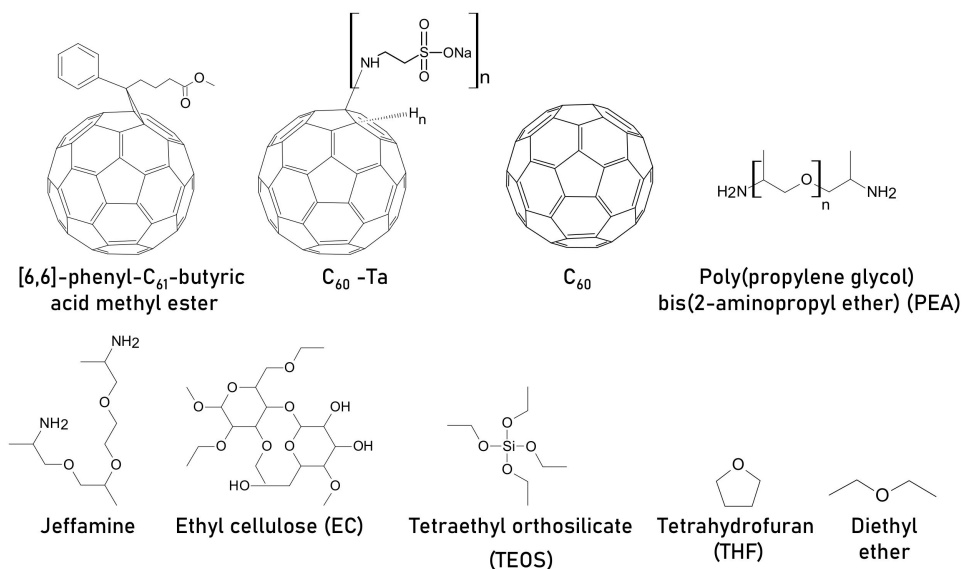


Figure 10. Chemical structures of ester and ether containing additives for MAPbI₃ PSC.

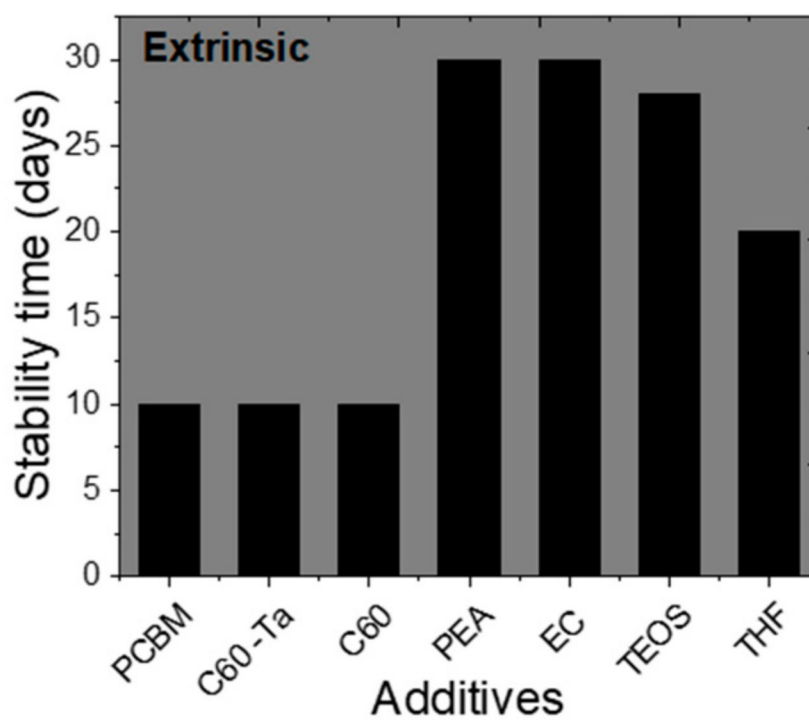


Figure 11. Influence of ester and ether-based additives on the stability of MAPbI₃ perovskite. The graph is plotted with data from [106,107,109,110,114], respectively.

Table 5. Ester and ether-based additives for MAPbI₃ and their role.

Additive in Active Layer	architecture	PCE, % (Pristine)	Stability (Pristine)	PCE, % (with Additive)	Amount of Additive	Stability with Additive	Stability Conditions	Role of Additive	Ref
[6,6]-phenyl-C ₆₁ -butyric acid methyl ester	FTO/c-TiO ₂ /m-TiO ₂ /mZrO ₂ /CH ₃ NH ₃ PbI ₃ /m-carbon	8.58	N/A	12.36	0.25 mg mL ⁻¹	N/A	N/A	Improved morphology, intermediate formation between C=O of PCBM and PbI ₂	[105]
PCBM				15.94	3.5 mg mL ⁻¹	Retained ~12% (absolute value) as of final PCE after 10 days			
C ₆₀ -Ta	Glass/ITO/CH ₃ NH ₃ PbI ₃ /PCBM/BPhen/Ag	13.94	Retained ~9% (absolute value) as of final PCE after 10 days	16.46	1.5 mg mL ⁻¹	Retained ~12% (absolute value) as of final PCE after 10 days	without encapsulation, ambient RH = 25–50%,	Improves crystallinity, passivates defects, suppress non radiative recombination	[106]
C ₆₀				16.59	0.1 mg mL ⁻¹	Retained ~11% (absolute value) as of final PCE after 10 days			
poly(propylene glycol) bis(2-aminopropyl ether) (PEA)	FTO/c-TiO ₂ /mp-TiO ₂ /CH ₃ NH ₃ PbI ₃ /Spiro-OMeTAD/Au	17.18	Maintains ~55% of its original PCE after 30 days	18.87	1 wt%	Maintains 95% of its original PCE after 30 days	dark, ambient, air, RH = 30 ± 5%	Grain boundary passivation, the oxygen atom from ether in PEA, acts as a crosslinking agent, reduces trap density and hysteresis	[107]
jeffamine	ITO/NiO _x /CH ₃ NH ₃ PbI ₃ /PC ₆₁ BM/BCP/Ag	14.5	Showed major cracks	16.8	0.05 wt%	Retained original morphology	10 cycles of stretching at 30% strain	Defect passivation through Lewis acid–base reaction of N atom and O atom with Pb ²⁺ or interaction of MA ⁺ and hydrogen bond of Jeffamine decrease trap density, enhances the ductility of the perovskite film to prevent cracking during stretching	[108]
ethyl cellulose (EC)	FTO/c-TiO ₂ /CH ₃ NH ₃ PbI ₃ /Spiro-OMeTAD/MoO ₃ /Ag	17.11	Completely died in 30 days	19.27	0.1 mg mL ⁻¹	Retained 80% PCE from initial after 30 days	non-encapsulated, dark, ambient, air, RH = 45%	Hydrogen bonding between EC and MAI passivates defects at the grain boundary, reduces hysteresis and improves stability	[109]
tetraethyl orthosilicate (TEOS)	TiO ₂ /CH ₃ NH ₃ PbI ₃ /Spiro-OMeTAD/Ag	15.96	Retained 73% of its initial PCE after 28 days	18.38	0.3 mol%	Retained 77% of its initial PCE after 28 days	ambient, 25 °C, RH = 30%, non-encapsulated,	Reduce trap density, improves carrier lifetime	[110]
THF	FTO/TiO ₂ /CH ₃ NH ₃ PbI ₃ /Spiro-OMeTAD/Au	11.3	Retained 35% PCE from initial after 20 days	15.1	THF: DMF (1:10) v/v	Retained 80% from initial PCE after 20 days	RH = 50%, unencapsulated,	Complex formation due to Lewis acid–base reaction	[113]
diethyl ether	Glass/ITO/NiO _x /CH ₃ NH ₃ PbI ₃ /PCBM/BCP/Ag	13.28	N/A	15.09	the molar ratio of 4% with matrix solvent	N/A	N/A	Grain size improvement	[114]

2.2.6. Hydroxyl/Alcohol

The Hydroxyl group can also play a vital part in interacting with perovskite through hydrogen bonding, further resulting in improved crystallinity and performance. For example, enhanced PCE and stability was observed when dibutyl hydroxyl toluene (BHT) additive containing a phenol group was mixed in MAPbI₃ precursor [115]. Furthermore, methanol and isopropanol showed larger grain size, reduced grain boundaries, lessened defect density, and demonstrated efficient charge carrier extraction at the interfaces, leading to improved PCE stability in ambient conditions without encapsulation. Similarly, improvement in PCE was also noticed due to other hydroxyl-based additives, such as 2-methoxy ethanol (ME), 2-ethoxy ethanol (EE), and 2-propoxy ethanol (PE) and n butanol [116–118]. The chemical structures of the discussed additives are shown in Figure 12. The influence of some of the alcohol additives on the stability of MAPbI₃ perovskite is displayed in Figure 13. Further, a summary of alcohol-based additives, their influence on the PCE, and their role with the perovskite framework is described in Table 6.

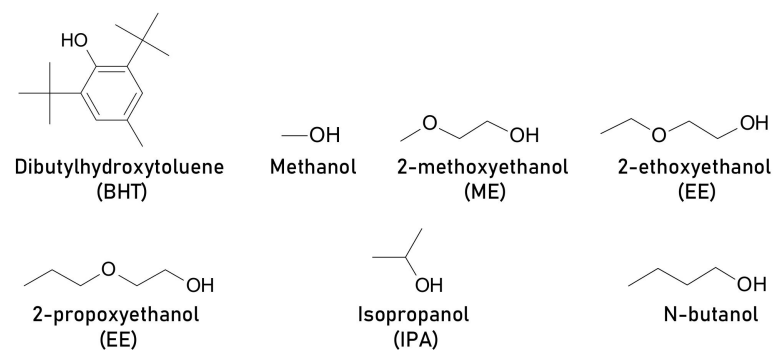


Figure 12. Chemical structures of alcohol additives for MAPbI₃ PSC.

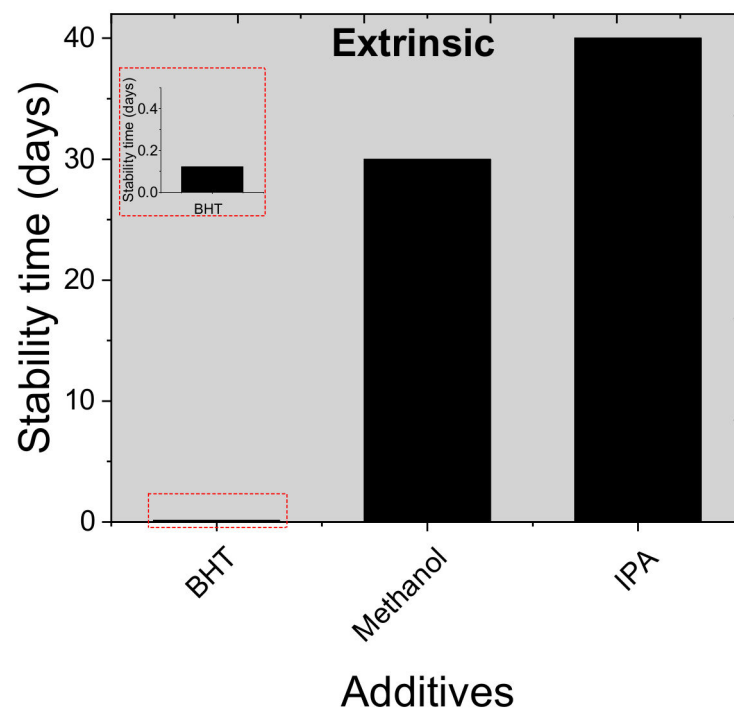


Figure 13. Influence of alcohols onto stability of MAPbI₃ PSC. The data to plot the graph are taken from references [115–117].

Table 6. Alcohol-based additives and their role in MAPbI₃ perovskite framework.

Additive in Active Layer	Architecture	PCE, % (Pristine)	Stability (Pristine)	PCE, % (with Additive)	Amount of Additive	Stability with Additive	Stability Conditions	Role of Additive	Ref
dibutylhydroxytoluene (BHT)	ITO/PEDOT: PSS/CH ₃ NH ₃ PbI ₃ /PC ₆₁ BM/ZnO/Al	17.1	Retained 85% from initial PCE after 180 min	18.1	0.02 M	Retained 93% of initial PCE after 180 min	light 100 mW cm ⁻² , RT, non-encapsulated, RH < 5%	intermolecular hydrogen bonds between the MA ⁺ and –OH groups of the BHT additive improves film crystallinity, reducing the sub-Eg states and carrier traps,	[115]
methanol	FTO/TiO ₂ /CH ₃ NH ₃ PbI ₃ /Spiro-OMeTAD/Au	16.53	Retained 40% from initial PCE after 30 days	19.51	5 vol%	Retained 90% from initial PCE after 30 days	Dark, ambient, nonencapsulated,	morphology control/enhancement	[116]
2-methoxyethanol ME				16.7				two-step interdiffusion protocol to prepare pin-hole free perovskite films, glycol ethers changes the lead iodide to perovskite conversion dynamics and enhances PCE resulting in more compact polycrystalline films, and it creates micrometer-sized perovskite crystals vertically-aligned across the photoactive layer	[118]
2-ethoxyethanol (EE),	ITO/ZnO/CH ₃ NH ₃ PbI ₃ /Spiro-OMeTAD/MoO _x /Ag	14.2	N/A	13.2	30 μL to 1 mL MAI solution	N/A	N/A		
2-propoxyethanol (PE)				15.1					
isopropanol (IPA)	FTO/compact-TiO ₂ /CH ₃ NH ₃ PbI ₃ /Spiro-OMeTAD/Au	16.02	Retained 40% PCE from initial after 40 days	19.70	precursor: IPA volume ratio = 4:1	Retained 85% PCE from initial after 40 days	unencapsulated, air, ambient, RT	morphology enhancement/control	[117]
n-butanol	FTO/CT-IO ₂ /mp-TiO ₂ /CH ₃ NH ₃ PbI ₃ /Spiro-OMeTAD/Ag	13.8	N/A	15.5	5.0 v% for 1 mL precursor	N/A	N/A	morphology enhancement	[119]

2.2.7. Oxygen-Based Multifunctional Group Containing Additives

Other than these additives, other oxygen atom-based additives with multiple functional groups, consisting of C=O, COOH, and OH, were also employed in the MAPbI₃ precursor. One of the examples is reduced graphene oxide (rGO), which was used to achieve fast electron transport rates toward anode, including the growth of large, uniform, smooth, and crystalline perovskite film, resulting in a massive improvement in device performance from 13.6% to 20% [120]. Another example includes poly (amic acid) (PAA) and polyimide (PI) additive. However, the PAA and PI additives also consisted of the N atom, other than C=O, COOH and the OH functional group. The O atoms in PAA and PI form hydrogen bonds with H atoms in CH₃NH₃⁺. The lone pair of electrons of N atoms interact with Pb ions, which stabilized the PVSK framework. Furthermore, these interactions improved the optoelectronic properties of the perovskite layer. As a result, an increment in the grain size was observed when 0.0497 mg/mL PAA-derived perovskite was employed, illustrating the Lewis acid–base interaction between C=O and Pb²⁺ that controls the crystallization process and defect passivation of PVSK. Moreover, both PAA and PI are hydrophobic and highly heat-resistant polymers and further contribute to the stability of PSC when operated in a humid and high-temperature environment [121]. The chemical structure of these additives and their influence on stability are shown in Figures 14 and 15, respectively. Table 7 presents the detailed description of these additives.

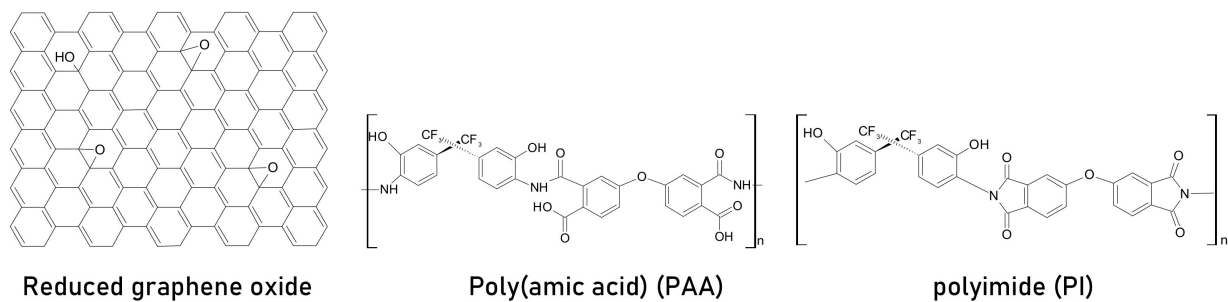


Figure 14. Chemical structures of oxygen-based multifunctional group containing additives.

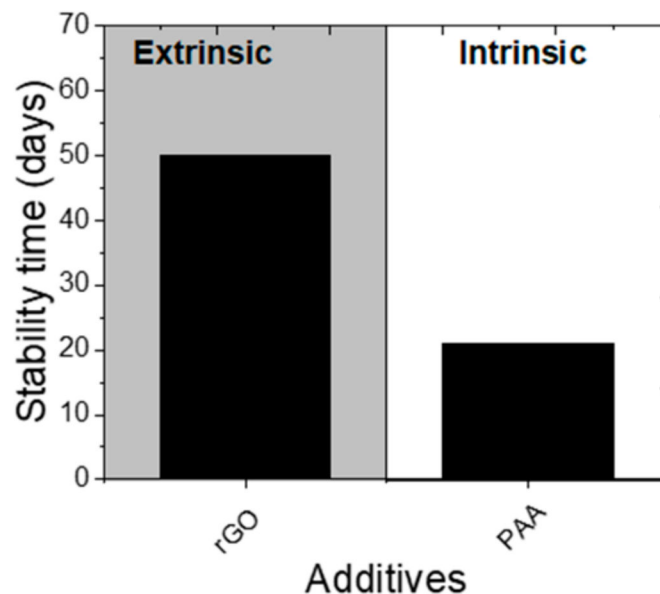


Figure 15. Other oxygen-based additives with multiple functional groups [120,121].

Table 7. Other oxygen atom-based additives with multifunctional group.

Additive in Active Layer	Architecture	PCE, % (Pristine)	Stability (Pristine)	PCE, % (with Additive)	Amount of Additive	Stability with Additive	Stability Conditions	Role of Additive	Ref
Reduced graphene oxide (rGO)	FTO/TiO ₂ /CH ₃ NH ₃ PbI ₃ /Spiro-OMeTAD/Ag	13.8	Retained 20% of their initial PCE after 50 days	16.5	9 μg mL ⁻¹	Retained 40% of their initial PCE after 50 days	dark, RH = 10%, unencapsulated,	Defect-free perovskite films of enhanced crystallinity, larger and evenly distributed grains, enhanced light harvesting potential, increasing the photocurrent density and the resulting improved PCE	[120]
Poly(amic acid) (PAA)	ITO/NiO _x /CH ₃ NH ₃ PbI ₃ /PC ₆₁ BM/BCP/Ag	14.16	(a) Remained 13% as of final PCE after 500 h (b) Retained 50% from initial PCE after 70 h	17.85	0.0497 mg mL ⁻¹	(a) Remained 16.57% as of final PCE after 500 h (b) Retained 88% from initial PCE after 70 h	Inert, dark, non-encapsulated, (b) 85 °C, RH = 45% without encapsulation, dark, in the glovebox	The O atoms in PAA and PI form hydrogen bonds with H atoms in CH ₃ NH ₃ ⁺ and lone pair of electrons of N atoms interact with Pb ions, which stabilized the PVSK framework.	[121]
polyimide (PI)				16.49	0.0990 mg mL ⁻¹	N/A	N/A		

2.3. S Donor Atom-Based Additives

2.3.1. Sulfide and Organosulfur Additives

Further, sulfur-based donor atoms have also improved crystallinity and device performance [28]. For instance, Yang and co-workers used dimethyl sulfide (DS) additive in MAPbI₃ precursor solution (based on DMSO precursor) and demonstrated a record high PCE of ~18.4% for a flexible perovskite solar cell. In addition, the formation of a stable intermediate complex between PbI₂ and DS molecule was observed, which further enhanced stability. The enhancement of stability due to DS solvent additive was ascribed to the smaller electronegativity of the sulfur atom (2.5) in the DS molecule compared to an oxygen atom (3.5) in the DMSO molecule, which allowed sulfur molecules to provide electrons to empty 5d Pb orbitals, ultimately resulting in a hexa-coordinated complex formation. Therefore, with better crystallization and stable intermediate formation, 86% of initial PCE remained for 60 days when unencapsulated devices were exposed to moisture RH~35% in the dark at room temperature [122]. Thiourea is another example of such an organosulfur compound, the addition of which, into the photoactive layer, results in improved performance and stability due to intermediate formation because of the Lewis acid–base reaction. However, the addition of thiourea in the active layer is often compared to the similar compound urea, where the O atom from the carbonyl group (in urea) is replaced with the S atom for thiourea. (i.e., the carbon atom is connected to different species—C=O for urea and C=S for thiourea). Both thiourea and urea were found to show similar effects of increasing grain size, crystallinity, grain boundary passivation, and coordination with PbI₂ in the MAPbI₃ framework [123]. Moreover, many other organosulfur derivatives were reported to form an adduct with PbI₂ as the Pb atom acts as the Lewis acid. One such example is a volatile Lewis base, thioacetamide (CH₃CSNH₂), abbreviated as TAA [124]. Another example is 2-pyridylthiourea, which has an S donor from thiourea, with a better ability to coordinate with PbI₂, and an N donor from pyridine, which can coordinate with PbI₂ as a Lewis acid base and regulate the co-ordination strength with PbI₂. This further resulted in an improvement in crystallinity, which in turn resulted in better light-harvesting ability, charge transport, the reduction of defect and recombination loss, leading to PCE of 18.2%. In addition, this allowed retaining the stability of PSC more than 90% when exposed to ambient conditions, at room temperature or at higher temperature in the dark [125]. Recently, Zhang and his co-workers combined thiourea with water and iodine (ITU) ions to reduce iodine defect vacancy produced during the film fabrication

process. Afterwards, the grain size was found increased with ITU (3.4 μm) compared to when thiourea was added (800–2000 nm), reducing the defects at grain boundaries. Moreover, PSCs with ITU additives displayed a higher V_{oc} , longer decay time, and longer carrier lifetime, with a lower charge recombination rate. Thus, overall, the addition of ITU resulted in improvement in PCE from 17.75% to 20.3%. In addition, the trap densities of the perovskite film significantly reduced as the ITU additive was incorporated into PSC, allowing PSC to stabilize and maintain $\sim 80\%$ of initial PCE after 100 h of exposure to 1.5 AMG solar irradiation and 30 days in the ambient atmosphere [126].

2.3.2. Thiocyanates

Thiocyanates (SCN^- containing anions) additives are another subcategory for S atom-based additives. It should be noted that thiocyanates are also considered pseudo halides. However, the role of thiocyanates in the perovskite film is very controversial. For example, Yanfa Yan et al. demonstrated that a small amount (5%) of $\text{Pb}(\text{SCN})_2$ addition in the precursor can significantly increase the grain size and crystalline quality of perovskite thin films using a one-step solution process method. This increased the average PCE from 15.57 to 17.80%. It was proposed that SCN^- anions do not incorporate in the perovskite film. SCN^- react with CH_3NH_3^+ and form volatile products HSCN and CH_3NH_2 . This allows excess Pb^{2+} and I^- to form PbI_2 at grain boundaries that sources passivation effect [127]. On the contrary, Kim et al. demonstrated that $\text{Pb}(\text{SCN})_2$ in $\text{CH}_3\text{NH}_3\text{PbI}_3$ partially substitutes I anions and forms $\text{CH}_3\text{NH}_3\text{Pb}(\text{SCN})_x\text{I}_{3-x}$ at lower temperatures. This phenomena was observed as not dependent on the concentration of $\text{Pb}(\text{SCN})_2$. However, similar reports of enhancement of crystal size were found. Thus, it was concluded that the influence of processing temperature could affect the purity of the final perovskite film when $\text{Pb}(\text{SCN})_2$ additive is used with MAPbI_3 [128]. Whereas, the addition of potassium thiocyanate (KSCN) also reported to form volatile products HSCN and CH_3NH_2 , consistent with earlier mentioned results, with no traces of SCN^- found in the final perovskite film [127]. In the case of the KSCN additive, however, the residue was KI instead of PbI_2 . Nevertheless, the authors illustrated that the final product upon KSCN incorporation was MAPbI_3 , not KPbI_3 , due to the smaller radius of the K cation. In addition, KI residue improves the crystal quality of perovskite film, resulting in enhancement of charge transport, reduced carrier recombination, and eliminating hysteresis [129].

Conversely, when NH_4SCN was incorporated in MAPbI_3 , it was reported to form an unstable intermediate phase $\text{NH}_4\text{PbI}_{3-x}\text{SCN}_x$ due to lower formation enthalpy (ΔHf) of the NH_4PbI_3 over MAPbI_3 , which later resulted in $\text{CH}_3\text{NH}_3\text{PbI}_{3-x}\text{SCN}_x$ a mixed halide perovskite after annealing of the films [130]. Therefore, when methylammonium thiocyanate (MASCN) was introduced as an additive to the precursor, a rapid vacuum-based drying approach was used to extract volatile intermediate product, so that MAPbI_3 was formed as the final product with no traces of SCN^- . The film fabricated, using this fabrication technique, was reported to gain grain size of more than one micrometer with uniform surface morphology, resulting in high crystallinity and significantly large carrier lifetimes ($\tau_1 = 931.94 \pm 89.43$ ns; $\tau_2 = 320.41 \pm 43.69$ ns), improving the ambient stability up to 1000 h [131]. However, when a larger cation guanidinium (Gu) was directly added in MAPbI_3 as GuSCN , GuPbI_3 was formed as an intermediate phase present with the MAPbI_3 phase. It was contradictory to the earlier belief and reports, which showed that Gu single-handedly could not form three-dimensional perovskite materials due to a larger ionic size (278 pm) over MA cation (217 pm). As a result, improved crystallinity, grain size, and reduced trap density were noticed further, resulting in improved PCE (from 15.57% to 16.70%) that maintained stability $\sim 90\%$ of the initial value after being stored for 15 days without encapsulation [132]. On the other hand, when guanidinium isothiocyanate was added in the PbI_2 precursor, with the dual step fabrication method; mixed cation perovskite was formed $(\text{GU})_x(\text{MA})_{(1-x)}\text{PbI}_3$ [133]. Nevertheless, most S donor atom-based additives (Figure 16) were found to influence ambient stability, as displayed in Figure 17. At a glance,

a summary of additives containing S atom and their role in the MAPbI₃ framework are presented in Table 8.

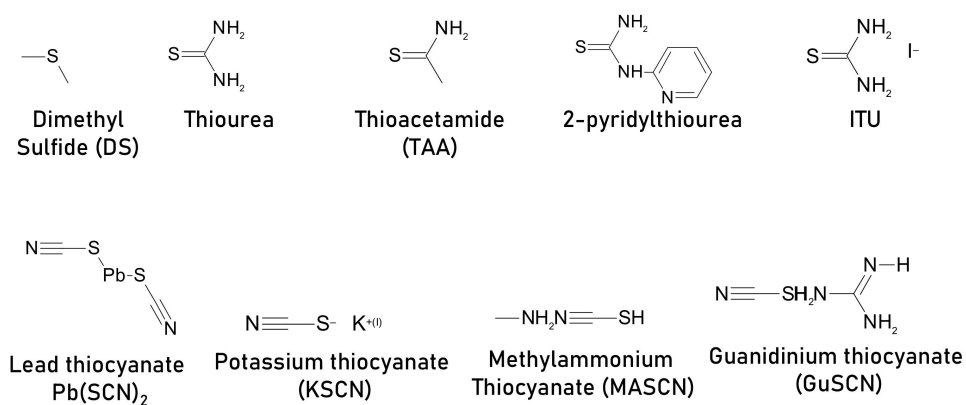


Figure 16. Chemical structures of organosulfur additives for MAPbI₃ PSC.

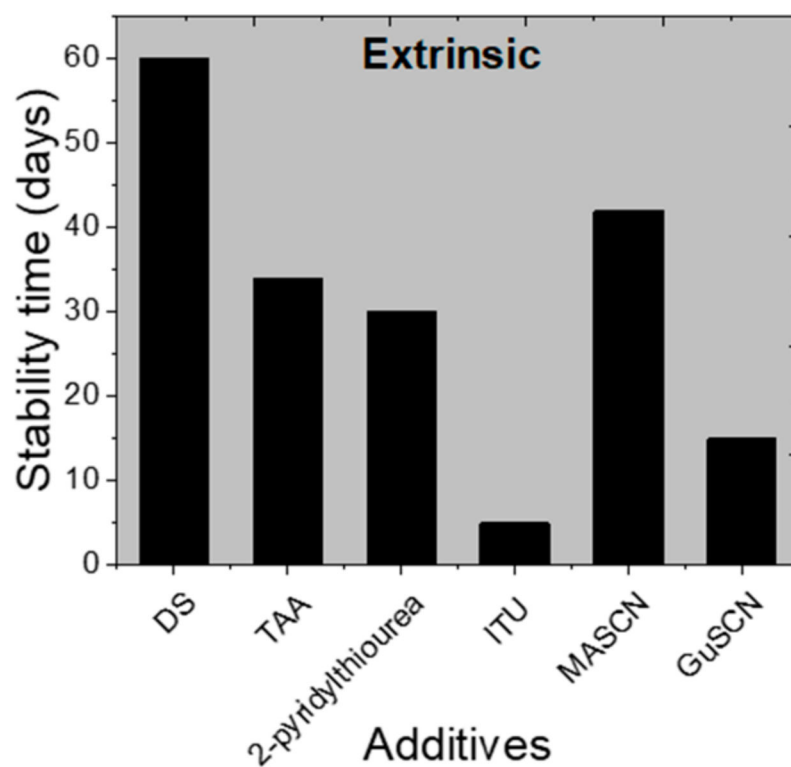


Figure 17. Influence of S donor atom onto stability of MAPbI₃-based PSC [122,124–126,131,132].

Table 8. S atom-based additive in MAPbI₃.

Additive in Active Layer	Architecture	PCE, % (Pristine)	Stability (Pristine)	PCE, % (with Additive)	Amount of Additive	Stability with Additive	Stability Conditions	Role of Additive	Ref
DS	MgF ₂ /PET/ITO/Nb ₂ O ₅ /CH ₃ NH ₃ PbI ₃ /Spiro-OMeTAD/Au	17.03	(a) Retained 50% PCE from initial after 60 days (b) N/A	18.40	10 vol% in 1 mL precursor	(a) Retained 86% PCE from initial after 60 days (b) 15.24 (83% of initial) as of final PCE after 5000 cycles	(a) unencapsulated, RH = 35%, dark, RT (b) bending stability-bending radius of 4 mm	Intermediate between Pb ²⁺ and S atom	[122]
thiourea	ITO/PEDOT:PSS/CH ₃ NH ₃ PbI ₃ /PCBM/Ag	13.4	N/A	16.2	0.5 vol%	N/A	N/A	Thiourea promotes grain growth, reduce trap states, passivate grain boundaries	[123]
thioacetamide (TAA)	ITO/SnO ₂ /CH ₃ NH ₃ PbI ₃ /Spiro-OMeTAD/Au	17	Retains ~75.1% of its initial performance after aging 816 h	18.9	1.0% (molar ratio to PbI ₂)	Retains 88.9% of its initial performance after aging 816 h	RH = 25–35%, unsealed, air,	Interaction of TAA with Pb ²⁺ improved grain size	[124]
2-pyridylthiourea	FTO/C-TiO ₂ /mp-TiO ₂ /CH ₃ NH ₃ PbI ₃ /Spiro-OMeTAD/Au	15.5	(a) Retained only ~10% PCE from initial after 30 days (b) Retained ~55% PCE from initial after 30 days	18.2	0.5 mg mL ⁻¹	(a) Retained ~95% PCE from initial after 30 days (b) Retained ~92% PCE from initial after 30 days	ambient, air, dark (a) RH = 55 ± 5%, dark, RT (b) 65 °C, RH = 30%, dark	N-donor and S-donor coordinate with PbI ₂ and slow down the formation of PbI ₂ . improved morphology, larger crystalline size, smooth compact, homogeneous film	[125]
ITU for I- and thiourea	ITO/SnO ₂ /CH ₃ NH ₃ PbI ₃ /Spiro-OMeTAD/Au	17.75	Retained 30% of the initial PCE after 100 h	20.3	0.003 mM	Retained 80% of the initial PCE after 100 h	AM 1.5 light, ambient atmosphere	Reduction of iodine ions and reduces defect state concentration, and defect passivation of grain boundaries crystalline quality, improve charge transport	[126]
lead thiocyanate Pb(SCN) ₂	FTO/SnO ₂ /CH ₃ NH ₃ PbI ₃ /Spiro-OMeTAD/Au	15.57	N/A	17.80	5% Pb(SCN) ₂ (molar ratio with respect to PbI ₂)	N/A	N/A	Forms volatile products HSCN and CH ₃ NH ₂ , resulting in formation of excess PbI ₂ that passivates GB	[127]
potassium thiocyanate (KSCN)	FTO/c-TiO ₂ /m-TiO ₂ /CH ₃ NH ₃ PbI ₃ /Spiro-OMeTAD/Ag	19.38	N/A	19.6	1 mol%	N/A	N/A	Grain size and crystallinity improvement reduced recombination density	[129]
methylammonium thiocyanate (MASCN) additive	Glass/FTO/TiO ₂ /CH ₃ NH ₃ PbI ₃ /Spiro-OMeTAD/Au	15.81	Died in 150 h.	18.71	40 mol%	Retained 16.34% as of final PCE after 1000 h ~89.7% from initial	air, RH = 20–25%, without encapsulation,	Rapid vacuum-based drying approach, high crystallinity, large carrier lifetimes	[131]
guanidinium thiocyanate (GuSCN)	FTO/TiO ₂ /CH ₃ NH ₃ PbI ₃ /PCBM/Ag	15.57	Retained 60% PCE from initial PCE after 15 days	16.70	10% mmol	Retained 90% PCE from initial PCE after 15 days	unencapsulated, dark, RH = 30–40%,	Enhance the crystallinity, enlarge the crystal size, and reduce the trap density of the perovskite film	[132]

2.4. Alkane Additives

Alkane-based additives are another class of additives that was briefly investigated within the MAPbI₃ framework. Additives such as poly(vinylidene fluoride-co-hexafluoropropylene) (PVDF-HFP) have shown interaction with MAI cation via hydrogen bonding with fluorine atoms in the additive. Such an additive is quite useful for indoor photovoltaic applications, as the additive is reported to control the nucleation and growth rate on a very thin (~150 nm) active layer of MAPbI₃ through a one-step solution processing method. Thinner light absorber perovskite is usually full of voids, results in a low fill factor, and lower internal quantum efficiency due to poor perovskite film quality. However, increasing the thickness is not suitable to obtain semi-transparent films [134]. As a solution to this problem, a poly(vinylidene fluoride-co-hexafluoropropylene) (PVDF-HFP) additive illustrated less rough morphology when a ~150 nm thick perovskite layer was obtained. In addition, it was found that perovskite solar cells with PVDF-HFP in the active layer have a higher charge transfer rate and lower carrier recombination rate [135]. Similar observations were seen when another derivative of PVDF polyvinylidene fluoride-trifluoroethylene polymer P(VDF-TrFE) was employed in a two-step fabrication process instead [136]. Other than these additives, some other haloalkane additives, such as diiodomethane (CH₂I₂) and diiodooctane (C₈H₁₆I₂), were also reported to reduce the trap states, resulting in improved morphology and enhanced PCE [137,138]. The chemical structures of alkane additives are shown in Figure 18. Further, Table 9 summarizes their role in the MAPbI₃ framework.

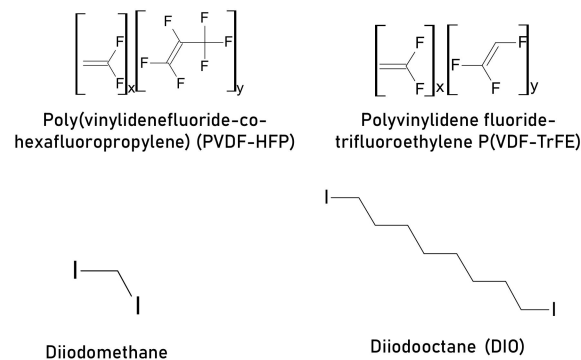


Figure 18. Chemical structures of alkane-based additives for MAPbI₃ PSC.

Table 9. Alkane-based additives and their role within MAPbI₃ framework.

Additive in Active Layer	Architecture	PCE, % (Pristine)	Stability (Pristine)	PCE, % (with Additive)	Amount of Additive	Stability with Additive	Stability Conditions	Role of Additive	Ref
poly(vinylidene-fluoride-co-hexafluoropropylene) (PVDF-HFP)	FTO/cTiO ₂ /CH ₃ NH ₃ PbI ₃ /Spiro-MeOTAD/Au	7.2	N/A	10.6	N/A	N/A	N/A	Interact with uncoordinated MAI molecule through hydrogen bonds between fluorine atoms. This can improve the carrier lifetimes and reduce the charge transfer resistance, which contributes to enhancing PCE	[135]
polyvinylidene fluoride-trifluoroethylene polymer P(VDF-TrFE)	FTO/cTiO ₂ /mesoporous-TiO ₂ /CH ₃ NH ₃ PbI ₃ /Spiro-MeOTAD/Ag	9.57 ± 0.25%	N/A	12.54 ± 0.40	N/A	N/A	N/A	Two-step deposition, improved crystallinity and morphology, reduced carrier recombination of charge carrier, increased carrier lifetime	[136]
diiodomethane CH ₂ I ₂	Glass/FTO/TiO ₂ /MAPbI ₃ /Spiro-OMeTAD/Au	10.0	N/A	16.5	0.25 mL in 1 mL precursor	N/A	N/A	Iodine liberation, morphology enhancement	[138]
Diiodooctane DIO	Glass/ITO/PEDOT:PSS/MAPbI ₃ /PCBM/Ag	10.61	N/A	17.74	1 vol% in 1 mL precursor	N/A	N/A	Intermediate formation and morphology enhancement	[137]

2.5. Quantum Dot-Based Additives

Recently, a new area of additive engineering has emerged, based on quantum dots containing different functional groups introduced in the precursor. This allows the functional group to chelate under coordinated Pb vacancy or iodine defect sites at the surface of the perovskite layer (Figure 19). At the same time, a quantum dot improves the crystallinity of film due to the quantum confinement effect and reduces non-radiative recombination centers; thus, passivating defects at grain boundaries [139–144]. In some cases, quantum dots can even promote charge transfer from the oxide surface to the perovskite layer, further reducing the charge trap density, boosting fill factor as high as 84% and efficiency as 21.04% [143,145]. The influence of incorporation of QDs onto the stability is shown in Figure 20. A summary of such additives based on quantum dots (QDs) is presented in Table 10.

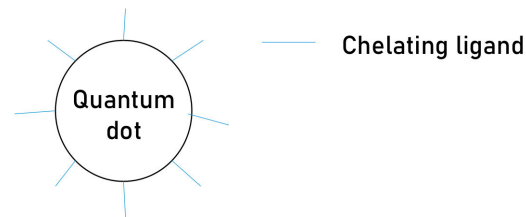


Figure 19. Schematic representation of quantum dots with chelating functional group/groups.

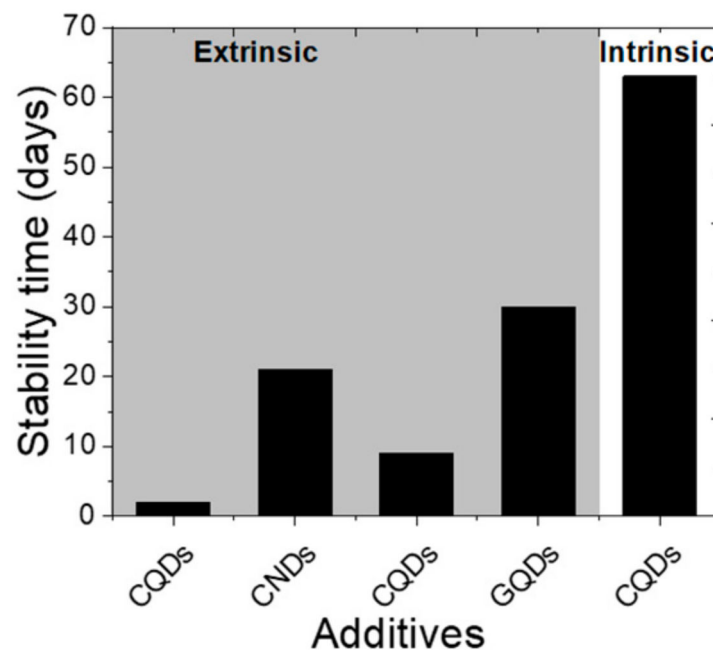


Figure 20. Quantum dots-based additives and their influence on stability of MAPbI₃. Data taken from [139,141,142,145] respectively.

Table 10. Quantum dots-based additives for MAPbI₃.

Additive in Active Layer	Architecture	PCE, % (Pristine)	Stability (Pristine)	PCE, % (with Additive)	Amount of Additive	Stability with Additive	Stability Conditions	Role of Additive	Ref
carbon quantum dot (CQD)	ITO/NiO _x /CH ₃ NH ₃ PbI ₃ /PCBM/Ag	15.25	Remained ~10% PCE from initial after 48 h	18.24	0.15 mg mL ⁻¹	Remained ~73.4% PCE from initial after 48 h	unencapsulated, dark, RT, RH = 80%,	Reduce non-radiative recombination loss, improve the crystallinity of film; thus, passivate grain boundaries and improve stability	[139]
carbon nanodots (CNDs)	ITO/NiO _x /CH ₃ NH ₃ PbI ₃ /PC ₆₁ BM/BCP/Ag	14.48% ± 0.39%	N/A	16.47% ± 0.26%	10 mg mL ⁻¹	Remained ~18% as of an absolute value of PCE after 500 h	dark, 25 °C, RH = 40% air, unencapsulated,	Increase in the crystal size, lower content of grain boundary defects, longer carrier lifetimes.	[142]
carbon quantum dots (CQDs)	FTO/TiO ₂ /CH ₃ NH ₃ PbI ₃ /Spiro-OMeTAD/Ag	17.59	(a) Retained 74% from initial PCE after 1500 h (b) Retained 17% from initial PCE after 216 h	18.81	0.05 mg mL ⁻¹	(a) Retained 90% from initial PCE after 1500 h (b) Retained 70% from initial PCE after 216 h	(a) unencapsulated, inert. (b) unencapsulated, RH = 50–60%,	Passivate the grain boundaries and decrease the trap-state density. The bonding between CQDs and MAPbI ₃ leads to a stable absorption of CQDs on the MAPbI ₃ surface, forming a protective layer to prevent the perovskite from coming in contact with water, thereby enhancing the stability of PSCs	[141]
nitrogen doped CQDs (N-CQDs),	ITO/PEDOT:PSS/CH ₃ NH ₃ PbI ₃ /PCBM/Al	8.34	N/A	13.936	3 vol%	N/A	N/A	N-CQDs act like an intermediate and help to form dense and smooth perovskite; passivate the trap states and decrease the non-radiative charge recombination	[140]
Nitrogen-doped carbon dots (NCDs)	FTO/blTiO ₂ /mL-TiO ₂ /CH ₃ NH ₃ PbI ₃ /Spiro-OMeTAD/Ag	12.12 ± 0.28%	N/A	15.93 ± 0.15%	0.05 mg mL ⁻¹	N/A	N/A	Coordinate with the iodide ions and lead cations on the surface of perovskite, which effectively passivates the surface traps and help reduce non-radiative charge carrier recombination; the nitrogen dopants with lone electron pairs in NCDs optimize the interfacial energy level to enhance the charge carrier extraction efficiency at photoactive layer/TiO ₂ interface	[144]

Table 10. Cont.

Additive in Active Layer	Architecture	PCE, % (Pristine)	Stability (Pristine)	PCE, % (with Additive)	Amount of Additive	Stability with Additive	Stability Conditions	Role of Additive	Ref
potassium cation (K ⁺) functionalized carbon nanodots (CNDs@K)	ITO/PTAA:F4TCNQ/CH ₃ NH ₃ PbI ₃ /PCBM/BPhen/Ag	18.25	N/A	21.04		N/A	N/A	Defects passivation and crystallization control of the perovskite film; K ⁺ in the grain boundary, and prevents excessive cations from occupying interstitial sites, thereby reducing microstrain of polycrystalline film, the synergistic effect of tailored crystal size, and suppressed grain boundary defects could reduce charge trap density, facilitate charge generation, and lengthen carrier lifetime	[143]
graphene quantum dots (GQDs)	FTO/c-TiO ₂ /mp-TiO ₂ /CH ₃ NH ₃ PbI ₃ /Spiro-OMeTAD/Au	16.83	Remained ~15.6% as of final PCE after 30 days	18.34	1.5 mg mL ⁻¹	Remained ~17.4% as of final PCE after 30 days	encapsulation, RH = 36%, atm	Promote charge transfer from the perovskite layer to TiO ₂ film. Faster electron extraction and a slower recombination rate passivate hanging bonds at the perovskite GBs	[145]

3. Inorganic Additives

Inorganic salts can be further explained as per the category in the periodic table, i.e., based on alkali metals, alkaline earth metals, transition metals, other metals, and other non-metals. These additives may exist in the form of inorganic halide salts or inorganic acids [146].

3.1. Alkali Metals Additives

Hydro halides are at the top, as hydrogen is the first element in group one of the periodic table. Soe et al. studied the incorporation of hydrohalic acids (HX, X=I, Br, Cl) in MAPbI₃ precursor prepared using DMF. It was found that HX incorporation in the perovskite layer alters the bandgap and unit cell parameters. The HI addition compressed bandgap, whereas HBr widens the bandgap at high concentrations (20–25 vol%). Further, these changes were found correlated with the types of defects present in polycrystalline perovskite thin films combined with the structural strain induced in very small crystallites. Thus, it was concluded that these acids could influence crystallization rate, surface coverage, and improve morphology. However, HCl incorporation showed no influence on bandgap [147,148]. The same was verified by Yan and co-workers who investigated HI (hydroiodic acid) as an iodine quencher in MAPbI₃ precursor solution (prepared with isopropyl alcohol (IPA)), that further lead to chemically passivate grain boundaries and increase in PCE from 16.13% (pristine) to 18.21% (with HI additive) [149]. Likewise, alkali metals, such as Li, Na, and K, combined with halogen counterparts, have been inspected as additives for the MAPbI₃ light absorber layer. Grätzel and Friend co-workers demonstrated the influence of NaI (sodium iodide) on the optical, excitonic, and electrical properties of CH₃NH₃PbI₃ perovskite prepared by a two-step sequential deposition technique. It was revealed that the NaI additive helps in the complete conversion of PbI₂ into CH₃NH₃PbI₃, leaving no unreacted PbI₂ and enhancing the crystallinity. Furthermore, KPFM measurements showed a reduction in work function (towards Au metal) for contact-potential difference (CPD) and proved the chemical passivation of perovskite surface due to additive incorporation in the precursor. Additionally, the hypothesis of partial substitution of Pb²⁺ with monovalent cations Na was discarded, because replacing Pb²⁺ with the Na cations required high energy, which could not be obtained at room temperature, since additives and films were processed at room temperature [150]. Similar reports were published from Chu and co-workers who investigated alkali metal chloride additives (LiCl, NaCl, and KCl) in MAPbI₃ and suggested that mixed halide formation does not occur as Cl atoms easily evaporate due to the annealing process, improving the crystallinity and carrier charge transport [151]. However, as the size of the nuclei increases, the perovskite shows partial replacement and forms a perovskite with a double cation (i.e., in the case of RbX and CsX, where X represents halide) [152]. The partial substitution of cation was also observed when alkaline earth metals were employed as additives in the precursor. Hence, they are not the center of attraction here and it is suggested that alkaline earth metals are best suited to replace Pb due to their divalent nature [153,154]. The chemical structures of alkali metal additives are presented in Figure 21. The example of the influence of alkali metal additives on the stability of MAPbI₃ PSC is shown in Figure 22. Further, the role of alkali metal additives in the MAPbI₃ framework is summarized in Table 11.

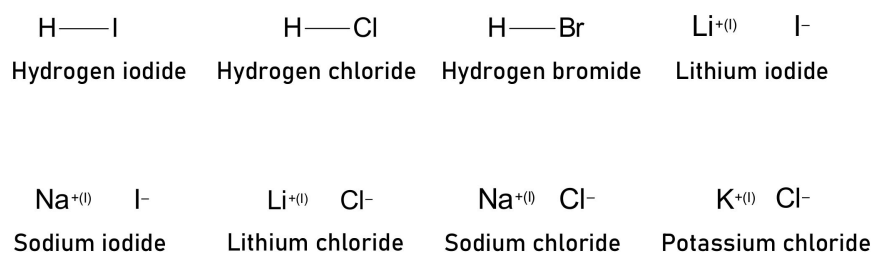


Figure 21. Chemical structures of alkali metal additives for MAPbI₃ PSC.

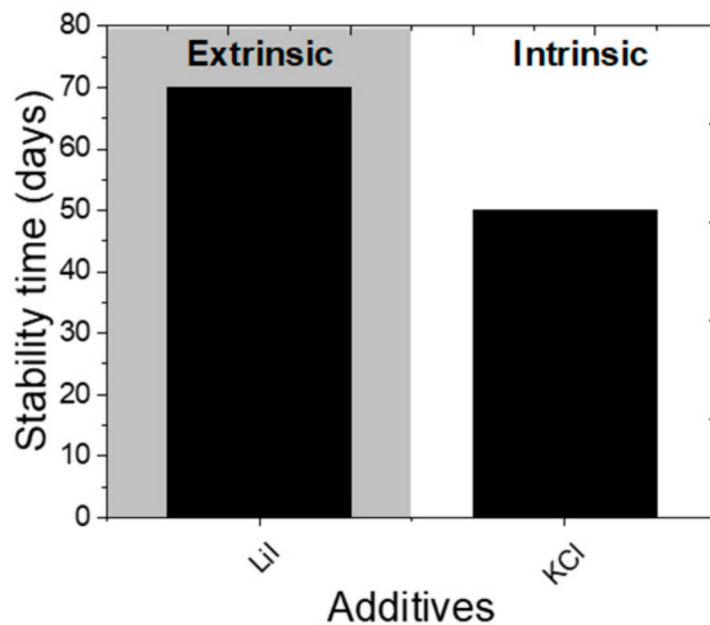


Figure 22. Influence of alkali metal additives onto stability of MAPbI₃. Data taken from references [151,155].

Table 11. Alkali metal additives and their role in MAPbI₃ perovskite.

Additive in Active Layer	Architecture	PCE, % (Pristine)	Stability (Pristine)	PCE, % (with Additive)	Amount of Additive	Stability with Additive	Stability Conditions	Role of Additive	Ref
hydroiodic acid (HI)	ITO/PTAA/CH ₃ NH ₃ PbI ₃ /PCBM/Ti/Au	16.1	N/A	18.21	0.004 vol%	N/A	N/A	Grain size improvement	[149]
hydrochloric acid (HCl)	Glass/TiO ₂ /CH ₃ NH ₃ PbI ₃ /Spiro-OMeTAD/Au	9.96	N/A	14.49	volume ratio 8%,	N/A	N/A	Grain size improvement and morphology enhancement	[156]
hydrobromic acid (HBr)				13.53	volume ratio 6%	N/A	N/A		
hydroiodic acid (HI)				15.21	volume ratio 8%	N/A	N/A		
lithium iodide (LiI)	FTO/TiO ₂ /CH ₃ NH ₃ PbI ₃ /electrode	11.3	Remained ~1% PCE as of final value after 25 days	17.01	12mg/mL	Retained ~6% PCE as of final value after 70 days	unencapsulated, ambient, air, RH = 40%,	Larger grain size and higher crystallinity and reduced PbI ₂ residue	[155]
sodium iodide (NaI)	FTO/compact TiO ₂ /mesoporous TiO ₂ /CH ₃ NH ₃ PbI ₃ /SpiroMeOTAD/Au	14.01	N/A	15.14	0.02 mol L ⁻¹	N/A	N/A	Improved crystallinity and grain boundary passivation	[150]
lithium chloride (LiCl)	Glass/ITO/PEDOT:PSS/CH ₃ NH ₃ PbI ₃ /PC ₆₁ BM/C ₆₀ /BCP/Al	11.40	Died in 50 days	9.98	0.25%, wt%	N/A	N/A	Improved crystallinity and homogenous nucleation, and crystallization	[151]
sodium chloride (NaCl)				12.77	1.0%, wt%	N/A	N/A		
potassium chloride (KCl)				15.08	0.75%, wt%	Remained ~85% after 50 days	unencapsulated, inert, dark		

3.2. Transition Metals Additives

Additionally, some transition metals were also reported as additives in MAPbI₃ precursor. One such example is n-type goethite (FeOOH) quantum dots that act as multifunctional additives. The addition of FeOOH QDs into precursor solution improves not only the performance, but also stability. The investigation by Wang and et al. showed that FeOOH QDs could produce heterogeneous nucleation, passivate the trap states, and obstruct the ion migration. The investigation demonstrated that the oxygen (in FeOOH) as a Lewis base could coordinate with Lewis acid Pb²⁺. The –OH group (in FeOOH) can coordinate with hydrogen atoms of MA⁺. This interaction delays crystal growth kinetics, resulting in good quality of perovskite films that result in high PCE. Further, the iron in FeOOH QDs as a Lewis acid interact with Lewis base I⁻. Thus, ion migration of I⁻ and MA⁺ is controlled, resulting in enhanced intrinsic stability of solar cells [157]. Further, the transitional metal halides, either with monovalent cations (i.e., AgI, CuI, CuBr), divalent cation (NiCl₂, CuCl₂, ZnCl₂, CdCl₂) [158–161], or trivalent cation (RhI₃) [162] frequently pointed out the improvement in crystallinity and grain boundary passivation.

Interestingly, in all these reports, chlorine-based additive salts were reported to form the MAPbI₃ phase without mixed iodide and chloride as it was proposed that Cl atoms evaporate while annealing the films. Similarly, trivalent cation, such as Rh³⁺, did not replace lead atoms when used in small quantities (e.g., 1 mol%). However, the addition of 5% could result in partial replacement of the Pb atom. Figures 23 and 24 demonstrate the chemical structures and the effect of transition metal additives on the stability of MAPbI₃ PSC, respectively. Further, Table 12 summarizes the details associated with transitional metal additives.

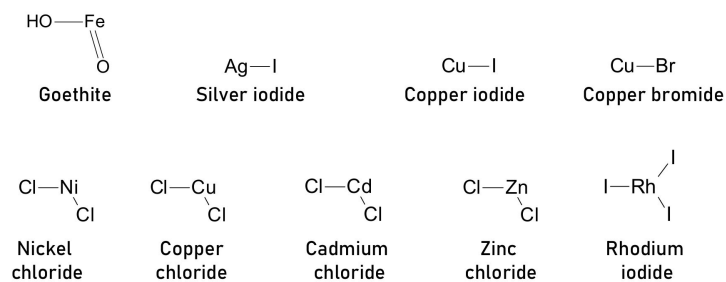


Figure 23. Chemical structures of transition metal additives.

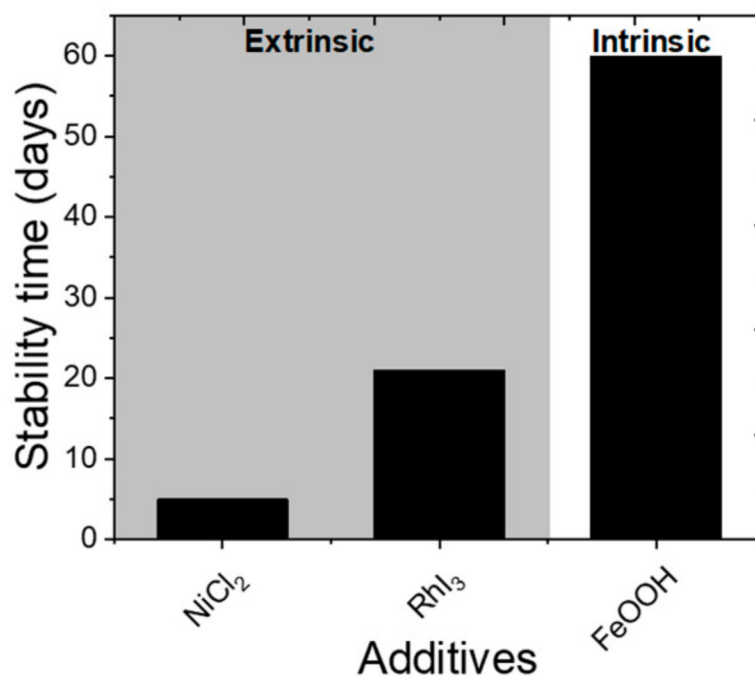


Figure 24. Influence of transition metal additive onto MAPbI₃. Data taken from references [157,158,162] respectively.

Table 12. Transition metal additives and their role in MAPbI₃ perovskite.

Additive in Active Layer	Architecture	PCE, % (Pristine)	Stability (Pristine)	PCE, % (with Additive)	Amount of Additive	Stability with Additive	Stability Conditions	Role of Additive	Ref
n-type goethite (FeOOH)	FTO/cTiO ₂ /mp-TiO ₂ /CH ₃ NH ₃ PbI ₃ /Spiro-OMeTAD/Au	15.4	(a) Remained only 5.7% as of final PCE after 360 h. (b) Retained 61% from initial PCE after 60 days. (c) Retained only 42% from initial PCE after 480 h	19.7	0.1 mg mL ⁻¹	(a) Retained 94% after 360 h, i.e., 17.9%. (b) Retained 97% from initial PCE after 60 days. (c) Retained 92% from initial PCE after 480 h	(a) inert, 85 °C, dark, non-encapsulated, (b) 10 ± 5% RH, (c) light 100 mW cm ⁻² , inert, RT, mpp tracking,	Improved quality of perovskite and inhibition of iodine and methylamine ion migration	[157]
silver iodide (AgI)	FTO/compact TiO ₂ /mesoporous TiO ₂ /CH ₃ NH ₃ PbI ₃ /SpiroMeOTAD/Au	14.01	N/A	14.18	0.02 mol L ⁻¹	N/A	N/A	Improved crystallinity and grain boundary passivation	[150]
copper iodide (CuI)				15.25		N/A			
copper bromide (CuBr)				15.61		N/A			
nickel chloride (NiCl ₂)	ITO/SnO ₂ /CH ₃ NH ₃ PbI ₃ /SpiroMeOTAD/Au	17.25	Retained ~70% PCE after 100 h	20.61	0.03 mM	Retained ~70% PCE after 100 h	en-capsulated, air, light 65 mW cm ⁻² , ~25 °C, RH = 45%, without ultraviolet filter	High crystallinity, GB passivation	[158]
copper chloride (CuCl ₂)	FTO/NiO _x /CH ₃ NH ₃ PbI ₃ /PCBM/BCP/Ag	9.73	N/A	15.22	2.5 mol%	N/A	N/A	Improves morphology	[159]
cadmium chloride (CdCl ₂)	FTO/SnO ₂ /CH ₃ NH ₃ PbI ₃ /Spiro-OMeTAD/Au	11.7	N/A	13.2	1% molar ratio	N/A	N/A	Enhance grain size and crystallinity	[160]
zinc chloride (ZnCl ₂)				13.76	0.1% molar ratio	N/A	N/A		
rhodium iodide (RhI ₃)	ITO/SnO ₂ /CH ₃ NH ₃ PbI ₃ /Spiro-OMeTAD/Ag	19.09	Retained 75% of efficiency after 500 h	20.71	1 mol%	Retained 92% of efficiency after 500 h	unencapsulated, dry air	Improved crystallinity and grain boundary passivation	[162]

3.3. Other Metals Additives

However, the most widely reported metal additive is PbI_2 . Several groups have suggested using excess PbI_2 as an additive and studied the effect of the stoichiometric and non-stoichiometric composition of PbI_2 in MAPbI_3 perovskite [163,164]. Reports suggest that the addition of excess PbI_2 in perovskite increases power conversion efficiency [163,165]. However, the influence of excess PbI_2 on photochemical stability is debatable [166]. Some research groups claim that excess PbI_2 passivates grain boundary [167]; thus, creates extra passivation [168]; enhancing performance and stability overall [164,169]. On the contrary, some reports showed that excess PbI_2 could increase PCE, but decreased PSC stability [170,171]. To resolve the issue, Stevenson et al. demonstrated that the stability associated with excess PbI_2 is affected by solvent coordination capacity with Pb atom, and suggested that excess PbI_2 can work as a stabilizer to improve intrinsic stability if the correct solvent (NMP) is chosen over commonly-used solvent DMF [172]. Other than PbI_2 , adding PbCl_2 also resulted in an equally good perovskite film quality with improved performance, but the outcome was reported as a mixed halide [173,174]. Hence, it is not focused on here. Interestingly, Ngo and the group demonstrated a different approach by using PbS quantum dots as capping ligands in the precursor solution to control nucleation and morphology. This approach allowed improving crystallinity and enhanced grain size, resulting in improved solar cell performance [175]. See Figure 25 for the chemical structures of PbI_2 and PbS. The influence of excess PbI_2 additive on the stability of MAPbI_3 is presented in Figure 26. Further, a relevant summary is presented in Table 13.



Figure 25. Chemical structures of other metal additives in MAPbI_3 .

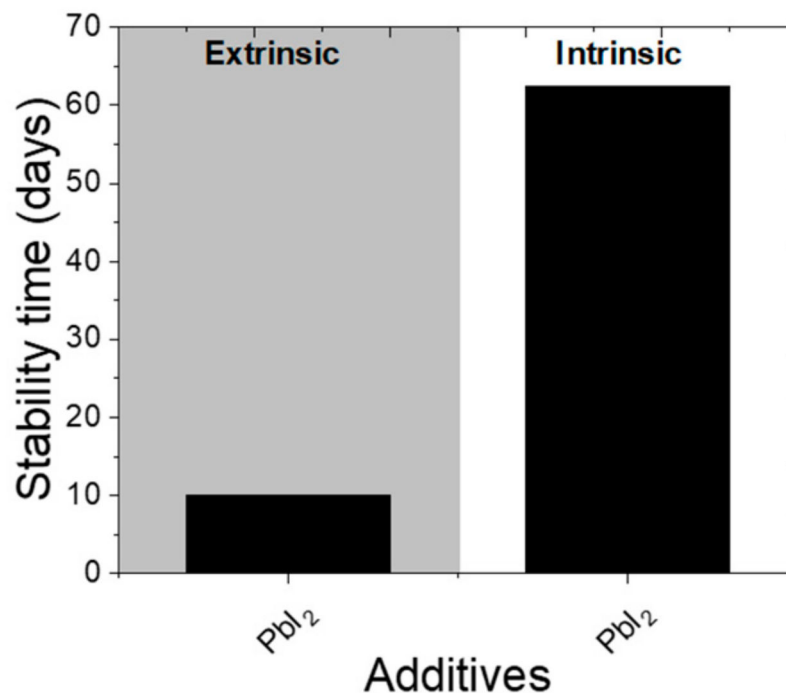


Figure 26. Ambient and inert stability due to excess PbI_2 [171,172].

Table 13. Other metal additive for MAPbI₃.

Additive in Active Layer	Architecture	PCE, % (Pristine)	Stability (Pristine)	PCE, % (with Additive)	Amount of Additive	Stability with Additive	Stability Conditions	Role of Additive	Ref
lead iodide (PbI ₂)	FTO/c-TiO ₂ /m-TiO ₂ /CH ₃ NH ₃ PbI ₃ /Spiro-OMeTAD/Au	15.95	N/A	18.42	10% excess PbI ₂	N/A	N/A	Improves the crystallinity	[163]
lead iodide (PbI ₂)	Glass/FTO/CH ₃ NH ₃ PbI ₃ /Spiro-OMeTAD/Electrode/Encapsulation (UV-epoxy)	16.2	Retained 80% PCE till 12 h	16.5	10 mg mL ⁻¹	Retained 80% PCE till 10 days	ambient air, 85 °C, 60% RH, light 1 sun	N/A	[171]
lead iodide (PbI ₂)	Glass/ITO/SnO ₂ /CH ₃ NH ₃ PbI ₃ /PTAA/MoO ₃ /Al	~8.9%	Remained ~40% PCE after 1500 h	~15.6%	15% excess	Remained ~95% PCE after 1500 h	light 30 mW cm ⁻² , 40 °C, inert	Excess PbI ₂ forms adduct with the cosolvent (NMP), improving PCE and stability.	[172]
lead iodide (PbI ₂)	FTO/TiO ₂ /CH ₃ NH ₃ PbI ₃ /Spiro-OMeTAD/Ag	7.23 ± 0.10	N/A	14.32 ± 0.28%	concentration ~N/A, by annealing @130 °C	N/A	N/A	Grain boundary passivation	[176]
lead sulfide (PbS QDs)	FTO/SnO ₂ /CH ₃ NH ₃ PbI ₃ /Spiro-OMeTAD/Au	15.2	N/A	15.7	12.5 mg mL ⁻¹	N/A	N/A	Capping ligand for surface functionalization to improve crystallinity	[175]

3.4. Non-Metal Inorganic Salts

Furthermore, the controlled nucleation, improved morphology, enhanced crystalline size, and grain size with lower trap density were also noticed with additives based on other non-metals salts. During the two-step method, which is one of the commonly used fabrication approaches to fabricate planar heterojunction complex lead halide perovskite solar cells, the complete conversion of PbI₂ into CH₃NH₃PbI₃ is often observed restricted by the inadequate diffusion of CH₃NH₃I into PbI₂ film, which affects the short circuit current density. To overcome this problem, Pathipati and co-workers used ammonium iodide (NH₄I) in a small quantity (5 wt%) in the PbI₂ solution and found this approach increases the porosity of the PbI₂ film, allowing to improve film morphology and increase grain size up to 500 nm. This, in turn, improves the fill factor and short circuit current density, improving the PCE compared to the pristine solar cell [177]. Similarly, a drastic improvement in fill factor (from 27.53 without additive to 80.11 with NH₄Cl additive) was noticed when NH₄Cl was added in the MAPbI₃ precursor. Moreover, as reported earlier, due to the quick evaporation of chlorine atoms, mixed halide formation did not take place [178]. Furthermore, improved performance and higher stability were observed with different ammonium halide salts (NH₄X, where X can be I, Cl, Br) even when using the single-step solution process method. Although, NH₄I showed the highest performance amongst all [177–179]. Another ammonium-based additive, NH₄H₂PO₂ (ammonium hypophosphite-AHP), was reported to show similar behavior. Surprisingly, one of the by-products (H₃PO₂) from CH₃NH₃I synthesis was found suppressing the formation of molecular iodine (i.e., the oxidation of I⁻ to I₂) [180,181]. This led to the idea of using NH₄H₂PO₂ (ammonium hypophosphite-AHP) as an additive in the PbI₂/CH₃NH₃I precursor. Huang and co-workers found that AHP forms a complex with PbI₂, which leads to improvement in crystallinity and grain size. In turn, this improves PV performance due to crystalline grain boundaries [182]. Moreover, in a recent report, it was illustrated that hydrazinium iodide (N₂H₅I), an iodine quencher in the MAPbI₃ active layer, can form an intermediate complex with PbI₂, and enhance crystallinity and grain size ~1100 nm, causing grain boundary passivation. This, in turn, reduces hysteresis in solar cells, improves efficiency, and intrinsic stability of solar cells

up to 4400 h [183]. There were similar reports by Huang et al., who reported hydrazinium chloride (N_2H_5Cl) incorporation in $MAPbI_3$ [184]. Whereas hypophosphorous acid (HPA) was used to assist crystallization dynamics for large area substrates [185]. The chemical structures and influence of non-metal inorganic additives on the stability of $MAPbI_3$ are presented in Figures 27 and 28, respectively. A summary of these additives is presented in Table 14.

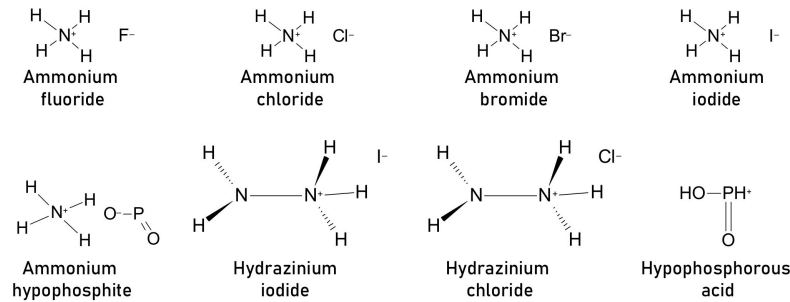


Figure 27. Chemical structure of non-metal halide additives for $MAPbI_3$.

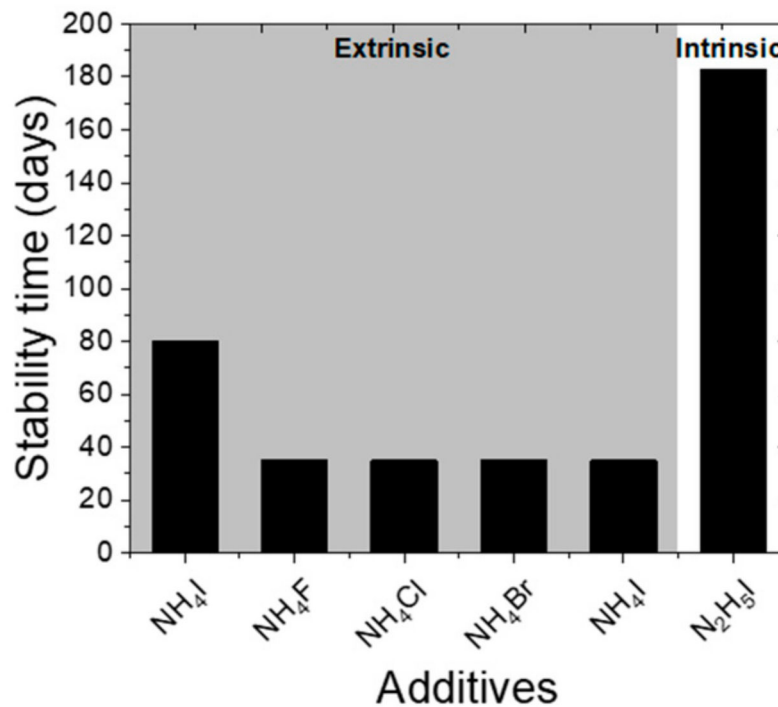


Figure 28. Influence of non-metal additives onto stability of the $MAPbI_3$ layer. Data were taken from references [177,179,183], respectively.

Table 14. Non-metal additives and their role in MAPbI₃ active layer.

Additive in Active Layer	Architecture	PCE, % (Pristine)	Stability (Pristine)	PCE, % (with Additive)	Amount of Additive	Stability with Additive	Stability Conditions	Role of Additive	Ref
ammonium iodide (NH ₄ I)	Glass/ITO/PTAA/CH ₃ NH ₃ PbI ₃ /PCBM/Ag	15.2	Retained ~70% PCE after 20 days	17.4	5 wt%	Retained ~80% PCE after 20 days	RH = 50 ± 5%, unencapsulated, ambient, air	Improved morphology, increased crystalline size and grain size, lower trap density	[177]
ammonium chloride (NH ₄ Cl)	ITO/PEDOT:PSS/CH ₃ NH ₃ PbI ₃ /PC ₆₁ BM/Al	7.97	N/A	9.93	17.5 mg mL ⁻¹	N/A	N/A	Improved morphology, increased crystalline size and grain size, lower trap density	[178]
ammonium fluoride (NH ₄ F)				15.15		Retained 82% PCE after 5 weeks			[179]
ammonium chloride (NH ₄ Cl)	ITO/PEDOT:PSS/CH ₃ NH ₃ PbI ₃ /PC ₆₁ BM/LiF/Al	13.74	Retained 70% PCE after 5 weeks	16.88	10 mol%	Retained 87% PCE after 5 weeks	encapsulated, air	Improved morphology, increased crystalline size and grain size, lower trap density	
ammonium bromide (NH ₄ Br)				16.85		Retained 89% PCE after 5 weeks			
ammonium iodide (NH ₄ I)				17.44		Retained 91% PCE after 5 weeks			
ammonium hypophosphate NH ₄ H ₂ PO ₂	ITO/PTAA:F4-TCNQ/CH ₃ NH ₃ PbI ₃ /PC ₆₁ BM/TrnBr/Ag	9.4 ± 1.0%	N/A	16.5 ± 0.7%	2.5 mg mL ⁻¹	N/A	N/A	Intermediate with Pb and improved crystallinity grain size	[182]
hydrazinium iodide (N ₂ H ₅ I)	Glass/ITO/SnO ₂ /CH ₃ NH ₃ PbI ₃ /PTAA/MoO _x /Al	14.98	Retained ~60% PCE after 4400 h	17.03	0.5%, wt%	Retained ~80% PCE after 4400 h	inert, light 60-70 mW cm ⁻² , 50 °C.	Intermediate between PbI ₂ and N ₂ H ₅ I, improved crystallinity, grain size	[183]
hydrazinium chloride (N ₂ H ₅ Cl)	ITO/PEDOT:PSS/CH ₃ NH ₃ PbI ₃ /PCBM/C ₆₀ /BCP/Ag	7.14	N/A	12.66	PbI ₂ /MAI/N ₂ H ₅ Cl molar ratio = 1:1:0.2	N/A	N/A	Intermediate between PbI ₂ and N ₂ H ₅ Cl, improved crystallinity, grain size	[184]
hypophosphorous acid (HPA)	Glass/FTO/TiO ₂ /CH ₃ NH ₃ PbI ₃ /ETL/electrode	5.1	N/A	8	0.75 uL mg ⁻¹ solution in 1 mL of MAI	N/A	N/A	Larger grains with a smoother surface, additive acts as a reducing agent for iodine	[185]

4. Conclusions and Outlook

To conclude, we covered the progress and updates in the area of additive engineering for the MAPbI₃ photoactive layer in perovskite solar cells. As known, the poor intrinsic and extrinsic stability causes a restriction in the substantial commercialization of the PSC. Intrinsic instability is considered due to the presence of under-coordinated Pb sites or escape of a volatile product or formation of molecular iodine; either of these creates a defect in the perovskite surface. Therefore, in this review, we summarized various additives that can coordinate with the mentioned defect sites and improve stability. Higher efficiency (more than 25%) was achieved, but achieving higher stability is still far away. Further, the role of additives into MAPbI₃ precursor was presented, which influences nucleation growth, film morphology, crystallinity, grain size, and grain boundary passivation via complex/intermediate formation were conferred. To understand the aforementioned, we classified additives based on organic and inorganic compounds. Furthermore, organic additives were scrutinized as per their functional group, and a relevant coordination mechanism that impacted stability was described. Similarly, inorganic additives were classified based on metal and non-metal halides. Moreover, we focused on additive influence on stability concerning different conditions (intrinsic/ambient/mechanical robustness). Our analysis suggests that amines, heterocyclic amines, and their derivatives, followed by carbonyl and acetate functional groups, can improve intrinsic stability. On the other hand, acid, esters, ether, and alcohol, and S atom-based additives can be mainly valuable to boost

ambient stability. This summary of additives further aims to boost designing new additives that can finally help achieve stability challenges.

Yet, further developments are required while adopting the additive approach in the fabrication of MAPbI₃-based PSCs. So far, additives employed in the MAPbI₃ light-absorbing layer do not have any rule of selection. The majority of additives have opted from existing literature available for DSSCs or organic solar cells, utilizing the N/O/S donor atoms to combine with under-coordinated Pb²⁺ sites to improve stability because of the Lewis acid–base reaction. Hence, the first and the topmost prospect is to design an additive that can help sustain MAPbI₃ under operational conditions, such as illumination, heat, moisture, oxygen, water. To do so, applying machine learning is highly recommended. While additives are primarily being experimented on (on a trial and error basis), the number of published reports are growing exponentially, with time, without any outcome to overcome stability issues. Therefore, a systematic empirical investigation should be conducted using analytical, statistical tools to understand the correlation of the additive, its properties, and its influence on morphology, optoelectronic properties, and stability with various conditions concerning numerous characterization techniques. This might help in the suitable material selections to further experiment by establishing the relationship between the chemical structure of additives and photovoltaic characteristics and lifetime. Thus, it would reduce the time and cost required for the experiment to improve stability, eventually driving industrial interest in product development.

The second prospect includes improved operational stability, which is reported to gain only a few thousand hours. While at least 10,000 h of operational stability is required to commercialize as the indoor application, with respect to thin-film photovoltaics. On the other hand, traditional photovoltaic has a lifetime of ~25 years. Thus, the second vision is to overcome short-term stability issues to commercialize the MAPbI₃-based PSC. Moreover, the duration of operational stability should also be reproducible. Henceforth, fabricating reproducible stability is the third prospect to work on, as testing short- or long-term reproducibility is a time-consuming process. The next challenge is upscaling. Currently, the majority of research reports are based on small area devices. Nevertheless, large-area devices will be required for commercial purpose. However, morphology, performance, distribution of surface defects, grain size, and trap states will be changed when the large area will be used. Therefore, the fabrication of large-area devices is another prospect that requires high PCE and stability. Another future scope of development is in the area of toxicity of PSC. Since some precursors used to prepare MAPbI₃ ink are not environment friendly. Hence, alternative, environment-friendly green solvent/precursors should be further explored to give equally good efficiency and stability.

In the end, we hope this review will help scientists and researchers to design and synthesize new additives that can provide the solution for the stability challenge of MAPbI₃. Thus, ultimately achieving stability by applying additive engineering, commercializing MAPbI₃-based PSC can be achieved.

Funding: This research received no external funding.

Institutional Review Board Statement: Not applicable.

Informed Consent Statement: Not applicable.

Data Availability Statement: Not applicable.

Conflicts of Interest: The authors declare no conflict of interests.

References

1. Wilson, G.M.; Al-Jassim, M.; Metzger, W.K.; Glunz, S.W.; Verlinden, P.; Xiong, G.; Mansfield, L.M.; Stanbery, B.J.; Zhu, K.; Yan, Y.; et al. The 2020 photovoltaic technologies roadmap. *J. Phys. D Appl. Phys.* **2020**, *53*, 493001. [[CrossRef](#)]
2. Pham, H.D.; Yang, T.C.; Jain, S.M.; Wilson, G.J.; Sonar, P. Development of Dopant-Free Organic Hole Transporting Materials for Perovskite Solar Cells. *Adv. Energy Mater.* **2020**, *10*. [[CrossRef](#)]
3. Fan, Y.; Meng, H.; Wang, L.; Pang, S. Review of Stability Enhancement for Formamidinium-Based Perovskites. *Sol. RRL* **2019**, *3*, 1900215. [[CrossRef](#)]
4. Roy, P.; Sinha, N.K.; Tiwari, S.; Khare, A. A review on perovskite solar cells: Evolution of architecture, fabrication techniques, commercialization issues and status. *Sol. Energy* **2020**, *198*, 665–688. [[CrossRef](#)]
5. Green, M.A.; Ho-Baillie, A.; Snaith, H.J. The emergence of perovskite solar cells. *Nat. Photonics* **2014**, *8*, 506–514. [[CrossRef](#)]
6. Huang, J.; Yuan, Y.; Shao, Y.; Yan, Y. Understanding the physical properties of hybrid perovskites for photovoltaic applications. *Nat. Rev. Mater.* **2017**, *2*, 17042. [[CrossRef](#)]
7. Leguy, A.M.A.; Hu, Y.; Campoy-Quiles, M.; Alonso, M.I.; Weber, O.; Azarhoosh, P.; van Schilfhaarde, M.; Weller, M.T.; Bein, T.; Nelson, J.; et al. Reversible Hydration of CH₃NH₃PbI₃ in Films, Single Crystals, and Solar Cells. *Chem. Mater.* **2015**, *27*, 3397–3407. [[CrossRef](#)]
8. Ke, J.C.-R.; Walton, A.S.; Lewis, D.J.; Tedstone, A.; O'Brien, P.; Thomas, A.G.; Flavell, W.R. In situ investigation of degradation at organometal halide perovskite surfaces by X-ray photoelectron spectroscopy at realistic water vapour pressure. *Chem. Commun.* **2017**, *53*, 5231–5234. [[CrossRef](#)]
9. Abdelmageed, G.; Jewell, L.; Hellier, K.; Seymour, L.; Luo, B.; Bridges, F.; Zhang, J.Z.; Carter, S. Mechanisms for light induced degradation in MAPbI₃ perovskite thin films and solar cells. *Appl. Phys. Lett.* **2016**, *109*, 233905. [[CrossRef](#)]
10. Bryant, D.; Aristidou, N.; Pont, S.; Sanchez-Molina, I.; Chotchunangatchaval, T.; Wheeler, S.; Durrant, J.R.; Haque, S.A. Light and oxygen induced degradation limits the operational stability of methylammonium lead triiodide perovskite solar cells. *Energy Environ. Sci.* **2016**, *9*, 1655–1660. [[CrossRef](#)]
11. Krishnan, U.; Kaur, M.; Kumar, M.; Kumar, A. Factors affecting the stability of perovskite solar cells: A comprehensive review. *J. Photonics Energy* **2019**, *9*, 021001. [[CrossRef](#)]
12. Manser, J.S.; Saidaminov, M.; Christians, J.; Bakr, O.M.; Kamat, P.V. Making and Breaking of Lead Halide Perovskites. *Acc. Chem. Res.* **2016**, *49*, 330–338. [[CrossRef](#)] [[PubMed](#)]
13. Aristidou, N.; Eames, C.; Sanchez-Molina, I.; Bu, X.; Kosco, J.; Islam, M.S.; Haque, S.A. Fast oxygen diffusion and iodide defects mediate oxygen-induced degradation of perovskite solar cells. *Nat. Commun.* **2017**, *8*, 15218. [[CrossRef](#)] [[PubMed](#)]
14. Li, B.; Li, Y.; Zheng, C.; Gao, D.; Huang, W. Advancements in the stability of perovskite solar cells: Degradation mechanisms and improvement approaches. *RSC Adv.* **2016**, *6*, 38079–38091. [[CrossRef](#)]
15. Aristidou, N.; Sanchez-Molina, I.; Chotchuangchutchaval, T.; Brown, M.; Martinez, L.; Rath, T.; Haque, S.A. The Role of Oxygen in the Degradation of Methylammonium Lead Trihalide Perovskite Photoactive Layers. *Angew. Chem. Int. Ed.* **2015**, *54*, 8208–8212. [[CrossRef](#)] [[PubMed](#)]
16. Kim, N.-K.; Min, Y.H.; Noh, S.; Cho, E.; Jeong, G.; Joo, M.; Ahn, S.-W.; Lee, J.S.; Kim, S.; Ihm, K.; et al. Investigation of Thermally Induced Degradation in CH₃NH₃PbI₃ Perovskite Solar Cells using In-situ Synchrotron Radiation Analysis. *Sci. Rep.* **2017**, *7*, 1–9. [[CrossRef](#)] [[PubMed](#)]
17. Akbulatov, A.F.; Frolova, L.A.; Dremova, N.N.; Zhidkov, I.S.; Martynenko, V.M.; Tsarev, S.A.; Luchkin, S.; Kurmaev, E.Z.; Aldoshin, S.M.; Stevenson, K.J.; et al. Light or Heat: What Is Killing Lead Halide Perovskites under Solar Cell Operation Conditions? *J. Phys. Chem. Lett.* **2020**, *11*, 333–339. [[CrossRef](#)]
18. Juarez-Perez, E.J.; Ono, L.K.; Maeda, M.; Jiang, Y.; Hawash, Z.; Qi, Y. Photodecomposition and thermal decomposition in methylammonium halide lead perovskites and inferred design principles to increase photovoltaic device stability. *J. Mater. Chem. A* **2018**, *6*, 9604–9612. [[CrossRef](#)]
19. Kim, M.; Ham, S.; Cheng, D.; Wynn, T.A.; Jung, H.S.; Meng, Y.S. Advanced Characterization Techniques for Overcoming Challenges of Perovskite Solar Cell Materials. *Adv. Energy Mater.* **2020**, *11*, 1–26. [[CrossRef](#)]
20. Latini, A.; Gigli, G.; Ciccio, A. A study on the nature of the thermal decomposition of methylammonium lead iodide perovskite, CH₃NH₃PbI₃: An attempt to rationalise contradictory experimental results. *Sustain. Energy Fuels* **2017**, *1*, 1351–1357. [[CrossRef](#)]
21. Brunetti, B.; Cavallo, C.; Ciccio, A.; Gigli, G.; Latini, A. Erratum: Corrigendum: On the Thermal and Thermodynamic (In)Stability of Methylammonium Lead Halide Perovskites. *Sci. Rep.* **2017**, *7*, 46867. [[CrossRef](#)] [[PubMed](#)]
22. Akbulatov, A.; Luchkin, S.Y.; Frolova, L.A.; Dremova, N.N.; Gerasimov, K.L.; Zhidkov, I.S.; Anokhin, D.V.; Kurmaev, E.Z.; Stevenson, K.J.; Troshin, P.A. Probing the Intrinsic Thermal and Photochemical Stability of Hybrid and Inorganic Lead Halide Perovskites. *J. Phys. Chem. Lett.* **2017**, *8*, 1211–1218. [[CrossRef](#)] [[PubMed](#)]
23. Juarez-Perez, E.J.; Hawash, Z.; Raga, S.R.; Ono, L.K.; Qi, Y. Thermal degradation of CH₃NH₃PbI₃ perovskite into NH₃ and CH₃I gases observed by coupled thermogravimetry–mass spectrometry analysis. *Energy Environ. Sci.* **2016**, *9*, 3406–3410. [[CrossRef](#)]
24. Deng, X.; Cao, Z.; Yuan, Y.; Chee, M.O.L.; Xie, L.; Wang, A.; Xiang, Y.; Li, T.; Dong, P.; Ding, L.; et al. Coordination modulated crystallization and defect passivation in high quality perovskite film for efficient solar cells. *Coord. Chem. Rev.* **2020**, *420*, 213408. [[CrossRef](#)]
25. Zhang, F.; Zhu, K. Additive Engineering for Efficient and Stable Perovskite Solar Cells. *Adv. Energy Mater.* **2020**, *10*. [[CrossRef](#)]

26. Azam, M.; Liu, K.; Sun, Y.; Wang, Z.; Liang, G.; Qu, S.; Fan, P.; Wang, Z. Recent advances in defect passivation of perovskite active layer via additive engineering: A review. *J. Phys. D Appl. Phys.* **2020**, *53*, 183002. [[CrossRef](#)]
27. Mahapatra, A.; Prochowicz, D.; Tavakoli, M.M.; Trivedi, S.; Kumar, P.; Yadav, P.K. A review of aspects of additive engineering in perovskite solar cells. *J. Mater. Chem. A* **2020**, *8*, 27–54. [[CrossRef](#)]
28. Zhang, L.; Cole, J.M. Anchoring Groups for Dye-Sensitized Solar Cells. *ACS Appl. Mater. Interfaces* **2015**, *7*, 3427–3455. [[CrossRef](#)]
29. Liao, K.; Yang, J.-A.; Li, C.; Li, T.S.; Hao, F. Off-Stoichiometric Methylammonium Iodide Passivated Large-Grain Perovskite Film in Ambient Air for Efficient Inverted Solar Cells. *ACS Appl. Mater. Interfaces* **2019**, *11*, 39882–39889. [[CrossRef](#)]
30. Dänekamp, B.; Droseros, N.; Palazon, F.; Sessolo, M.; Banerji, N.; Bolink, H.J. Efficient Photo- and Electroluminescence by Trap States Passivation in Vacuum-Deposited Hybrid Perovskite Thin Films. *ACS Appl. Mater. Interfaces* **2018**, *10*, 36187–36193. [[CrossRef](#)]
31. Xie, Y.; Shao, F.; Wang, Y.; Xu, T.; Wang, D.; Huang, F. Enhanced Performance of Perovskite CH₃NH₃PbI₃ Solar Cell by Using CH₃NH₃I as Additive in Sequential Deposition. *ACS Appl. Mater. Interfaces* **2015**, *7*, 12937–12942. [[CrossRef](#)]
32. Yang, Y.; Song, J.; Zhao, Y.; Zhu, L.; Gu, X.; Gu, Y.; Che, M.; Qiang, Y. Ammonium-iodide-salt additives induced photovoltaic performance enhancement in one-step solution process for perovskite solar cells. *J. Alloys. Compd.* **2016**, *684*, 84–90. [[CrossRef](#)]
33. Xu, C.; Zhang, Z.; Hu, Y.; Sheng, Y.; Jiang, P.; Han, H.; Zhang, J. Printed hole-conductor-free mesoscopic perovskite solar cells with excellent long-term stability using PEAI as an additive. *J. Energy Chem.* **2018**, *27*, 764–768. [[CrossRef](#)]
34. Wang, Y.; Liu, S.; Zeng, Q.; Wang, R.; Qin, W.; Cao, H.; Yang, L.; Li, L.; Yin, S.; Zhang, F. Enhanced performance and stability of inverted planar perovskite solar cells by incorporating 1,6-diaminohexane dihydrochloride additive. *Sol. Energy Mater. Sol. Cells* **2018**, *188*, 140–148. [[CrossRef](#)]
35. Laskar, A.R.; Luo, W.; Ghimire, N.; Chowdhury, A.H.; Bahrami, B.; Gurung, A.; Reza, K.M.; Pathak, R.; Bobba, R.S.; Lamsal, B.S.; et al. Phenylhydrazinium Iodide for Surface Passivation and Defects Suppression in Perovskite Solar Cells. *Adv. Funct. Mater.* **2020**, *30*, 1–11. [[CrossRef](#)]
36. Du, C.; Wang, S.; Miao, X.; Sun, W.; Zhu, Y.; Wang, C.; Ma, R. Polyvinylpyrrolidone as additive for perovskite solar cells with water and isopropanol as solvents. *Beilstein J. Nanotechnol.* **2019**, *10*, 2374–2382. [[CrossRef](#)]
37. Wang, N.; Liu, Z.; Zhou, Z.; Zhu, H.; Zhou, Y.; Huang, C.; Wang, Z.; Xu, H.; Jin, Y.; Fan, B.; et al. Reproducible One-Step Fabrication of Compact MAPbI_{3-x}Cl_x Thin Films Derived from Mixed-Lead-Halide Precursors. *Chem. Mater.* **2014**, *26*, 7145–7150. [[CrossRef](#)]
38. Yu, H.; Wang, F.; Xie, F.; Li, W.; Chen, J.; Zhao, N. The Role of Chlorine in the Formation Process of “CH₃NH₃PbI_{3-x}Cl_x” Perovskite. *Adv. Funct. Mater.* **2014**, *24*, 7102–7108. [[CrossRef](#)]
39. Yefang, J.; Ru, D.; Xuediao, C.; Jiangshan, F.; Zhike, L.; Shengzhong, L. Effect of Amphiphilic Quaternary Ammonium Salt Additive on Performance and Stability of Perovskite Solar Cells. *J. Chin. Univ.* **2019**, *40*, 1697–1705. [[CrossRef](#)]
40. Mateen, M.; Arain, Z.; Liu, X.; Iqbal, A.; Ren, Y.; Zhang, X.; Liu, C.; Chen, Q.; Ma, S.; Ding, Y.; et al. Boosting optoelectronic performance of MAPbI₃ perovskite solar cells via ethylammonium chloride additive engineering. *Sci. China Mater.* **2020**, *63*, 2477–2486. [[CrossRef](#)]
41. Yao, J.; Wang, H.; Wang, P.; Gurney, R.S.; Intaniwet, A.; Ruankham, P.; Choopun, S.; Liu, D.; Wang, T. Trap passivation and efficiency improvement of perovskite solar cells by a guanidinium additive. *Mater. Chem. Front.* **2019**, *3*, 1357–1364. [[CrossRef](#)]
42. Wang, P.; Wang, H.; Ye, F.; Zhang, H.; Chen, M.; Cai, J.; Li, D.; Liu, D.; Wang, T. Contrasting Effects of Organic Chloride Additives on Performance of Direct and Inverted Perovskite Solar Cells. *ACS Appl. Mater. Interfaces* **2019**, *11*, 37833–37841. [[CrossRef](#)] [[PubMed](#)]
43. Zheng, G.; Li, L.; Wang, L.; Gao, X.; Zhou, H. The investigation of an amidine-based additive in the perovskite films and solar cells. *J. Semicond.* **2017**, *38*, 14001. [[CrossRef](#)]
44. Bae, S.; Jo, J.W.; Lee, P.; Ko, M.J. Controlling the Morphology of Organic-Inorganic Hybrid Perovskites through Dual Additive-Mediated Crystallization for Solar Cell Applications. *ACS Appl. Mater. Interfaces* **2019**, *11*, 17452–17458. [[CrossRef](#)] [[PubMed](#)]
45. Wang, Y.; Song, N.; Feng, L.; Deng, X. Effects of Organic Cation Additives on the Fast Growth of Perovskite Thin Films for Efficient Planar Heterojunction Solar Cells. *ACS Appl. Mater. Interfaces* **2016**, *8*, 24703–24711. [[CrossRef](#)] [[PubMed](#)]
46. Chen, C.-C.; Hong, Z.; Li, G.; Chen, Q.; Zhou, H.; Yang, Y. One-step, low-temperature deposited perovskite solar cell utilizing small molecule additive. *J. Photonics Energy* **2015**, *5*, 057405. [[CrossRef](#)]
47. Mangrulkar, M.; Luchkin, S.Y.; Boldyreva, A.G.; Troshin, P.A.; Stevenson, K.J. Influence of pyridine-based ligands on photostability of MAPbI₃ thin films. *Mendeleev Commun.* **2021**, *31*, 319–322. [[CrossRef](#)]
48. Frolova, L.A.; Davlethanov, A.I.; Dremova, N.N.; Zhidkov, I.S.; Akbulatov, A.F.; Kurmaev, E.Z.; Aldoshin, S.M.; Stevenson, K.J.; Troshin, P. Efficient and Stable MAPbI₃-Based Perovskite Solar Cells Using Polyvinylcarbazole Passivation. *J. Phys. Chem. Lett.* **2020**, *11*, 6772–6778. [[CrossRef](#)]
49. Zhen, J.; Zhou, W.; Chen, M.; Li, B.; Jia, L.; Wang, M.; Yang, S. Pyridine-functionalized fullerene additive enabling coordination interactions with CH₃NH₃PbI₃ perovskite towards highly efficient bulk heterojunction solar cells. *J. Mater. Chem. A* **2019**, *7*, 2754–2763. [[CrossRef](#)]
50. Fu, S.; Li, X.; Wan, L.; Wu, Y.; Zhang, W.; Wang, Y.; Bao, Q.; Fang, J. Efficient Passivation with Lead Pyridine-2-Carboxylic for High-Performance and Stable Perovskite Solar Cells. *Adv. Energy Mater.* **2019**, *9*, 1–10. [[CrossRef](#)]

51. Cheng, F.; Jing, X.; Chen, R.; Cao, J.; Yan, J.; Wu, Y.; Huang, X.; Wu, B.; Zheng, N. N-Methyl-2-pyrrolidone as an excellent coordinative additive with a wide operating range for fabricating high-quality perovskite films. *Inorg. Chem. Front.* **2019**, *6*, 2458–2463. [[CrossRef](#)]
52. Lee, S.; Tang, M.-C.; Munir, R.; Barrit, D.; Kim, Y.-J.; Kang, R.; Yun, J.-M.; Smilgies, D.-M.; Amassian, A.; Kim, D.-Y. In situ study of the film formation mechanism of organic–inorganic hybrid perovskite solar cells: Controlling the solvate phase using an additive system. *J. Mater. Chem. A* **2020**, *8*, 7695–7703. [[CrossRef](#)]
53. Xia, R.; Fei, Z.; Drigo, N.; Bobbink, F.D.; Huang, Z.; Jasiūnas, R.; Franckevičius, M.; Gulbinas, V.; Mensi, M.; Fang, X.; et al. Retarding Thermal Degradation in Hybrid Perovskites by Ionic Liquid Additives. *Adv. Funct. Mater.* **2019**, *29*. [[CrossRef](#)]
54. Luo, C.; Li, G.; Chen, L.; Dong, J.; Yu, M.; Xu, C.; Yao, Y.; Wang, M.; Song, Q.; Zhang, S. Passivation of defects in inverted perovskite solar cells using an imidazolium-based ionic liquid. *Sustain. Energy Fuels* **2020**, *4*, 3971–3978. [[CrossRef](#)]
55. Zheng, X.; Jiang, T.; Bai, L.; Chen, X.; Chen, Z.; Xu, X.; Song, D.; Xu, X.; Li, B.; Yang, Y. Enhanced thermal stability of inverted perovskite solar cells by interface modification and additive strategy. *RSC Adv.* **2020**, *10*, 18400–18406. [[CrossRef](#)]
56. Chen, S.; Pan, Q.; Li, J.; Zhao, C.; Guo, X.; Zhao, Y.; Jiu, T. Grain boundary passivation with triazine-graphdiyne to improve perovskite solar cell performance. *Sci. China Mater.* **2020**, *63*, 2465–2476. [[CrossRef](#)]
57. Liao, J.-F.; Wu, W.-Q.; Zhong, J.-X.; Jiang, Y.; Wang, L.; Kuang, D.-B. Enhanced efficacy of defect passivation and charge extraction for efficient perovskite photovoltaics with a small open circuit voltage loss. *J. Mater. Chem. A* **2019**, *7*, 9025–9033. [[CrossRef](#)]
58. Jiang, L.-L.; Wang, Z.-K.; Li, M.; Zhang, C.-C.; Ye, Q.-Q.; Hu, K.-H.; Lu, D.-Z.; Fang, P.; Liao, L.-S. Passivated Perovskite Crystallization via g-C₃N₄ for High-Performance Solar Cells. *Adv. Funct. Mater.* **2018**, *28*, 1–8. [[CrossRef](#)]
59. Hu, L.; Liu, T.; Sun, L.; Xiong, S.; Qin, F.; Jiang, X.; Jiang, Y.; Zhou, Y. Suppressing generation of iodine impurity via an amidine additive in perovskite solar cells. *Chem. Commun.* **2018**, *54*, 4704–4707. [[CrossRef](#)] [[PubMed](#)]
60. Li, L.; Chen, Y.; Liu, Z.; Chen, Q.; Wang, X.; Zhou, H. The Additive Coordination Effect on Hybrids Perovskite Crystallization and High-Performance Solar Cell. *Adv. Mater.* **2016**, *28*, 9862–9868. [[CrossRef](#)] [[PubMed](#)]
61. Hao, X.; Bo-Xin, Z.; Wei, J.; Qing-Hong, Z.; Hua-Qing, X. Polymer PVP Additive for Improving Stability of Perovskite Solar Cells. *J. Inorg. Mater.* **2019**, *34*, 96–102. [[CrossRef](#)]
62. Zhang, T.; Cao, Z.; Shang, Y.; Cui, C.; Fu, P.; Jiang, X.; Wang, F.; Xu, K.; Yin, D.; Qu, D.; et al. Multi-functional organic molecules for surface passivation of perovskite. *J. Photochem. Photobiol. A Chem.* **2018**, *355*, 42–47. [[CrossRef](#)]
63. Zhi, L.; Li, Y.; Cao, X.; Li, Y.; Cui, X.; Ci, L.; Wei, J. Perovskite Solar Cells Fabricated by Using an Environmental Friendly Aprotic Polar Additive of 1,3-Dimethyl-2-imidazolidinone. *Nanoscale Res. Lett.* **2017**, *12*, 632. [[CrossRef](#)] [[PubMed](#)]
64. Gao, L.; Wang, L.; Ding, X.; Zhao, E.; Yang, S.; Zhao, Y.; Li, Y.; Wang, S.; Ma, T. Incredible PCE enhancement induced by damaged perovskite layers: Deeply understanding the working principle of additives in bulk heterojunction perovskite solar cells. *J. Mater. Chem. A* **2018**, *6*, 4365–4373. [[CrossRef](#)]
65. Li, Y.; Li, L.; Yerramilli, A.; Chen, Y.; Fang, D.; Shen, Y.; Alford, T. Enhanced power conversion efficiency and preferential orientation of the MAPbI₃ perovskite solar cells by introduction of urea as additive. *Org. Electron.* **2019**, *73*, 130–136. [[CrossRef](#)]
66. Han, L.; Cong, S.; Yang, H.; Lou, Y.; Wang, H.; Huang, J.; Zhu, J.; Wu, Y.; Chen, Q.; Zhang, B.; et al. Environmental-Friendly Urea Additive Induced Large Perovskite Grains for High Performance Inverted Solar Cells. *Sol. RRL* **2018**, *2*, 1–9. [[CrossRef](#)]
67. Wen, X.; Cai, Q.; Shen, G.; Xu, X.; Dong, P.; Du, Y.; Dong, H.; Mu, C. Enhanced crystallization of solution-processed perovskite using urea as an additive for large-grain MAPbI₃ perovskite solar cells. *Nanotechnology* **2021**, *32*, 30LT02. [[CrossRef](#)]
68. Lee, J.-W.; Bae, S.-H.; Hsieh, Y.-T.; De Marco, N.; Wang, M.; Sun, P.; Yang, Y. A Bifunctional Lewis Base Additive for Microscopic Homogeneity in Perovskite Solar Cells. *Chem* **2017**, *3*, 290–302. [[CrossRef](#)]
69. Liu, B.; Wang, S.; Ma, Z.; Ma, J.; Ma, R.; Wang, C. High-performance perovskite solar cells with large grain-size obtained by the synergy of urea and dimethyl sulfoxide. *Appl. Surf. Sci.* **2019**, *467–468*, 708–714. [[CrossRef](#)]
70. Liu, S.; Li, S.; Wu, J.; Wang, Q.; Ming, Y.; Zhang, D.; Sheng, Y.; Hu, Y.; Rong, Y.; Mei, A.; et al. Amide Additives Induced a Fermi Level Shift To Improve the Performance of Hole-Conductor-Free, Printable Mesoscopic Perovskite Solar Cells. *J. Phys. Chem. Lett.* **2019**, *10*, 6865–6872. [[CrossRef](#)]
71. Shi, X.; Wu, Y.; Chen, J.; Cai, M.; Yang, Y.; Liu, X.; Tao, Y.; Guli, M.; Ding, Y.; Dai, S. Thermally stable perovskite solar cells with efficiency over 21% via a bifunctional additive. *J. Mater. Chem. A* **2020**, *8*, 7205–7213. [[CrossRef](#)]
72. Lv, Y.; Zhang, H.; Wang, J.; Chen, L.; Bian, L.; An, Z.; Qian, Z.; Ren, G.; Wu, J.; Nüesch, F.; et al. All-in-One Deposition to Synergistically Manipulate Perovskite Growth for High-Performance Solar Cell. *Research* **2020**, *2020*, 1–10. [[CrossRef](#)]
73. Qin, C.; Matsushima, T.; Fujihara, T.; Adachi, C. Multifunctional Benzoquinone Additive for Efficient and Stable Planar Perovskite Solar Cells. *Adv. Mater.* **2017**, *29*, 1–8. [[CrossRef](#)]
74. Yu, W.; Yu, S.; Zhang, J.; Liang, W.; Wang, X.; Guo, X.; Li, C. Two-in-one additive-engineering strategy for improved air stability of planar perovskite solar cells. *Nano Energy* **2018**, *45*, 229–235. [[CrossRef](#)]
75. Kuo, D.-W.; Liu, G.-Z.; Lee, R.-H. Star-shaped molecule with planar triazine core and perylene diimide branches as an n-type additive for bulk-heterojunction perovskite solar cells. *Dye. Pigment.* **2019**, *170*, 107562. [[CrossRef](#)]
76. Li, H.; Zhu, K.; Zhang, K.; Huang, P.; Li, D.; Yuan, L.; Cao, T.; Sun, Z.; Li, Z.; Chen, Q.; et al. 3,4-Dihydroxybenzhydrazide as an additive to improve the morphology of perovskite films for efficient and stable perovskite solar cells. *Org. Electron.* **2019**, *66*, 47–52. [[CrossRef](#)]
77. Xiong, S.; Song, J.; Yang, J.; Xu, J.; Zhang, M.; Ma, R.; Li, D.; Liu, X.; Liu, F.; Duan, C.; et al. Defect-Passivation Using Organic Dyes for Enhanced Efficiency and Stability of Perovskite Solar Cells. *Sol. RRL* **2020**, *4*, 1–9. [[CrossRef](#)]

78. Lan, Y.; Wang, Y.; Song, Y. Efficient flexible perovskite solar cells based on a polymer additive. *Flex. Print. Electron.* **2020**, *5*, 014001. [[CrossRef](#)]
79. Song, C.; Li, X.; Wang, Y.; Fu, S.; Wan, L.; Liu, S.; Zhang, W.; Song, W.; Fang, J. Sulfonyl-based non-fullerene electron acceptor-assisted grain boundary passivation for efficient and stable perovskite solar cells. *J. Mater. Chem. A* **2019**, *7*, 19881–19888. [[CrossRef](#)]
80. Cao, X.B.; Li, C.; Zhi, L.L.; Li, Y.H.; Cui, X.; Yao, Y.W.; Ci, L.J.; Wei, J.Q. Fabrication of high quality perovskite films by modulating the Pb–O bonds in Lewis acid–base adducts. *J. Mater. Chem. A* **2017**, *5*, 8416–8422. [[CrossRef](#)]
81. Cao, X.; Zhi, L.; Li, Y.; Cui, X.; Ci, L.; Ding, K.; Wei, J. Enhanced performance of perovskite solar cells by strengthening a self-embedded solvent annealing effect in perovskite precursor films. *RSC Adv.* **2017**, *7*, 49144–49150. [[CrossRef](#)]
82. Gregorio, R.; Borges, D.S. Effect of crystallization rate on the formation of the polymorphs of solution cast poly(vinylidene fluoride). *Polymer* **2008**, *49*, 4009–4016. [[CrossRef](#)]
83. Hao, F.; Stoumpos, C.; Guo, P.; Zhou, N.; Marks, T.J.; Chang, R.P.H.; Kanatzidis, M.G. Solvent-Mediated Crystallization of $\text{CH}_3\text{NH}_3\text{SnI}_3$ Films for Heterojunction Depleted Perovskite Solar Cells. *J. Am. Chem. Soc.* **2015**, *137*, 11445–11452. [[CrossRef](#)]
84. Cao, X.; Zhi, L.; Li, Y.; Fang, F.; Cui, X.; Yao, Y.; Ci, L.; Ding, K.; Wei, J. Control of the morphology of PbI_2 films for efficient perovskite solar cells by strong Lewis base additives. *J. Mater. Chem. C* **2017**, *5*, 7458–7464. [[CrossRef](#)]
85. Ren, Y.; Ding, X.; Zhu, J.; Hayat, T.; Alsaedi, A.; Li, Z.; Xu, X.; Ding, Y.; Yang, S.; Kong, M.; et al. A Bi-functional additive for linking PbI_2 and decreasing defects in organo-halide perovskites. *J. Alloys Compd.* **2018**, *758*, 171–176. [[CrossRef](#)]
86. Foley, B.J.; Girard, J.; Sorenson, B.A.; Chen, A.Z.; Niezgoda, J.S.; Alpert, M.; Harper, A.; Smilgies, D.-M.; Clancy, P.; Saidi, W.A.; et al. Controlling nucleation, growth, and orientation of metal halide perovskite thin films with rationally selected additives. *J. Mater. Chem. A* **2017**, *5*, 113–123. [[CrossRef](#)]
87. Gutwald, M.; Rolston, N.; Printz, A.D.; Zhao, O.; Elmaraghi, H.; Ding, Y.; Zhang, J.; Dauskardt, R.H. Perspectives on intrinsic toughening strategies and passivation of perovskite films with organic additives. *Sol. Energy Mater. Sol. Cells* **2020**, *209*, 110433. [[CrossRef](#)]
88. Lin, C.-T.; De Rossi, F.; Kim, J.; Baker, J.; Ngiam, J.; Xu, B.; Pont, S.; Aristidou, N.; Haque, S.A.; Watson, T.; et al. Evidence for surface defect passivation as the origin of the remarkable photostability of unencapsulated perovskite solar cells employing aminovaleric acid as a processing additive. *J. Mater. Chem. A* **2019**, *7*, 3006–3011. [[CrossRef](#)]
89. Santhosh, N.; Sitaaraman, S.; Pounraj, P.; Govindaraj, R.; Pandian, M.S.; Ramasamy, P. Fabrication of hole-transport-free perovskite solar cells using 5-ammonium valeric acid iodide as additive and carbon as counter electrode. *Mater. Lett.* **2019**, *236*, 706–709. [[CrossRef](#)]
90. Li, N.; Xu, F.; Qiu, Z.; Liu, J.; Wan, X.; Zhu, X.; Yu, H.; Li, C.; Liu, Y.; Cao, B. Sealing the domain boundaries and defects passivation by Poly(acrylic acid) for scalable blading of efficient perovskite solar cells. *J. Power Sources* **2019**, *426*, 188–196. [[CrossRef](#)]
91. Chen, H.; Liu, T.; Zhou, P.; Li, S.; Ren, J.; He, H.; Wang, J.; Wang, N.; Guo, S. Efficient Bifacial Passivation with Crosslinked Thioctic Acid for High-Performance Methylammonium Lead Iodide Perovskite Solar Cells. *Adv. Mater.* **2020**, *32*, 1905661. [[CrossRef](#)]
92. Zhang, C.; Luo, Q.; Deng, X.; Zheng, J.; Ou-Yang, W.; Chen, X.; Huang, S. Enhanced efficiency and stability of carbon based perovskite solar cells using terephthalic acid additive. *Electrochim. Acta* **2017**, *258*, 1262–1272. [[CrossRef](#)]
93. Su, L.; Xiao, Y.; Han, G.; Lu, L.; Li, H.; Zhu, M. Performance enhancement of perovskite solar cells using trimesic acid additive in the two-step solution method. *J. Power Sources* **2019**, *426*, 11–15. [[CrossRef](#)]
94. Su, L.; Xiao, Y.; Lu, L.; Han, G.; Zhu, M. Enhanced stability and solar cell performance via π -conjugated Lewis base passivation of organic inorganic lead halide perovskites. *Org. Electron.* **2020**, *77*, 105519. [[CrossRef](#)]
95. Yao, X.; Zheng, L.; Zhang, X.; Xu, W.; Hu, W.; Gong, X. Efficient Perovskite Solar Cells through Suppressed Nonradiative Charge Carrier Recombination by a Processing Additive. *ACS Appl. Mater. Interfaces* **2019**, *11*, 40163–40171. [[CrossRef](#)]
96. Pockett, A.; Raptis, D.; Meroni, S.M.P.; Baker, J.; Watson, T.M.; Carnie, M. Origin of Exceptionally Slow Light Soaking Effect in Mesoporous Carbon Perovskite Solar Cells with AVA Additive. *J. Phys. Chem. C* **2019**, *123*, 11414–11421. [[CrossRef](#)]
97. Han, F.; Luo, J.; Malik, H.A.; Zhao, B.; Wan, Z.; Jia, C. A functional sulfonic additive for high efficiency and low hysteresis perovskite solar cells. *J. Power Sources* **2017**, *359*, 577–584. [[CrossRef](#)]
98. Gao, C.; Dong, H.; Bao, X.; Zhang, Y.; Saparbaev, A.; Yu, L.; Wen, S.; Yang, R.; Dong, L. Additive engineering to improve the efficiency and stability of inverted planar perovskite solar cells. *J. Mater. Chem. C* **2018**, *6*, 8234–8241. [[CrossRef](#)]
99. Wang, M.; Li, B.; Siffalovic, P.; Chen, L.-C.; Cao, G.; Tian, J. Monolayer-like hybrid halide perovskite films prepared by additive engineering without antisolvents for solar cells. *J. Mater. Chem. A* **2018**, *6*, 15386–15394. [[CrossRef](#)]
100. Wu, Y.; Xie, F.; Chen, H.; Yang, X.; Su, H.; Cai, M.; Zhou, Z.; Noda, T.; Han, L. Thermally Stable MAPbI_3 Perovskite Solar Cells with Efficiency of 19.19% and Area over 1 cm^2 achieved by Additive Engineering. *Adv. Mater.* **2017**, *29*, 1–8. [[CrossRef](#)] [[PubMed](#)]
101. Wu, Q.; Zhou, P.; Zhou, W.; Wei, X.; Chen, T.; Yang, S. Acetate Salts as Nonhalogen Additives To Improve Perovskite Film Morphology for High-Efficiency Solar Cells. *ACS Appl. Mater. Interfaces* **2016**, *8*, 15333–15340. [[CrossRef](#)] [[PubMed](#)]
102. Zhang, Z.; Fan, W.; Wei, X.; Zhang, L.; Yang, Z.; Wei, Z.; Shen, T.; Si, H.; Qi, J. Promoted performance of carbon based perovskite solar cells by environmentally friendly additives of $\text{CH}_3\text{COONH}_4$ and $\text{Zn}(\text{CH}_3\text{COO})_2$. *J. Alloys Compd.* **2019**, *802*, 694–703. [[CrossRef](#)]
103. Tang, G.; You, P.; Tai, Q.; Wu, R.; Yan, F. Performance Enhancement of Perovskite Solar Cells Induced by Lead Acetate as an Additive. *Sol. RRL* **2018**, *2*, 1–9. [[CrossRef](#)]

104. Wang, Y.; Wu, Y.; Fu, S.; Song, C.; Wan, L.; Zhang, W.; Li, X.; Yang, W.; Song, W.; Fang, J. Barium acetate as an additive for high performance perovskite solar cells. *J. Mater. Chem. C* **2019**, *7*, 11411–11418. [[CrossRef](#)]
105. Guan, Y.; Mei, A.; Rong, Y.; Duan, M.; Hou, X.; Hu, Y.; Han, H. Fullerene derivative as an additive for highly efficient printable mesoscopic perovskite solar cells. *Org. Electron.* **2018**, *62*, 653–659. [[CrossRef](#)]
106. Hu, L.; Li, S.; Zhang, L.; Liu, Y.; Zhang, C.; Wu, Y.; Sun, Q.; Cui, Y.; Zhu, F.; Hao, Y.; et al. Unravelling the role of C60 derivatives as additives into active layers for achieving high-efficiency planar perovskite solar cells. *Carbon* **2020**, *167*, 160–168. [[CrossRef](#)]
107. Chen, N.; Yi, X.; Zhuang, J.; Wei, Y.; Zhang, Y.; Wang, F.; Cao, S.; Li, C.; Wang, J. An Efficient Trap Passivator for Perovskite Solar Cells: Poly(propylene glycol) bis(2-aminopropyl ether). *Nano-Micro Lett.* **2020**, *12*, 1–13. [[CrossRef](#)]
108. Hsu, H.-L.; Jiang, B.-H.; Chung, C.-L.; Yu, Y.-Y.; Jeng, R.-J.; Chen, C.-P. Commercially available jeffamine additives for p–i–n perovskite solar cells. *Nanotechnol.* **2020**, *31*, 274002. [[CrossRef](#)]
109. Yang, J.; Xiong, S.; Qu, T.; Zhang, Y.; He, X.; Guo, X.; Zhao, Q.; Braun, S.; Chen, J.; Xu, J.; et al. Extremely Low-Cost and Green Cellulose Passivating Perovskites for Stable and High-Performance Solar Cells. *ACS Appl. Mater. Interfaces* **2019**, *11*, 13491–13498. [[CrossRef](#)]
110. Guan, M.; Zhang, Q.; Wang, F.; Liu, H.; Zhao, J.; Jia, C.; Chen, Y. Employing tetraethyl orthosilicate additive to enhance trap passivation of planar perovskite solar cells. *Electrochim. Acta* **2019**, *293*, 174–183. [[CrossRef](#)]
111. De Carvalho, B.A.; Kavadiya, S.; Huang, S.; Niedzwiedzki, D.; Biswas, P. Highly Stable Perovskite Solar Cells Fabricated Under Humid Ambient Conditions. *IEEE J. Photovoltaics* **2017**, *7*, 532–538. [[CrossRef](#)]
112. Isa, M.J.A.; Sulistianto, J.; Kevin, L.; Poespawati, N.R. Optimization of Perovskite Solar Cell Performance using Optimized Level of Tetraethyl Orthosilicate Concentration. In Proceedings of the 2019 11th International Conference on Information Technology and Electrical Engineering (ICITEE), Pattaya, Thailand, 10–11 October 2019; Volume 7. [[CrossRef](#)]
113. Chaudhary, B.; Kulkarni, A.; Jena, A.K.; Ikegami, M.; Miyasaka, T. Tetrahydrofuran as an Oxygen Donor Additive to Enhance Stability and Reproducibility of Perovskite Solar Cells Fabricated in High Relative Humidity (50%) Atmosphere. *Energy Technol.* **2020**, *8*, 1–8. [[CrossRef](#)]
114. Wang, H.; Zeng, W.; Xia, R. Antisolvent diethyl ether as additive to enhance the performance of perovskite solar cells. *Thin Solid Film.* **2018**, *663*, 9–13. [[CrossRef](#)]
115. Kumar, S.; Choi, Y.; Kang, S.-H.; Oh, N.K.; Lee, J.; Seo, J.; Jeong, M.; Kwon, H.W.; Seok, S.I.; Yang, C.; et al. Multifaceted Role of a Dibutylhydroxytoluene Processing Additive in Enhancing the Efficiency and Stability of Planar Perovskite Solar Cells. *ACS Appl. Mater. Interfaces* **2019**, *11*, 38828–38837. [[CrossRef](#)]
116. Feng, M.; You, S.; Cheng, N.; Du, J. High quality perovskite film solar cell using methanol as additive with 19.5% power conversion efficiency. *Electrochim. Acta* **2019**, *293*, 356–363. [[CrossRef](#)]
117. You, S.; Bi, S.; Qiushuang, J.; Jia, Q.; Yuan, Y.; Xia, Y.; Xiao, Z.; Sun, Z.; Liu, J.; Sun, S.; et al. Additive-Enhanced Crystallization of Solution Process for Planar Perovskite Solar Cells with Efficiency Exceeding 19 %. *Chem. A Eur. J.* **2017**, *23*, 18140–18145. [[CrossRef](#)] [[PubMed](#)]
118. Ugur, E.; Sheikh, A.D.; Munir, R.; Khan, J.I.; Barrit, D.; Amassian, A.; Laquai, F. Improved Morphology and Efficiency of n–i–p Planar Perovskite Solar Cells by Processing with Glycol Ether Additives. *ACS Energy Lett.* **2017**, *2*, 1960–1968. [[CrossRef](#)]
119. Wu, W.; Li, H.; Liu, S.; Zheng, B.; Xue, Y.; Liu, X.; Gao, C. Tuning PbI₂ layers by n-butanol additive for improving CH₃NH₃PbI₃ light harvesters of perovskite solar cells. *RSC Adv.* **2016**, *6*, 89609–89613. [[CrossRef](#)]
120. Balis, N.; Zaky, A.A.; Athanasekou, C.; Silva, A.; Sakellis, E.; Vasilopoulou, M.; Stergiopoulos, T.; Kontos, A.G.; Falaras, P. Investigating the role of reduced graphene oxide as a universal additive in planar perovskite solar cells. *J. Photochem. Photobiol. A Chem.* **2020**, *386*, 112141. [[CrossRef](#)]
121. Yu, Y.-Y.; Tseng, C.; Chien, W.-C.; Hsu, H.-L.; Chen, C.-P. Photovoltaic Performance Enhancement of Perovskite Solar Cells Using Polyimide and Polyamic Acid as Additives. *J. Phys. Chem. C* **2019**, *123*, 23826–23833. [[CrossRef](#)]
122. Feng, J.; Zhu, X.; Yang, Z.; Zhang, X.; Niu, J.; Wang, Z.; Zuo, S.; Priya, S.; Liu, F.; Yang, D. Record Efficiency Stable Flexible Perovskite Solar Cell Using Effective Additive Assistant Strategy. *Adv. Mater.* **2018**, *30*, 1801418. [[CrossRef](#)]
123. Hsieh, C.-M.; Liao, Y.-S.; Lin, Y.-R.; Chen, C.-P.; Tsai, C.-M.; Diao, E.W.-G.; Chuang, S.-C. Low-temperature, simple and efficient preparation of perovskite solar cells using Lewis bases urea and thiourea as additives: Stimulating large grain growth and providing a PCE up to 18.8%. *RSC Adv.* **2018**, *8*, 19610–19615. [[CrossRef](#)]
124. Cui, C.; Xie, D.; Lin, P.; Hu, H.; Che, S.; Xiao, K.; Wang, P.; Xu, L.; Yang, D.; Yu, X. Thioacetamide additive assisted crystallization of solution-processed perovskite films for high performance planar heterojunction solar cells. *Sol. Energy Mater. Sol. Cells* **2020**, *208*, 110435. [[CrossRef](#)]
125. Sun, M.; Zhang, F.; Liu, H.; Li, X.; Xiao, Y.; Wang, S. Tuning the crystal growth of perovskite thin-films by adding the 2-pyridylthiourea additive for highly efficient and stable solar cells prepared in ambient air. *J. Mater. Chem. A* **2017**, *5*, 13448–13456. [[CrossRef](#)]
126. Gao, Y.; Wu, Y.; Liu, Y.; Chen, C.; Bai, X.; Yang, L.; Shi, Z.; Yu, W.W.; Dai, Q.; Zhang, Y. Dual Functions of Crystallization Control and Defect Passivation Enabled by an Ionic Compensation Strategy for Stable and High-Efficient Perovskite Solar Cells. *ACS Appl. Mater. Interfaces* **2019**, *12*, 3631–3641. [[CrossRef](#)]
127. Ke, W.; Xiao, C.; Wang, C.; Saporov, B.; Duan, H.-S.; Zhao, D.; Xiao, Z.; Schulz, P.; Harvey, S.P.; Liao, W.; et al. Employing Lead Thiocyanate Additive to Reduce the Hysteresis and Boost the Fill Factor of Planar Perovskite Solar Cells. *Adv. Mater.* **2016**, *28*, 5214–5221. [[CrossRef](#)] [[PubMed](#)]

128. Kim, M.K.; Jeon, T.; Park, H.I.; Lee, J.M.; Nam, S.A.; Kim, S.O. Effective control of crystal grain size in $\text{CH}_3\text{NH}_3\text{PbI}_3$ perovskite solar cells with a pseudohalide $\text{Pb}(\text{SCN})_2$ additive. *CrystEngComm* **2016**, *18*, 6090–6095. [[CrossRef](#)]
129. Zhang, R.; Li, M.; Huan, Y.; Xi, J.; Zhang, S.; Cheng, X.; Wu, H.; Peng, W.; Bai, Z.; Yan, X. A potassium thiocyanate additive for hysteresis elimination in highly efficient perovskite solar cells. *Inorg. Chem. Front.* **2019**, *6*, 434–442. [[CrossRef](#)]
130. Zhang, H.; Hou, M.; Xia, Y.; Wei, Q.; Wang, Z.; Cheng, Y.; Chen, Y.; Huang, W. Synergistic effect of anions and cations in additives for highly efficient and stable perovskite solar cells. *J. Mater. Chem. A* **2018**, *6*, 9264–9270. [[CrossRef](#)]
131. Han, Q.; Bai, Y.; Liu, J.; Du, K.; Li, T.; Ji, D.; Zhou, Y.; Cao, C.; Shin, D.; Ding, J.; et al. Additive engineering for high-performance room-temperature-processed perovskite absorbers with micron-size grains and microsecond-range carrier lifetimes. *Energy Environ. Sci.* **2017**, *10*, 2365–2371. [[CrossRef](#)]
132. Cheng, N.; Li, W.; Zhang, M.; Wu, H.; Sun, S.; Zhao, Z.; Xiao, Z.; Sun, Z.; Zi, W.; Fang, L. Enhance the performance and stability of methylammonium lead iodide perovskite solar cells with guanidinium thiocyanate additive. *Curr. Appl. Phys.* **2019**, *19*, 25–30. [[CrossRef](#)]
133. Zou, J.; Liu, W.; Deng, W.; Lei, G.; Zeng, S.; Xiong, J.; Gu, H.; Hu, Z.; Wang, X.; Li, J. An efficient guanidinium isothiocyanate additive for improving the photovoltaic performances and thermal stability of perovskite solar cells. *Electrochim. Acta* **2018**, *291*, 297–303. [[CrossRef](#)]
134. Correa-Baena, J.-P.; Anaya, M.; Lozano, G.; Tress, W.; Domanski, K.; Saliba, M.; Matsui, T.; Jacobsson, J.; Calvo, M.; Abate, A.; et al. Unbroken Perovskite: Interplay of Morphology, Electro-optical Properties, and Ionic Movement. *Adv. Mater.* **2016**, *28*, 5031–5037. [[CrossRef](#)]
135. Zhang, S.; Lu, Y.; Lin, B.; Zhu, Y.; Zhang, K.; Yuan, N.-Y.; Ding, J.-N.; Fang, B. PVDF-HFP additive for visible-light-semi-transparent perovskite films yielding enhanced photovoltaic performance. *Sol. Energy Mater. Sol. Cells* **2017**, *170*, 178–186. [[CrossRef](#)]
136. Sun, C.; Guo, Y.; Fang, B.; Yang, J.; Qin, B.; Duan, H.; Chen, Y.; Li, H.; Liu, H. Enhanced Photovoltaic Performance of Perovskite Solar Cells Using Polymer P(VDF-TrFE) as a Processed Additive. *J. Phys. Chem. C* **2016**, *120*, 12980–12988. [[CrossRef](#)]
137. Eze, V.O.; Seike, Y.; Mori, T. Synergistic Effect of Additive and Solvent Vapor Annealing on the Enhancement of MAPbI_3 Perovskite Solar Cells Fabricated in Ambient Air. *ACS Appl. Mater. Interfaces* **2020**, *12*, 46837–46845. [[CrossRef](#)] [[PubMed](#)]
138. AnkiReddy, K.; Ghahremani, A.H.; Martin, B.; Gupta, G.; Druffel, T. Rapid thermal annealing of $\text{CH}_3\text{NH}_3\text{PbI}_3$ perovskite thin films by intense pulsed light with aid of diiodomethane additive. *J. Mater. Chem. A* **2018**, *6*, 9378–9383. [[CrossRef](#)]
139. Ma, Y.; Zhang, H.; Zhang, Y.; Hu, R.; Jiang, M.; Zhang, R.; Lv, H.; Tian, J.; Chu, L.; Zhang, J.; et al. Enhancing the Performance of Inverted Perovskite Solar Cells via Grain Boundary Passivation with Carbon Quantum Dots. *ACS Appl. Mater. Interfaces* **2018**, *11*, 3044–3052. [[CrossRef](#)]
140. Kırbıyık, Ç.; Toprak, A.; Başlak, C.; Kuş, M.; Ersöz, M. Nitrogen-doped CQDs to enhance the power conversion efficiency of perovskite solar cells via surface passivation. *J. Alloys Compd.* **2020**, *832*, 154897. [[CrossRef](#)]
141. Guo, Q.; Yuan, F.; Zhang, B.; Zhou, S.; Zhang, J.; Bai, Y.; Fan, L.; Hayat, T.; Alsaedi, A.; Tan, Z. Passivation of the grain boundaries of $\text{CH}_3\text{NH}_3\text{PbI}_3$ using carbon quantum dots for highly efficient perovskite solar cells with excellent environmental stability. *Nanoscale* **2019**, *11*, 115–124. [[CrossRef](#)] [[PubMed](#)]
142. Hsu, H.-L.; Hsiao, H.-T.; Juang, T.-Y.; Jiang, B.-H.; Chen, S.-C.; Jeng, R.-J.; Chen, C.-P. Carbon Nanodot Additives Realize High-Performance Air-Stable p-i-n Perovskite Solar Cells Providing Efficiencies of up to 20.2%. *Adv. Energy Mater.* **2018**, *8*, 1–9. [[CrossRef](#)]
143. Li, Z.; Wang, F.; Liu, C.; Gao, F.; Shen, L.; Guo, W. Efficient perovskite solar cells enabled by ion-modulated grain boundary passivation with a fill factor exceeding 84%. *J. Mater. Chem. A* **2019**, *7*, 22359–22365. [[CrossRef](#)]
144. Wang, Y.; Zhang, J.; Chen, S.; Zhang, H.; Li, L.; Fu, Z. Surface passivation with nitrogen-doped carbon dots for improved perovskite solar cell performance. *J. Mater. Sci.* **2018**, *53*, 9180–9190. [[CrossRef](#)]
145. Fang, X.; Ding, J.; Yuan, N.; Sun, P.; Lv, M.; Ding, G.; Zhu, C. Graphene quantum dot incorporated perovskite films: Passivating grain boundaries and facilitating electron extraction. *Phys. Chem. Chem. Phys.* **2017**, *19*, 6057–6063. [[CrossRef](#)] [[PubMed](#)]
146. Brakkee, R.; Williams, R.M. Minimizing Defect States in Lead Halide Perovskite Solar Cell Materials. *Appl. Sci.* **2020**, *10*, 3061. [[CrossRef](#)]
147. Soe, C.M.M.; Stoumpos, C.C.; Harutyunyan, B.; Manley, E.F.; Chen, L.X.; Bedzyk, M.J.; Marks, T.J.; Kanatzidis, M.G. Room Temperature Phase Transition in Methylammonium Lead Iodide Perovskite Thin Films Induced by Hydrohalic Acid Additives. *ChemSusChem* **2016**, *9*, 2656–2665. [[CrossRef](#)] [[PubMed](#)]
148. Zhang, T.; Guo, N.; Li, G.; Qian, X.; Zhao, Y. A controllable fabrication of grain boundary PbI_2 nanoplates passivated lead halide perovskites for high performance solar cells. *Nano Energy* **2016**, *26*, 50–56. [[CrossRef](#)]
149. Wen, Y.; Tang, Y.-G.; Yan, G.-Q. Large grain size $\text{CH}_3\text{NH}_3\text{PbI}_3$ film for perovskite solar cells with hydroic acid additive. *AIP Adv.* **2018**, *8*, 095226. [[CrossRef](#)]
150. Abdi-Jalebi, M.; Dar, M.I.; Sadhanala, A.; Senanayak, S.P.; Franckevicius, M.; Arora, N.; Hu, Y.; Nazeeruddin, M.K.; Zakeeruddin, S.M.; Grätzel, M.; et al. Impact of Monovalent Cation Halide Additives on the Structural and Optoelectronic Properties of $\text{CH}_3\text{NH}_3\text{PbI}_3$ Perovskite. *Adv. Energy Mater.* **2016**, *6*, 1502472. [[CrossRef](#)]
151. Boopathi, K.M.; Mohan, R.; Huang, T.-Y.; Budiawan, W.; Lin, M.-Y.; Lee, C.-H.; Ho, K.-C.; Chu, C.-W. Synergistic improvements in stability and performance of lead iodide perovskite solar cells incorporating salt additives. *J. Mater. Chem. A* **2016**, *4*, 1591–1597. [[CrossRef](#)]

152. Park, I.J.; Seo, S.; Park, M.A.; Lee, S.; Kim, D.H.; Zhu, K.; Shin, H.; Kim, J.Y. Effect of Rubidium Incorporation on the Structural, Electrical, and Photovoltaic Properties of Methylammonium Lead Iodide-Based Perovskite Solar Cells. *ACS Appl. Mater. Interfaces* **2017**, *9*, 41898–41905. [[CrossRef](#)]
153. Chan, S.-H.; Wu, M.-C.; Lee, K.-M.; Chen, W.-C.; Lin, T.-H.; Su, W.-F. Enhancing perovskite solar cell performance and stability by doping barium in methylammonium lead halide. *J. Mater. Chem. A* **2017**, *5*, 18044–18052. [[CrossRef](#)]
154. Chen, C.; Xu, Y.; Wu, S.; Zhang, S.; Yang, Z.; Zhang, W.; Zhu, H.; Xiong, Z.; Chen, W.; Chen, W. CaI₂: A more effective passivator of perovskite films than PbI₂ for high efficiency and long-term stability of perovskite solar cells. *J. Mater. Chem. A* **2018**, *6*, 7903–7912. [[CrossRef](#)]
155. Mabrouk, S.; Bahrami, B.; Gurung, A.; Reza, K.M.; Adhikari, N.; Dubey, A.; Pathak, R.; Yang, S.; Qiao, Q. Higher efficiency perovskite solar cells using additives of LiI, LiTFSI and BMIm in the PbI₂ precursor. *Sustain. Energy Fuels* **2017**, *1*, 2162–2171. [[CrossRef](#)]
156. Duan, B.; Ren, Y.; Xu, Y.; Chen, W.; Ye, Q.; Huang, Y.; Zhu, J.; Dai, S. Identification and characterization of a new intermediate to obtain high quality perovskite films with hydrogen halides as additives. *Inorg. Chem. Front.* **2017**, *4*, 473–480. [[CrossRef](#)]
157. Chen, H.; Luo, Q.; Liu, T.; Ren, J.; Li, S.; Tai, M.; Lin, H.; He, H.; Wang, J.; Wang, N. Goethite Quantum Dots as Multifunctional Additives for Highly Efficient and Stable Perovskite Solar Cells. *Small* **2019**, *15*, e1904372. [[CrossRef](#)]
158. Gong, X.; Guan, L.; Pan, H.; Sun, Q.; Zhao, X.; Li, H.; Pan, H.; Shen, Y.; Shao, Y.; Sun, L.; et al. Highly Efficient Perovskite Solar Cells via Nickel Passivation. *Adv. Funct. Mater.* **2018**, *28*, 1804286. [[CrossRef](#)]
159. Kayesh, E.; Matsui, K.; Chowdhury, T.H.; Kaneko, R.; Noda, T.; Islam, A. Enhanced Photovoltaic Performance of Perovskite Solar Cells by Copper Chloride (CuCl₂) as an Additive in Single Solvent Perovskite Precursor. *Electron. Mater. Lett.* **2018**, *14*, 712–717. [[CrossRef](#)]
160. Almutawah, Z.S.; Wathage, S.C.; Song, Z.; Ahangharnejhad, R.H.; Subedi, K.K.; Shrestha, N.; Phillips, A.B.; Yan, Y.; Ellingson, R.J.; Heben, M.J. Enhanced Grain Size and Crystallinity in CH₃NH₃PbI₃ Perovskite Films by Metal Additives to the Single-Step Solution Fabrication Process. *MRS Adv.* **2018**, *3*, 3237–3242. [[CrossRef](#)]
161. Wathage, S.C.; Song, Z.; Shrestha, N.; Phillips, A.B.; Liyanage, G.K.; Roland, P.J.; Ellingson, R.J.; Heben, M.J. Impact of Divalent Metal Additives on the Structural and Optoelectronic Properties of CH₃NH₃PbI₃ Perovskite Prepared by the Two-Step Solution Process. *MRS Adv.* **2017**, *2*, 1183–1188. [[CrossRef](#)]
162. Liu, W.; Liu, N.; Ji, S.; Hua, H.; Ma, Y.; Hu, R.; Zhang, J.; Chu, L.; Li, X.; Huang, W. Perfection of Perovskite Grain Boundary Passivation by Rhodium Incorporation for Efficient and Stable Solar Cells. *Nano-Micro Lett.* **2020**, *12*, 119. [[CrossRef](#)]
163. Carmona, C.R.; Gratia, P.; Zimmermann, I.; Grancini, G.; Gao, P.; Graetzel, M.; Nazeeruddin, M.K. High efficiency methylammonium lead triiodide perovskite solar cells: The relevance of non-stoichiometric precursors. *Energy Environ. Sci.* **2015**, *8*, 3550–3556. [[CrossRef](#)]
164. Rafizadeh, S.; Wienands, K.; Schulze, P.S.C.; Bett, A.J.; Andreani, L.C.; Hermle, M.; Glunz, S.W.; Goldschmidt, J.C. Efficiency Enhancement and Hysteresis Mitigation by Manipulation of Grain Growth Conditions in Hybrid Evaporated–Spin-coated Perovskite Solar Cells. *ACS Appl. Mater. Interfaces* **2019**, *11*, 722–729. [[CrossRef](#)] [[PubMed](#)]
165. Chen, Y.; Yerramilli, A.; Shen, Y.; Zhao, Z.; Alford, T. Effect of excessive Pb content in the precursor solutions on the properties of the lead acetate derived CH₃NH₃PbI₃ perovskite solar cells. *Sol. Energy Mater. Sol. Cells* **2018**, *174*, 478–484. [[CrossRef](#)]
166. Yerramilli, A.; Chen, Y.; Sanni, D.; Asare, J.; Theodore, N.D.; Alford, T. Impact of excess lead on the stability and photo-induced degradation of lead halide perovskite solar cells. *Org. Electron.* **2018**, *59*, 107–112. [[CrossRef](#)]
167. Barbé, J.; Newman, M.; Lilliu, S.; Kumar, V.; Lee, H.K.H.; Charbonneau, C.; Rodenburg, C.; Lidzey, D.G.; Tsoi, W.C. Localized effect of PbI₂ excess in perovskite solar cells probed by high-resolution chemical–optoelectronic mapping. *J. Mater. Chem. A* **2018**, *6*, 23010–23018. [[CrossRef](#)]
168. Li, Z.; Zhang, C.; Shao, Z.; Fan, Y.; Liu, R.; Wang, L.; Pang, S. Controlled surface decomposition derived passivation and energy-level alignment behaviors for high performance perovskite solar cells. *J. Mater. Chem. A* **2018**, *6*, 9397–9401. [[CrossRef](#)]
169. Meier, T.; Gujar, T.P.; Schönleber, A.; Olthof, S.; Meerholz, K.; van Smaalen, S.; Panzer, F.; Thelakkat, M.; Köhler, A. Impact of excess PbI₂ on the structure and the temperature dependent optical properties of methylammonium lead iodide perovskites. *J. Mater. Chem. C* **2018**, *6*, 7512–7519. [[CrossRef](#)]
170. Gujar, T.P.; Unger, T.; Schönleber, A.; Fried, M.; Panzer, F.; van Smaalen, S.; Köhler, A.; Thelakkat, M. The role of PbI₂ in CH₃NH₃PbI₃ perovskite stability, solar cell parameters and device degradation. *Phys. Chem. Chem. Phys.* **2018**, *20*, 605–614. [[CrossRef](#)]
171. Liu, F.; Dong, Q.; Wong, M.K.; Djurišić, A.B.; Ng, A.; Ren, Z.; Shen, Q.; Surya, C.; Chan, W.K.; Wang, J.; et al. Is Excess PbI₂ Beneficial for Perovskite Solar Cell Performance? *Adv. Energy Mater.* **2016**, *6*, 1502206. [[CrossRef](#)]
172. Mangrulkar, M.; Luchkin, S.Y.; Akbulatov, A.F.; Zhidkov, I.; Kurmaev, E.Z.; Troshin, P.A.; Stevenson, K.J. Rationalizing the effect of overstoichiometric PbI₂ on the stability of perovskite solar cells in the context of precursor solution formulation. *Synth. Met.* **2021**, *278*, 116823. [[CrossRef](#)]
173. Zhang, Z.; Yue, X.; Wei, D.; Li, M.; Fu, P.; Xie, B.; Song, D.; Li, Y. DMSO-based PbI₂ precursor with PbCl₂ additive for highly efficient perovskite solar cells fabricated at low temperature. *RSC Adv.* **2015**, *5*, 104606–104611. [[CrossRef](#)]
174. Jiang, F.; Rong, Y.; Liu, H.; Liu, T.; Mao, L.; Meng, W.; Qin, F.; Jiang, Y.; Luo, B.; Xiong, S.; et al. Synergistic Effect of PbI₂ Passivation and Chlorine Inclusion Yielding High Open-Circuit Voltage Exceeding 1.15 V in Both Mesoscopic and Inverted Planar CH₃NH₃PbI₃(Cl)-Based Perovskite Solar Cells. *Adv. Funct. Mater.* **2016**, *26*, 8119–8127. [[CrossRef](#)]

175. Ngo, T.T.; Masi, S.; Méndez, P.F.; Kazes, M.; Oron, D.; Seró, I.M. PbS quantum dots as additives in methylammonium halide perovskite solar cells: The effect of quantum dot capping. *Nanoscale Adv.* **2019**, *1*, 4109–4118. [[CrossRef](#)]
176. Wang, S.; Dong, W.; Fang, X.; Zhang, Q.; Zhou, S.; Deng, Z.; Tao, R.; Shao, J.; Xia, R.; Song, C.; et al. Credible evidence for the passivation effect of remnant PbI_2 in $\text{CH}_3\text{NH}_3\text{PbI}_3$ films in improving the performance of perovskite solar cells. *Nanoscale* **2016**, *8*, 6600–6608. [[CrossRef](#)] [[PubMed](#)]
177. Pathipati, S.R.; Shah, M.N. Performance enhancement of perovskite solar cells using NH_4I additive in a solution processing method. *Sol. Energy* **2018**, *162*, 8–13. [[CrossRef](#)]
178. Zuo, C.; Ding, L. An 80.11% FF record achieved for perovskite solar cells by using the NH_4Cl additive. *Nanoscale* **2014**, *6*, 9935–9938. [[CrossRef](#)]
179. Jahandar, M.; Khan, N.; Jahankhan, M.; Song, C.E.; Lee, H.K.; Lee, S.K.; Shin, W.S.; Lee, J.-C.; Im, S.H.; Moon, S.-J. High-performance $\text{CH}_3\text{NH}_3\text{PbI}_3$ inverted planar perovskite solar cells via ammonium halide additives. *J. Ind. Eng. Chem.* **2019**, *80*, 265–272. [[CrossRef](#)]
180. Zhang, W.; Pathak, S.; Sakai, N.; Stergiopoulos, T.; Nayak, P.K.; Noel, N.K.; Haghghirad, A.A.; Burlakov, V.M.; Dequillettes, D.W.; Sadhanala, A.; et al. Enhanced optoelectronic quality of perovskite thin films with hypophosphorous acid for planar heterojunction solar cells. *Nat. Commun.* **2015**, *6*, 10030. [[CrossRef](#)]
181. Xiao, Z.; Wang, D.; Dong, Q.; Wang, Q.; Wei, W.; Dai, J.; Zeng, X.; Huang, J. Unraveling the hidden function of a stabilizer in a precursor in improving hybrid perovskite film morphology for high efficiency solar cells. *Energy Environ. Sci.* **2016**, *9*, 867–872. [[CrossRef](#)]
182. Xu, W.; Lei, G.; Tao, C.; Zhang, J.; Liu, X.; Xu, X.; Lai, W.-Y.; Gao, F.; Huang, W. Precisely Controlling the Grain Sizes with an Ammonium Hypophosphite Additive for High-Performance Perovskite Solar Cells. *Adv. Funct. Mater.* **2018**, *28*, 1802320. [[CrossRef](#)]
183. Mangrulkar, M.; Boldyreva, A.G.; Lipovskikh, S.A.; Troshin, P.A.; Stevenson, K.J. Influence of hydrazinium iodide on the intrinsic photostability of MAPbI_3 thin films and solar cells. *J. Mater. Res.* **2021**, *36*, 1846–1854. [[CrossRef](#)]
184. Zhang, X.; Yuan, S.; Lu, H.; Zhang, H.; Wang, P.; Cui, X.; Zhang, Y.; Liu, Q.; Wang, J.; Zhan, Y.; et al. Hydrazinium Salt as Additive To Improve Film Morphology and Carrier Lifetime for High-Efficiency Planar-Heterojunction Perovskite Solar Cells via One-Step Method. *ACS Appl. Mater. Interfaces* **2017**, *9*, 36810–36816. [[CrossRef](#)] [[PubMed](#)]
185. Abzieher, T.; Mathies, F.; Hetterich, M.; Welle, A.; Gerthsen, D.; Lemmer, U.; Paetzold, U.W.; Powalla, M. Additive-Assisted Crystallization Dynamics in Two-Step Fabrication of Perovskite Solar Cells. *Phys. Status Solidi Appl. Mater. Sci.* **2017**, *214*, 1–9. [[CrossRef](#)]